Aus dem
Universitätsklinikum Tübingen
Institut für Pathologie und Neuropathologie
Abteilung Allgemeine und Molekulare Pathologie und Pathologische Anatomie

Characterization of inflammatory skin diseases using 3D skin models, patient samples and highly multiplexed microscopy

Inaugural-Dissertation
zur Erlangung des Doktorgrades der Medizin

der Medizinischen Fakultät
der Eberhard Karls Universität
zu Tübingen

vorgelegt von
Jäger, Annika

2025

Dekan: Professor Dr. rer. nat. Bernd Pichler

1. Berichterstatter: Professor Dr. Schürch
2. Berichterstatter: Professor Dr. Thorwarth

Tag der Disputation: 20.08.2025

Dedication

To my loving parents.

Table of contents

List of Tables and Figures 4

List of Abbreviations 8

1 Introduction 9

1.1 Highly multiplexed imaging by CODEX 9

1.2 Inflammatory skin diseases 10

1.2.1 Atopic dermatitis (AD) 11

1.2.2 Psoriasis (PS) 12

1.3 Role of Neutrophil Infiltration in inflammatory skin 13

1.4 Colonization of inflammatory skin with *Staphylococcus Aureus* 14

1.4.1 Disruption of the skin barrier 14

1.4.2 Differences in AD and PS 17

1.5 In vitro 3D skin modelling 18

1.6 Proposal: Neutrophils and NETs enhance *S. aureus* colonization 19

1.6.1 Background 19

1.6.2 Characterization of AD and PS patient samples for the presence of activated neutrophils 20

1.6.3 Validation of suitability of 3D human inflammatory skin models for surrogate use in functional assays in vitro 21

1.6.4 CODEX analysis of key markers representative for AD and PS . 22

2 Materials and Methods 23

2.1 Materials 23

2.1.1 Biological Materials 23

2.1.2 Conjugation of DNA oligonucleotides to antibodies 23

2.1.3 Purified antibodies 24

2.1.4 CODEX antibody staining 24

2.1.5 Equipment 25

2.1.6 Antibodies and oligonucleotides 27

2.2 Determination of suitable antibodies for characterization of AD and PS 30

2.3 Tissue selection for patient samples and 3D models 30

2.4 3D human skin models 31

2.4.1 Naïve CD4+ T cell isolation and TH1 cell generation 32
2.4.2 Bacterial strains and culture conditions 32
2.4.3 3D human skin equivalents on fibroblast matrix 32
2.4.4 3D human skin equivalents on collagen matrix 33
2.4.5 Equivalents of inflammatory skin 34
2.4.6 Infection of 3D skin models with Staphylococcus aureus 34
2.5 CODEX 35
2.5.1 Establishment of the CODEX technology 35
2.5.2 Conjugation of selected antibodies to oligonucleotides 35
2.5.3 Validation of conjugated antibodies using FACS analysis 39
2.5.4 Validation of conjugated antibodies using hand-staining with fluorescent labeling 42
2.5.5 Multicycle imaging with CODEX 44
2.5.6 Panel design 45
2.6 Immunohistochemistry 46
2.7 Cell culture 48
2.7.1 Cutaneous T-cell Lymphoma 3D skin model 48
2.8 Statistics and computation 49
3 Results 50
3.1 Skin equivalents 52
3.1.1 Multiplexed imaging of phenotypic hallmark expression in 3D skin models 52
3.1.2 Epithelial barrier in inflammatory skin equivalents 54
3.1.3 Inflammatory hallmarks and distinction markers 56
3.1.4 Staphylococcus aureus colonization 58
3.2 Patient samples 59
3.2.1 Epithelial barrier proteins 59
3.2.2 Inflammatory hallmarks 64
3.2.3 S. aureus 70
3.3 Cell culture and Lymphoma 72
3.3.1 CD3 staining for cell lines HH and HUT 78 72
3.3.2 CD3 staining for TH-17 HSEs with HUT 78 72

4 Discussion 74
4.1 Skin equivalents 74
4.1.1 Atopic dermatitis (AD) Multiplexed imaging of phenotypic hallmark expression in 3D skin models 74
4.1.2 Multiplexed imaging validates phenotypic hallmark expression in 3D skin models 74
4.1.3 Epithelial barrier function of HSEs mimics inflammatory skin 75
4.1.4 NOS2 as psoriatic disease classifier 77
4.1.5 Nitric oxide donors present a new therapeutic perspective for psoriasis 78
4.1.6 Staphylococcus aureus colonization is enhanced by an abundance of Polymorphonuclear Neutrophils 79
4.2 Patient samples 80
4.2.1 Changes to epithelial barrier proteins in inflammatory skin diseases 80
4.2.2 Neutrophil abundance in inflammatory skin and NETosis 83
4.2.3 Interaction of inflammatory markers in response to reactive oxygen species 86
4.2.4 S. aureus colonization is enhanced by presence of PMNs and NET formation 92
4.3 Cell culture 93
4.3.1 CD3 staining for TH-17 HSEs with HUT 78 93
4.4 Outlook 94
5 Conclusion 95
6 Bibliography 97
7 Declaration of Originality 104
8 Publications 105
9 Acknowledgment 106

List of Tables and Figures

Table 1: Overview of antibodies for characterization of inflammatory skin 22
Table 2: List of antibodies including clones and manufacturer 28
Table 3: List of oligo sequences and conjugated antibodies 30
Table 4: Gating of data generated in FACS. forward scatter A (FSC A), sideward scatter A (SSC A), Allophycocyanin A (APC A) 41
Table 5: Final Panel Design 3D skin equivalents 45
Table 6: Final panel design patient samples 46

Figure 1: Schematic workflow of CODEX for inflammatory skin models and patient samples 11
Figure 2: Schematic of production of 3D cytokine model. Figure created with Biorender.com. 33
Figure 3: Schematic of CODEX procedure. Figure created with Biorender.com. Adaptation from publication in (Scheurer et al., 2024). 38
Figure 4: FACS analysis of conjugated antibodies. 51
Figure 5: Hand staining of antibodies pNFkB, NOS2 and OGG1 on lung and skin. Dilutions and exposure times according to labels. 51
Figure 6: Overlay of representative 3D human skin models, showing the epithelial markers Filaggrin, Loricrin and Elafin, Ki-67, NOS2 and the nuclear stain DRAQ5. Published in (Scheurer et al., 2024). 52
Figure 7: Collagen IV and Ki67 staining of human skin equivalents. Partly published in (Scheurer et al., 2024). 53
Figure 8: CODEX fluorescence image comparison of Filaggrin expression in untreated control, TH-17 and TH-2 3D human skin models. 3-day cytokine treatment, six-well collagen matrix. Published in (Scheurer et al., 2024). 55
Figure 9: Comparison and unpaired two-tailed t-test of mean Filaggrin expression per unit area in the epidermis of all analyzed 3D human skin models (n=4). Bars represent the mean ± SD; ns, not significant; $p < 0.05$*. Published in (Scheurer et al., 2024). 55
Figure 10: Elafin and Loricrin expression in HSEs. Statistical comparison of Elafin and Loricrin expression per epidermal cell by unpaired t-test. Bars

represent the mean ± SD; ns, not significant; p < 0.001***. Published in (Scheurer et al., 2024). 56
Figure 11: CODEX fluorescence image comparison of NOS2 expression in untreated control, TH-17 and TH-2 3D human skin models. 3-day cytokine treatment, six-well collagen matrix. Squares in top images indicate magnified regions in bottom images. Published in (Scheurer et al., 2024). 57
Figure 12: Statistical comparison of NOS2 expression per epithelial (left) or dermal (right) cell by unpaired two-tailed t-test. Bars represent the mean ± SD; p < 0.05*; p < 0.0001****. Published in (Scheurer et al., 2024). 57
Figure 13: CODEX fluorescence image comparison of S. aureus expression in S. aureus-infected untreated control, S. aureus-infected TH-17 and S. aureus-infected TH-2 3D human skin models. 3-day cytokine treatment, six-well collagen matrix. Scale bars: 75 µm. Published in (Scheurer et al., 2024). 58
Figure 14: Comparison and unpaired two-tailed t-test of mean marker expression of S. aureus per area in the epidermis of infected 3D human skin models (n=2). Unpaired two-tailed t-test was used. Bars represent the mean ± SD; p < 0.01**. Published in (Scheurer et al., 2024). 58
Figure 15: CODEX image of Loricrin expression and statistical comparison of mean epidermal marker expression. Bars represent the mean ± SD; ns, not significant. 61
Figure 16: CODEX images of Loricrin and MPO expression (top). Statistical analysis of epidermal Loricrin and MPO expression per cell (bottom). Total, nuclear and cytoplasmic marker expression quantified using QuPath; unpaired two-tailed t-tests, p < 0.0001****. Bars represent the mean ± SD. 61
Figure 17: CODEX image comparisons of Filaggrin and Elafin expression and statistical analysis of mean marker expression. Bars represent the mean ± SD; ns, not significant. 62
Figure 18: Comparison of Mean Marker Expression and Signal to noise ratio for epidermal barrier proteins Filaggrin, Elafin and Loricrin. Quantification and statistical analysis performed using QuPath, unpaired two-tailed t-tests. Bars represent the mean ± SD; ns, not significant, p < 0.05*, p < 0.01**, p < 0.001***. 62

Figure 19: CODEX images of Filaggrin and NE expression (top). Statistical analysis of epidermal Filaggrin and NE expression per cell (bottom). Total, nuclear and cytoplasmic marker expression quantified using QuPath; unpaired two-tailed t-tests, p < 0.0001****. Bars represent the mean ± SD. 63
Figure 20: CODEX images of OGG1 and Elafin expression (top). Statistical analysis of epidermal OGG1 and Elafin expression per cell (bottom). Total, nuclear and cytoplasmic marker expression quantified using QuPath; unpaired two-tailed t-tests, p < 0.0001****. Bars represent the mean ± SD. 63
Figure 21: CODEX image comparisons of MPO expression and statistical analysis of mean marker expression by unpaired two-tailed t-tests. Bars represent the mean ± SD; p < 0.05*. 67
Figure 22: CODEX image of Neutrophil Elastase expression and statistical comparison of mean epidermal marker expression by unpaired two-tailed t-tests. Bars represent the mean ± SD; p < 0.01**. Published in (Focken et al., 2023). 67
Figure 23: CODEX image of OGG1 expression and statistical comparison of mean epidermal marker expression by unpaired two-tailed t-tests. Bars represent the mean ± SD; p < 0.05*. 68
Figure 24: CODEX image of HMGB1 expression and statistical comparison of mean epidermal marker expression by unpaired two-tailed t-tests. Bars represent the mean ± SD; p < 0.05*. Published in (Focken et al., 2023). 68
Figure 25: HMGB1 expression in the skin of AD patients compared to healthy controls A-C: Total, nuclear and cytoplasmic HMGB1 expression quantified using QuPath; unpaired two-tailed t-tests. Bars represent the mean ± SD; p < 0.0001****. Published in (Focken et al., 2023)..... 68
Figure 26: CODEX images of HMGB1 and CitH3 expression (top). Statistical analysis of epidermal HMGB1 and CitH3 expression per cell (bottom). Total, nuclear and cytoplasmic marker expression quantified using QuPath; unpaired two-tailed t-tests, p < 0.0001****. Bars represent the mean ± SD. 69
Figure 27: CODEX image of citH3 expression and statistical comparison of mean epidermal marker expression by unpaired two-tailed t-tests Bars represent the mean ± SD; ns, not significant. 69

Figure 28: Comparison of mean marker expression of inflammatory hallmark proteins p-NF-kB, p-ERK and p-p38. Statistical analysis performed in QuPath, unpaired two-tailed t-tests. Bars represent the mean ± SD; p < 0.05*, p < 0.01**. 70
Figure 29: Comparison of mean marker expression of inflammatory hallmark proteins Histone H3, LL37 and HBD3. Statistical analysis performed in QuPath, unpaired two-tailed t-tests. Bars represent the mean ± SD; p < 0.05*, p < 0.01**. 70
Figure 30: CODEX images of S. aureus expression (top). Statistical analysis of epidermal S. aureus expression per cell (bottom left). Descriptive statistics for epidermal cytoplasmic S. aureus expression per cell (bottom right). Total, nuclear and cytoplasmic marker expression quantified using QuPath; unpaired two-tailed t-tests, p < 0.0001****. Bars represent the mean ± SD. 71
Figure 31: CODEX image of S. aureus expression and statistical comparison of mean epidermal marker expression by unpaired two-tailed t-tests, Bars represent the mean ± SD; p < 0.05*. Published in (Focken et al., 2023). 72
Figure 32: CD3 staining for sewed $5x10^5$ HUT 78 cells on Control, non-cytokine and TH-17 cytokine model after 6 days. Scale bars indicate 200 µm. 73
Figure 33: CD3 staining for sewed $6x10^6$ HUT 78 cells on non-cytokine treated and TH-17 cytokine skin model after 6 days. Scale bars indicate 200 µm. 73
Figure 34: Overview of interactions between inflammation markers. Figure created using Biorender.com. Adapted from (Chen, Kang and Tang, 2022; Md Jaffri, 2023). Blue labels indicate markers included in the CODEX panel for characterization of inflammatory skin. 88

List of Abbreviations

AD	Atopic Dermatitis
cAMP	Cyclic adenosine monophosphate
CODEX	Co-Detection by Imaging
CTCL	Cutaneous T-cell lymphoma
EDC	Epidermal differentiation complex
FACS	Fluorescence Activated Cell Sorting
FLG	Filaggrin
HMGB1	High-mobility-group-protein B1
HSE	Human Skin Equivalent
ICAM-1	Intercellular adhesion molecule 1
IgE	Immunoglobulin E
IL	Interleukin
MDA	Malondialdehyde
MPO	Myeloperoxidase
NE	Neutrophil Elastase
NET	Neutrophil Extracellular Trap
OGG1	8-Oxoguanine glycosylase
PCA	Pyrrolidone carboxylic acid
PDE4	Phosphodiesterase 4
PMN	Polymorphonuclear neutrophil
PS	Psoriasis
TGFβ	Transforming Growth Factor β
TLSP	Thymic stromal lymphoprotein
UCA	Urocanic acid

1 Introduction

1.1 Highly multiplexed imaging by CODEX

Microscopy-based techniques facilitate the portrayal of histological structures in three dimensions for individual cells, typically assisted by the visualization of cellular components. To understand the organization of multiple cell types, their interactions and activation states, it's necessary to concurrently detect numerous cellular markers. Microscopy using immunofluorescence commonly manages to identify only four markers due to overlaps in spectral properties. However, recent advancements in multiplex tissue imaging allow for the simultaneous spatial identification of over 50 cellular markers with single-cell resolution (Baertsch, Nolan and Hickey, 2022). Consequently, multiplex tissue imaging is now capable of pinpointing various immune, stromal, and epithelial cell types and subsets, enabling the mapping of tissue structure and the characterization of interactions among different cell types.

Co-Detection-by indexing (CODEX) utilizes antibodies linked to oligonucleotides conjugated to barcodes and is compatible with both formalin-fixed, paraffin-embedded, and fresh frozen samples (Black *et al.*, 2021). It is based on iterative annealing and subsequent chemical stripping of fluorescently labeled DNA probes that bind to DNA-conjugated barcoded antibodies (Black *et al.*, 2021). The process involves imaging three fluorescent-dye conjugated oligonucleotides that are complementary to the antibody barcodes. Afterward, the fluorescent oligonucleotides are removed, and another set of three fluorescently labeled oligonucleotides, complementary to different barcodes, are attached and imaged. This sequence is repeated until all the antibodies within the panel have been imaged (Schürch *et al.*, 2020).

Progress in multiplexed imaging techniques has significantly enhanced our capacity to examine both healthy and diseased tissues at the individual cell level. The CODEX approach provides an intricate insight into the spatial relationships among individual cells within tissues and is intended to catalyze discoveries in areas such as developmental biology, diseases, and therapeutic progress (Kuswanto, Nolan and Lu, 2023). My work specifically focused on utilization of CODEX for mapping the spatial distribution of immune, stromal, and epithelial

elements in cases of inflammatory skin diseases. The examination of immune responses within tissues has unveiled the diverse roles played by the immune system, spanning from overall organism metabolism to tissue regeneration and repair and will continue to promote further scientific research.

Equally significant alongside the technical strides in multiplexed tissue imaging are the advancements in bioinformatic methodologies. These methods are used to process and interpret the complex single-cell data in high dimensions, aiming to extract biological and clinical insights. Recent progress in computational analysis has enabled rapid image preprocessing, reliable cell segmentation, precise quantification of protein markers, followed by the identification of cell types and spatial analysis. These methodologies allow for the measurement of marker expression in individual cells, as well as the assessment of multi-scale spatial relationships that characterize tissue structure and function (Kuswanto, Nolan and Lu, 2023).

1.2 Inflammatory skin diseases

Inflammatory skin diseases, including atopic dermatitis (AD) and psoriasis (PS), are among the most common human diseases, affecting millions of individuals worldwide (Nørreslet, Agner and Clausen, 2020). In addition to physical discomfort and the increased susceptibility to infections, patients suffering from AD or PS face an impaired quality of life due to emotional distress and social stigma, leading to a higher incidence of psychiatric disorders and increased number of suicides among affected patients (Noormohammadpour *et al.*, 2015; Pompili *et al.*, 2016; Gochnauer *et al.*, 2017). Diagnosis of AD or PS has a substantial effect on patients' quality of life, especially for adults who often present refractory to adequate topical treatment with corticosteroids or calcineurin inhibitors. This only leaves systemic treatment as the last option (Megna *et al.*, 2016). In the proposed project, we will use CODEX to characterize the differences in the two main inflammatory skin diseases, first aiming to validate the use of 3D human inflammatory skin models and second focusing on NET distribution and activity in AD. Significant results will help in developing therapies based on immunological and molecular grounds of AD and PS respectively,

without the use of mouse models. Especially, influences upon the skin barrier resulting in enhanced inflammatory processes could be limited with further knowledge about pathways among NET activation and colonization of *S. aureus*.

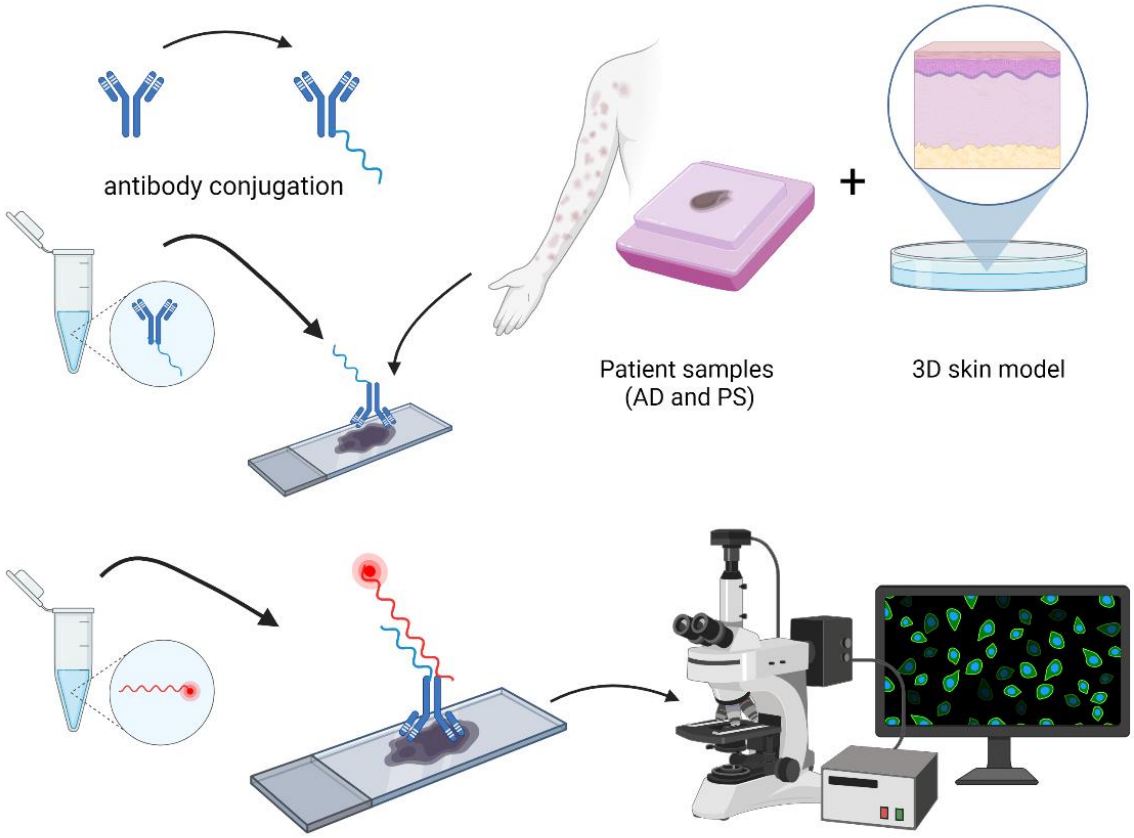

Figure 1: Schematic workflow of CODEX for inflammatory skin models and patient samples

1.2.1 Atopic dermatitis (AD)

Atopic dermatitis (AD) is the most common chronic inflammatory skin disease, with a lifetime prevalence of up to 20 % and substantial effects on quality of life (Balato *et al.*, 2019). Patients are often diagnosed before adolescence, but progression can be chronically relapsing until late adulthood. AD is characterized by intense itch, recurrent eczematous lesions and a fluctuating course, has a strong heritability component and is closely related to and commonly co-occurs with other atopic diseases such as asthma and allergic rhinitis. Several pathophysiological mechanisms contribute to AD etiology and clinical manifestations. One of the main factors for development of phenotypic AD relys

on impairment of epidermal barrier function. This can be led by a deficiency in the structural protein Filaggrin and promotes inflammation by T cell infiltration (Weidinger *et al.*, 2018). The immune response in AD is skewed towards T helper 2 cell-mediated pathways and can in turn favor epidermal barrier disruption (Balato *et al.*, 2019). Another factor contributing to AD onset includes dysbiosis of the skin microbiota. In particular overgrowth of *Staphylococcus aureus* and systemic immune responses including immunoglobulin E (IgE)-mediated sensitization and neuroinflammation are vital drivers to developing pruritus (Weidinger *et al.*, 2018). Current treatments for AD rely on topical moisturizers and anti-inflammatory agents such as corticosteroids, calcineurin inhibitors and cyclic adenosine monophosphate (cAMP)-specific 3',5'-cyclic phosphodiesterase 4 (PDE4) inhibitors, phototherapy and systemic immunosuppressants (Noormohammadpour *et al.*, 2015; Gochnauer *et al.*, 2017).

1.2.2 Psoriasis (PS)

Another example of an inflammatory skin disease is PS, which affects up to 4 % of the world's population (Balato *et al.*, 2019). Earlier thought of as a genetic disorder of keratinocyte proliferation, it is now accepted as a more complex series of events responsible for the disease. The pathogenesis of PS involves stimuli such as infections, trauma or medication leading to an activation of the innate immune system. Following the release of auto-antigens, activated dendritic cells support the activation and proliferation of T helper 17 $CD4^+$ T cells (TH-17 cells) and IL-17 releasing $CD8^+$ T cells by secreting interleukin 23 (IL-23) and transforming growth factor β (TGFβ) (Balato *et al.*, 2019; Ho and Kupper, 2019). Psoriatic skin lesions show leukocyte infiltrates as part of a dysregulated cell-mediated adaptive immune response consisting of $CD4^+$ and $CD8^+$ T cells that home to the skin using adhesion molecules including E-selectin and intercellular adhesion molecule-1 (ICAM-1) (Valdimarsson *et al.*, 1995; Robert and Kupper, 1999). In addition, in PS plaques cytokines like interferon-γ, IL-2 and IL-12 are upregulated, which are signature cytokines of a T helper 1 (Th1) phenotype, and lesioned skin shows an abundance of TH-17 and IL-17 producing $CD8^+$ T cells (Balato *et al.*, 2019).

1.3 Role of Neutrophil Infiltration in inflammatory skin

The innate immune system plays a major role in the pathway leading to TH-17 activation in psoriasis. Polymorphonuclear neutrophils (PMNs) are the most abundant innate immune effector cells of the human immune system and act as a first line of defense. Their activation is regulated by phagocytosis, degranulation of cytotoxic molecules and a cell-own mechanism of PMNs leading to the release of neutrophil extracellular traps (NETs) (Hu *et al.*, 2016). The formation of NETs is a process by which neutrophils externalize web-like chromatin strands coated with antimicrobial peptides (Rada, 2019). NETs are important in neutralization of bacteria and viruses and play a role in the pathogenesis of immune-related diseases. NETosis is the process of NET production and release by neutrophils through a cell death program.

The formation of NETs is led by a break-up of the nuclear envelope as well as granular membranes, releasing decondensed chromatin and granular components into the cytoplasm. Thereafter chromatin threads and granular components are released but the cytoplasmic membrane of polymorphonuclear cells (PMNs) stays intact during this process. The antimicrobial proteins and chromatin stay enucleated and still perform phagocytosis until inevitable cell death (Sabbatini, Magnelli and Renò, 2021).

In a study conducted in 2016, PS patients showed a higher amount of neutrophils undergoing NETosis compared to control groups, showed increased ability to induce NET formation and depicted NET amounts that correlated with severity of the disease (Hu *et al.*, 2016). Current research focuses on the identification of molecules that modulate the release of NETs (Hoffmann and Enk, 2016).

In contrast to PS, AD is defined as a T helper type 2 cell (TH-2) disease associated with cytokines like IL-4, IL-5 and IL-13 (Landgren *et al.*, 2006). While it is established that neutrophil abundance in PS contributes to cutaneous inflammation, little is known about the abundance and function of neutrophils in AD inflammation and immunity (Dhingra *et al.*, 2013). AD is characterized by heightened colonization of lesional and non-lesional skin by *S. aureus* (Weidinger *et al.*, 2018). Recent findings suggest that *S. aureus* is capable of TH-17 / IL-17

induction, which implicates an increasing role for the TH-17 / IL-17 axis and its downstream neutrophil-associated molecules in cases of *S. aureus* infection in AD (Dhingra *et al.*, 2013). Furthermore, recent evidence shows that *S. aureus* skin colonization is enhanced by the interaction of NETs with keratinocytes in the skin indicating that neutrophils play an essential role in the aggravation of AD (Bitschar *et al.*, 2020). However, little is known about the abundance of neutrophils and NETs in AD patients with *S. aureus* skin colonization. In addition, PS patients, whose skin is rarely colonized with *S. aureus,* have increased numbers of neutrophils (Chiang *et al.*, 2019). However, neutrophil interaction with keratinocytes in the induction of NET-formation, and their effect on *S. aureus* skin colonization, have not been addressed so far. Therefore, there is need for an improved understanding and research in the role of skin barrier function, NETs, and *S. aureus* colonization in PS and AD.

1.4 Colonization of inflammatory skin with *Staphylococcus Aureus*

1.4.1 Disruption of the skin barrier

As previously mentioned, pathogenesis of AD is associated with a disruption of the natural protection the skin represents as a barrier for irritants like bacteria. Furthermore, immune dysregulation in affected patients leads to subsequent and additional damage of the skin barrier. Especially for lesioned skin, the probability of disruptive factors successfully crossing the natural barrier is much higher than in healthy skin. This creates a vicious cycle, as the entering of the disruptors into the skin triggers an inflammatory response, again causing further weakening of the skins barrier (Williams and Gallo, 2015).

Moreover, the existing microbiota on the skin can be diminished in this process, which plays an important role in the prevention of pathogen proliferation and maintenance of homeostasis. In lesioned skin the compromised diversity of the microflora allows growth of pathogens like *S. aureus*, which is inter alia caused by a reduction in bacteria usually associated with anti-*S. aureus* activity (Nakatsuji *et al.*, 2017).

The process itself is understood as that with the penetration of the skin barrier by an allergen, expression of thymic stromal lymphoprotein (TLSP) is induced. TLSP function lies in stimulation of Th0 cells, supporting differentiation into TH-2 cells. The cascade triggers IgE production by B cells, which then target the allergen. Cytokines released by the developed TH-2 cells stimulate pruritus and interfere with differentiation of corneocytes, causing further disruption of the skin barrier. In a chronic state, TH-1 cells develop and play a leading role in development of the AD phenotype by releasing proinflammatory cytokines like IFN-g (Geoghegan, Irvine and Foster, 2018).

Interestingly, the colonization of *S. aureus* in AD skin samples has been known for over 40 years (Leyden, Marples and Kligman, 1974) but the preferential occurrence in AD in contrast to other inflammatory skin diseases like psoriasis is still not understood. One hypothesis proposes a contribution of the composition of the stratum corneum and corneocytes: Fibronectin, a protein assisting in tissue organization and composition of the extracellular matrix, is expressed in the stratum corneum of AD skin but not in healthy skin (Cho *et al.*, 2001). Staphylococcus aureus can therefore bind to skin in AD patients via surface proteins like fibronectin-binding proteins (FnBP) A and B (Foster *et al.*, 2014). Another surface protein expressed on the *S. aureus* bacterium is clumping factor B (ClfB), which mediates adherence to squamous epithelial cells by binding to epithelial proteins Loricrin and cytokeratin 10 (Mulcahy *et al.*, 2012). Adding to that, corneocytes in AD skin with low natural moisturizing factors, like breakdown products of Filaggrin, differ in their morphology from healthy ones. The appearance has been described previously as “villus-like projections” extending from the apical surface of the corneocytes. The tips of the villi hereby express corneodesmosin, which is associated with cell-to-cell connection and thereby presents an unusual location of this protein. This implies possible accessibility of additional ligands in the environment created by the disrupted skin barrier in AD patients (Geoghegan, Irvine and Foster, 2018).

One more proposal is, that by incorporation of fatty acids into the cytoplasmic membrane, *S. aureus* has an increased membrane fluidity, increases

proinflammatory properties (Nguyen *et al.*, 2016) and can be a factor in tolerating oxidative stress (Sun *et al.*, 2012).

Additionally, bacterial as well as host proteases act in favor of a disruption in the skin's barrier. Proteases like Staphopain protect the bacterium from antimicrobial peptides, amongst others cleaving LL-37 (Sieprawska-Lupa *et al.*, 2004). This is supported by AD skin showing reduced levels of antimicrobial peptides like LL-37 (Chieosilapatham, Ogawa and Niyonsaba, 2017), which are inhibited by cytokines IL-4 and IL-13 produced by TH-2 cells (Geoghegan, Irvine and Foster, 2018). Bacterial proteases assist penetration of the epidermis while *S. aureus* additionally stimulates expression of endogenous peptidases in keratinocytes, therefore leading to a reciprocal induction of disruptions in the skin barrier (Nakatsuji *et al.*, 2016; Williams *et al.*, 2017). Altogether the mentioned factors induce a disbalance in the microbial environment of the skin and enable colonization with *S. aureus*.

With relevance to corneocyte morphology, natural moisturizing factors are important in the maintenance of a functional skin barrier. Two of those factors are urocanic acid (UCA) and pyrrolidone carboxylic acid (PCA), which are both a breakdown product of Filaggrin. Filaggrin (FLG) is an important epidermal protein as mutations in the FLG gene lead to an AD phenotype in 42 % of all carriers, but are also associated with asthma, hay fever and peanut allergy (Irvine, McLean and Leung, 2011). Thus, mutations in the FLG gene also cause reduced levels of UCA and PCA respectively, which results in low levels of natural moisturizing factors for maintenance of the skin barrier. This is accompanied by the induced differentiation of TH-0 to TH-2 cells, which release IL-4 and IL-13, synergistically reducing FLG as well as Loricrin expression, which affects corneocyte function (Cornelissen *et al.*, 2012). This means, that even without being a carrier of the mutation, UCA and PCA levels will be reduced in AD lesions (Kezic *et al.*, 2011) reducing skin barrier integrity.

1.4.2 Differences in AD and PS

Although AD and PS are very different diseases pathologically, they still share some characteristics like dry skin and disturbed epidermal differentiation. While PS is known for infiltration of macrophages, neutrophils and dendritic cells into the epidermis and dermis causing hyperproliferation of keratinocytes, AD shows infiltration of eosinophils and mast cells (Bowcock, 2004). This relates to chemokines increased in AD skin like CCL13, CCL18 and CCL27. In PS chemokines reported are CCL4, CCL20, CXCL2 and MCP1. Increased keratinocyte proliferation may be a result of an upregulation of certain genes summarized as the epidermal differentiation complex (EDC) also involved in upregulation of the mentioned chemokines. Upregulations of those genes cannot be seen in AD and involve Elafin, protease, lipocalin and PRP2C (Nakatani *et al.*, 2001). Elafin is a psoriasis-specific biomarker and was found to be upregulated even in non-lesional skin of PS patient, while not being elevated in patients with eczema (Berekmeri *et al.*, 2024). The EDC has been described as a complex of genes involved in transcription of genes that may modify immune processes in the epithelium. Moreover, it has been shown that PS is associated with HLA alleles that could not be found in AD. This may stand in relation to hyperproliferation of keratinocytes or infections. However, the polymorphic nature of genes expressed in the skin outline a complex interplay of factors comprising genetic and external stimuli.

Adding to that, the expression of antimicrobial peptides shows significant differences between both inflammatory diseases: While AD showed lower levels for beta-defensin, LL-37 and other innate immune effector molecules, Nel-like protein 2 showed a strong induction only in AD skin. Next to beta-defensin 2, Elafin, interleukin 1F9 and vanin 3 were strongly expressed in psoriasis, while carbonic anhydrase II was not, which can be found in every form of eczema (Kamsteeg *et al.*, 2010).

Recently, Garzorz-Stark et al. showed a correlation of mRNA levels of nitric oxidase synthase (NOS2) and CCL27 to clinical and histological features of psoriasis and eczema. NOS2 and CCL27 both showed antagonistic properties to histological hallmarks, thus NOS2 was found to be significantly upregulated in

lesional psoriatic skin compared to healthy skin or AD (Garzorz-Stark *et al.*, 2016).

This not only proves molecular differences between the diseases but also suggests a possibility to visualize the differences in form of expression patterns as an indicator for further findings.

1.5 In vitro 3D skin modelling

To characterize the inflammation-induced changes in the epidermis in PS and AD in depth, the workgroup of Birgit Schittek at the Institute of Dermatology has developed *in vitro* 3D human skin models that comprise a stratified, terminally differentiated epidermal compartment with primary human keratinocytes. These are seeded on a dermal compartment consisting of primary human fibroblasts, either embedded in collagen or on a fibroblast matrix without collagen. To mimic the two inflammatory skin diseases AD and PS *in vitro*, 3D human skin equivalents (HSE) are treated with cytokine cocktails. For the PS model, either the TH-17 specific cytokines IL-17 and IL-22 or the TH1 cytokines TNF-α, IL-6 and IL-1α are used while the AD models are treated with the TH-2 specific cytokines IL-4, IL-5, and IL-13. 3D models are exposed to the respective cytokines for 3-5 days during airlift cultivation. The HSE models manage to successfully recapitulate inflammatory skin diseases after treatment with the respective cytokines, which has been presented in (Scheurer *et al.*, 2024).

Filaggrin, a key protein for skin barrier maintenance, is downregulated in diseases with epidermal barrier disruption (McGrath and Uitto, 2008) while Elafin, an important antimicrobial peptide and a serine protease inhibitor with anti-inflammatory properties as well as stimulatory effects on cellular proliferation, is increased in PS (Elgharib *et al.*, 2018). In both 3D skin models, a thickening of the epidermis is detectable while Elafin expression is increased only for the PS HSE and Filaggrin expression is decreased (Scheurer *et al.*, 2024).

Moreover, HSEs have been established and are currently being improved by inducing skin inflammation through the introduction of TH-1 or TH-2 effector T cells into the culture. This successfully created a PS-like model by introducing

TH-1 human effector T cells in replacement of the cytokine treatment. This model shows a phenotype like the PS model induced with cytokines, with higher expression of Elafin and lower expression of Filaggrin. However, the TH-1-induced PS model must be further validated using more markers specific for PS and an AD model by introduction of TH-2 effector T cells has not been established so far, not allowing comparison of the two diseases yet (Scheurer *et al.*, 2024).

To determine the validity of the AD and PS models *in vitro* on a functional level, analysis of efficient *S. aureus* colonization was performed for the PS and AD 3D models. Excitingly, *S. aureus* efficiently colonizes the AD skin models, but not the PS model, which correlates well with the clinical phenotypes in the respective patients.

1.6 Proposal: Neutrophils and NETs enhance *S. aureus* colonization

The role of neutrophils during staphylococcal skin colonization has been described previously and found that the depletion of neutrophils *in vivo* reduces *S. aureus* colonization, and *in vitro* coculture of primary human keratinocytes with neutrophils promotes *S. aureus* skin colonization. This demonstrates that the interaction of NETs with keratinocytes is responsible for increased *S. aureus* skin colonization (Bitschar *et al.*, 2020) and suggests that AD patients who suffer from *S. aureus* skin colonization have more activated neutrophils producing NETs than PS patients or healthy people.

1.6.1 Background

Using our recently established cytokine and T cell induced 3D human inflammatory skin models resembling PS and AD, respectively, we aim to characterize the interplay of specific immune cell types, the epithelium, antimicrobial proteins, and *S. aureus* using CODEX. This will indicate whether these 3D models are suitable models to analyze the interplay between epithelial barrier proteins, immune cells and microbes concerning disease severity on a functional level and offers the opportunity to test potential new therapy targets to diminish the disease phenotype.

Recent data concerning the role of neutrophils and NETs in enhancing *S. aureus* skin colonization let us hypothesize that AD patients who show *S. aureus* skin colonization in lesional and non-lesional skin have more infiltrating and activated NET-producing neutrophils than AD patients without *S. aureus* colonization, PS patients or healthy persons (Bitschar *et al.*, 2020). We therefore aim to characterize patient material from AD and PS patients and healthy control samples for the presence and abundance of activated neutrophils and NETs, and their influence on epithelial barrier proteins and *S. aureus* skin colonization, using CODEX.

1.6.2 Characterization of AD and PS patient samples for the presence of activated neutrophils

The aim is characterization of the interplay of epithelial barrier proteins with integrated T cells and *S. aureus* in 3D inflammatory skin models using CODEX highly multiplexed microscopy. To achieve a successful characterization of the change of the epithelial barrier in the PS and AD models, we will analyze the expression of epithelial barrier proteins listed in Table 1 in detail using CODEX as well as structural proteins known to play an important role in structural details of the epidermis and dermis. For instance, Collagen IV is found as a major component of the dermal-epidermal junction and can be used to identify the basement membrane (Abreu-Velez and Howard, 2012). In addition, markers known to be dysregulated specifically in AD or PS patients will be analyzed including antimicrobial peptides, proinflammatory cytokines and T cell markers (see Table 1 and (Quaranta *et al.*, 2014)). Translational research has fostered the development of targeted small molecules and biologic therapies, especially for moderate-to-severe disease (McGrath and Uitto, 2008). Hereby, using CODEX, the phenotypical histological resemblance will be validated on a molecular basis.

1.6.3 Validation of suitability of 3D human inflammatory skin models for surrogate use in functional assays in vitro

We strive to achieve a characterization of the abundance of neutrophils and NETs in skin samples from AD and PS patients and correlation with *S. aureus* skin colonization. First, we will investigate whether the abundance, location and activation of infiltrated neutrophils and NETs differ in patient samples of AD and PS. Therefore, patient material will be stained for myeloperoxidase (MPO) as an inflammatory marker, citrullinated histone H3 (citH3) which potentiates NET formation, Neutrophil Elastase (NE) to locate NETs and 8-Oxoguanine glycosylase (OGG1), which is involved in base excision repair and marks for exposure to reactive oxygen species (ROS). To correlate the abundance of neutrophils and NETs with *S. aureus* skin colonization, we will stain the patient samples with an antibody against protein A, which allows detecting *S. aureus*. Since we have preliminary data that NETs induce oxidative stress in keratinocytes, we will stain the patient samples with antibodies against phospho-histone H2Ax (pH2Ax) as a marker for DNA damage and malondialdehyde (MDA) as a marker for lipid peroxidation because of ROS. Our *in vitro* data showed that the NET-mediated colonizing-enhancing effect depends on the effect via high-mobility-group-protein B1 (HMGB1) release, as a necrotic marker, toll-like receptor (TLR4) and proposedly receptor for advanced glycation end products (RAGE) signaling in keratinocytes. Therefore, we will investigate if the expression of TLR4, RAGE and HMGB1 is increased in AD patients and if this correlates with *S. aureus* colonization. Moreover, co-incubation of keratinocytes with NETs mediates activation of phosphorylated nuclear factor kB (p-NF-kB), a transcription factor regulating proliferation, apoptosis and immune response and Mitogen-activated protein kinase (MAPK) in keratinocytes. Inhibition of these pathways reduces the colonizing-enhancing effect. By staining for p-NF-kB, protein kinase R-like endoplasmic reticulum kinase (p-ERK) and MAPK p-38 the activity of this signaling pathway will be characterized using the CODEX technique. CODEX offers the possibility to use imaging for elaboration of the role of NETs and identification of the processes on a molecular level.

1.6.4 CODEX analysis of key markers representative for AD and PS

The panel used for multiplexed imaging is designed to ensure illustration of a representative phenotype of the two diseases compared to a healthy patient control sample or an untreated 3D model. Markers were chosen from different subgroups of antibodies to visualize the effects on immune as well as DNA damage and epithelial markers. Data analysis can be performed using images created by CODEX that are then processed and segmented with the AKOYA Processor and later on characterized on a single-cell level to enable clustering of cells. An overview of all markers can be found in Table 1.

T cell & tumor	**Macrophages**	**Cytokines and inflammation**	**Lymphocytes**	**Epithelium**	**Anti-microbial**
CD3	CD11b	CCL27	CD45	Cytokeratin	Anti-*S. aureus*
TCR-b	CD68	HMGB1	CD45RA	Filaggrin	HBD3
CD8	CD163	pNFkB	CD45RO	Elafin	LL37
FoxP3	CD206	S100A9	CD62L	Loricrin	MPO
				Involucrin	NOS2
Nuclei	**Granulocytes**	**Oxidative Stress**	**Dendritic cells**	**Proliferation & activation**	**Extracellular matrix**
DRAQ5	CD15	OGG1	CD1a	Granzyme B	Collagen IV
Hoechst	Mast cell tryptase	pH2AX	CD11c	p53	
Multifunctional	**Neutrophils**	**Blood & plasma cells**	**Blood vessels**	Ki-67	**NK cells**
B-catenin	citH3	CD20	CD31	pERK	CD56
HLA-DR	Neutrophil Elastase	CD38	CD34	HistoneH3	**Cytoplasm**
a-SMA	MPO	CD138		pp38	Vimentin
				pSTAT3	

Table 1: Overview of antibodies for characterization of inflammatory skin

2 Materials and Methods

2.1 Materials

2.1.1 Biological Materials

Human tissue was prepared according to standard pathology procedures for FFPE (Goldblum *et al.*, 2018). The tissues used in this dissertation were taken from patients who gave their written informed consent to have their tissue used for research. The samples were fully de-identified, and therefore the study was exempt from ethics approval (no human subjects research). Patient samples were from patients with AD and PS phenotypes before treatment and taken from lesional skin. 3D skin model samples were taken from cultivated skin tissue using primary human keratinocytes.

Two Tissue Micro-Arrays were created in the course of the project, one for patient samples and a second one for 3D skin models to enable simultaneous imaging of 15 samples and ensure comparability among the results. Each TA contained punches of five control samples, five AD samples and five PS samples or five untreated models, five AD models and five PS models respectively. Punches were made for previously defined regions chosen from H&E slides of the blocks and of 2 mm diameter. Both TAs were prepared with approval of all parties and only used for the mentioned project.

2.1.2 Conjugation of DNA oligonucleotides to antibodies

- Tween 20 (Sigma, cat. no. P1379)
- Dulbecco's PBS (DPBS), 1×, no calcium or magnesium (Thermo Fisher Scientific, cat. no. 14190-250)
- Trizma HCl (Sigma, cat. no. T3253)
- Trizma base (Sigma, cat. no. T1503)
- Tris-(2-carboxyethyl) phosphine hydrochloride (TCEP; Thermo Fisher Scientific, cat. no. 77720; Sigma,
- cat. no. C4706-10G)
- 500 mM EDTA, pH 8.0 (Teknova, cat. no. E0308)

- 1 M Tris, pH 8.0 (Teknova, cat. no. T1080)
- NaCl (Thermo Fisher Scientific, cat. no. S271-10)
- DNA oligonucleotides (TriLink Biotechnologies)
- Candor PBS antibody stabilizer solution (Thermo Fisher Scientific, cat. no. NC0436689)
- Sodium azide (NaN_3; Sigma-Aldrich, cat. no. S-8032)

2.1.3 Purified antibodies

- 100 µg of purified, carrier-free antibody with specificity against the target of interest.

For efficient conjugation, antibodies must be free of cysteine-containing proteins, such as BSA, which can compete for maleimide-functionalized groups. A list of the DNA-conjugated antibodies used in the presented CODEX multicycle is provided in Table 2.

2.1.4 CODEX antibody staining

- Vectabond (Vector Labs, cat. no. SP-1800)
- Acetone (Thermo Fisher Scientific, cat. no. A929-4)
- Xylene (Thermo Fisher Scientific, cat. no. X5-4)
- Ethanol, 100 % (Sigma, cat. no. E7023)
- 10× PBS, pH 7.4 (Thermo Fisher Scientific, cat. no. 70011069)
- Dako target retrieval solution, pH 9.0 (Agilent, cat. no. S236784-2)
- Tris-buffered saline (TBS) IHC wash buffer with Tween 20 (Cell Marque, cat. no. 935B-09)
- Bondic polyacrylamide gel pen (Amazon, cat. no. B018IBEHQU).
- DPBS, 1×, no calcium or magnesium (Thermo Fisher Scientific, cat. no. 14190-250)
- Mouse IgG (Sigma, cat. no. I5381-10MG)
- Rat IgG (Sigma, cat. no. I4131)
- Blocking component 4 (BC4)

- Salmon sperm DNA, sheared, 10 mg/ml (Thermo Fisher Scientific, cat. no. AM9680)
- BSA (Sigma, cat. no. A3059)
- Disodium phosphate (Na_2HPO_4; Sigma, cat. no. S7907)
- Sodium phosphate monobasic monohydrate ($NaH_2PO_4 \cdot H_2O$; Sigma, cat. no. S9638)
- Magnesium chloride hexahydrate ($MgCl_2 \cdot 6H_2O$; Sigma, cat. no. M2670)
- NaOH (Sigma, cat. no. S8263)
- Triton X-100 (Sigma, cat. no. T8787)
- Paraformaldehyde ampoules, 16 % (wt/vol) (Thermo Fisher Scientific, cat. no. 50-980-487)
- Methanol, 100 % (Thermo Fisher Scientific, cat. no. A412-4)
- Bis (sulfosuccinimidyl) suberate (BS3; Thermo Fisher Scientific, cat. no. 21580)
- Dimethyl sulfoxide (DMSO) ampule (Sigma, cat. no. D2650)
- DMSO (Sigma-Aldrich, cat. no. D2650-5X5ML)
- Hoechst 33342 (Thermo Fisher Scientific, cat. no. 62249)
- DRAQ5 (Cell Signaling Technology, cat. no. 4084L)
- Fluorescent reporter oligonucleotides (Integrated DNA Technologies (IDT)
- Hematoxylin, ready-to-use solution (Agilent, cat. no. S330930-2)
- Eosin Y solution (Sigma, cat. no. HT110116)
- Cytoseal XYL (VWR Scientific, cat. no. 48212-196)
- UltraComp eBead compensation beads (Thermo Fisher Scientific, cat. no. 01-2222-42)
- XT OptiView DAB IHC v3 (Roche, cat. no. 06396500001)
- Antibody Diluent (Zytomed Systems no. ZUC025-500)

2.1.5 Equipment

- 4 °C, −20 °C and −80 °C storage units
- UV-visible spectrophotometer (Thermo Fisher Scientific, model no. NanoDrop 2000)

- Tabletop microcentrifuge (Eppendorf, model no. 5424)
- 50-kDa Amicon Ultra 0.5-ml centrifugal filter column (EMD Millipore, cat. no. UFC505096)
- Eppendorf tubes, 1.7 ml (VWR Scientific, cat. no. 87003-294)
- Microcentrifuge tubes with socket screw-cap, 1.5 ml (VWR Scientific, cat. no. 89004-294)
- Glass coverslips, 22 × 22 mm, 1.5-inch thickness (Electron Microscopy Sciences, cat. no. 72204-10)
- Frosted glass microscope slides (Thermo Fisher Scientific, cat. no. 12-550-343)
- Glass coverslip storage box (Qintay, cat. no. CS-22)
- Wheaton coverslip glass jar (Thermo Fisher Scientific, cat. no. 02-912-637)
- Microscope slide–staining glass jar (Ted Pella, cat. no. 432-1)
- Dumont #5/45 coverslip forceps (Fine Science Tools, cat. no. 11251-33)
- Six-well tissue culture plates (Thermo Fisher Scientific, cat. no. 07-20083)
- Digital mini incubator (VWR Scientific, cat. no. 10055-006)
- ST4020 small linear stainer (Leica, cat. no. 14050946425)
- Lab Vision PT module (Thermo Fisher Scientific, cat. no. A80400012)
- Slide chamber for antigen retrieval (Electron Microscopy Sciences, cat. no. 62705-01)
- Humidity chamber, sealable (we use a pipette tip box with a wet paper towel soaked in ddH_2O on the bottom)
- Adjustable speed orbital shaker (Mophorn, cat. no. B07FCY2S1P)
- Heavy-duty, single-edge razor blade (Amazon, cat. no. B003O3EOFM)
- Kimberly-Clark Professional Kimwipes (Thermo Fisher Scientific, cat. no. 06-666-1A)
- Falcon round-bottom polypropylene tubes, 5 ml (Corning, cat. no. 352053)
- CODEX acrylic plate (Bayview Plastic Solutions, custom; blueprints available upon request)
- DMSO-resistant mounting gasket, 22 × 22 mm (Qintay, cat. no. TMG-22)
- Corning black 96-well plates (Thermo Fisher Scientific, cat. no. 07-200-762)

- Axygen aluminum sealing film (VWR Scientific, cat. no. 47734-817)
- BZ-X710 inverted fluorescence microscope (Keyence); the currently available model for purchase is X810.
- CFI Plan Apo ƛ 2×/0.10 objective (Nikon)
- CFI Plan Apo ƛ 20×/0.75 objective (Nikon)
- Akoya microfluidics device (Akoya Biosciences)
- Keyence accessory kit: microscope objective liquid collector device and microscope liquid collector cup (Akoya Biosciences, cat. no. 9000020)
- Ventana BenchMark XT IHC/ISH Staining Module (Roche)

2.1.6 Antibodies and oligonucleotides

Antibody	**Clone**	**Manufacturer**	**Preexisting (P), Newly established (N), Reconjugated (R)**
a-SMA	poly	abcam	P
Anti-Staphylococcus aureus	polyclonal	Thermofisher	N
beta catenin	14	Cell Marque	P/R
CCL27	124308	R&D Systems	N
CD11b	EPR1344	abcam	P
CD11c	EP1347Y	abcam	P
CD138	B-A38	Invitrogen	P
CD15	HI98	BD Biosciences	P
CD163	EDHu-1	Novus	P
CD1a	O10 + C1A/711	Novus	P
CD20	rIGEL/773	Novus	P
CD206	MM0820-48L31	abcam	P
CD3	MRQ-39	Cell Marque	P
CD31	C31.3 + C31.7 + C31.10	Novus	P
CD34	QBEnd/10	Novus	P
CD38	EPR4106	abcam	P
CD4	EPR6855	abcam	P
CD45	2B11 + PD7/26	Novus	P
CD45RA	HI100	BD Biosciences	P
CD45RO	UCH-L1	BioLegend	P
CD56	MRQ-42	Cell Marque	P
CD62L	B-8	Santa Cruz	N
CD68	KP-1	BioLegend	P
CD69	polyclonal	Novus	P
CD8a	C8/144B	Santa Cruz BT	P

citH3	polyclonal	abcam	N
Collagen IV	polyclonal	abcam	P
Cytokeratin	AE1/AE3	BioLegend	P/R
Elafin	H-2	Santa Cruz	N
Filaggrin	AE21	Santa Cruz BT	N
Foxp3	236A/E7	eBioscience	P
Granzyme B	EPR20129-217	abcam	P
HBD-3	polyclonal	Novus	N
Histone H3	E191	SB	P
HLA-DR	EPR3692	abcam	P
HMGB1	polyclonal	R&D Systems	N
Involucrin	SY5	Novus	N
Ki67	B56	BD Biosciences	P
LL-37	polyclonal	Novus	N
Loricrin	Poly19051	BioLegend	N
Mast cell tryptase	AA1	BioLegend	P
MDA	1,10E+04	Novus	N
MMP9	L51/82	BioLegend	P/R
MPO	polyclonal	Novus	N
Neutrophil Elastase	ELA2	R&D Systems	N
NOS2	poly	Novus	N
OGG1	polyclonal	Novus	N
P-p38	polyclonal	Novus	N
P53	DO7	Cell Marque	N
pERK	polyclonal	Cell Signal	N
pH2AX	EP854(2)Y	abcam	N
pNFkB	polyclonal	Thermofisher	N
pSTAT3	4	BD Biosciences	P
RAGE	polyclonal	R&D Systems	N
S100A9	MAC387	Invitrogen	P/R
TCR-b	G-11	Santa Cruz BT	P
TCR-g/d	H-41	Santa Cruz	P
TLR4	polyclonal	R&D Systems	N
Vimentin	RV202	BD Biosciences	P

Table 2: List of antibodies including clones and manufacturer

Top oligo	Top oligo sequence (5'-3')	Fluorescent oligo sequences (5'-3')	Antibody
A2	/mal/ATGGTTTAGGACTAC	/5ATTO550N/GTAGTCCTAAACCAT	CD45RO
A3	/mal/TACTCCTCGCCG	/5Alex488N/CGGCGAGGAGTA	TCR-b
A5	/mal/TCTCCCATTAGTCGG	/5Alex488N/CCGACTAATGGGAGA	pH2AX
A6	/mal/TGGATGTGTTACGAT	/5Alex647N/ATCGTAACACATCCA	Ki67
A7	/mal/CGCTAAGATATTCTAAG	/5Alex488N/CTTAGAATATCTTAGCG	Vimentin
A8	/mal/CGCAGATGAATATTC	/5Alex488N/GAATATTCATCTGCG	CD8
A11	/mal/GGGTTATACACTCGT	/5ATTO550N/ACGAGTGTATAACCC	*S. aureus*
A14	/mal/AGATTCAGTCTCTCG	/5ATTO550N/CGAGAGACTGAATCT	P-p38
A15	/mal/CTGTAATAGGCACTA	/5Alex488N/TAGTGCCTATTACAG	CD15
A20	/mal/ATGTAGGATGGTCTC	/5ATTO550N/GAGACCATCCTACAT	pSTAT3
A21	/mal/CGTGCCGTTTCAC	/5Alex488N/GTGAAACGGCACG	CCL27
A24	/mal/ATAAGGGCTCATTGT	/5ATTO550N/ACAATGAGCCCTTAT	Beta catenin
A25	/mal/GCACGCCCTTTTA	/5Alex647N/TAAAAGGGCGTGC	P53
A26	/mal/CACTTGTCTAACCAA	/5Alex647N/TTGGTTAGACAAGTG	Filaggrin
A28	/mal/TGGTCCACTAACGTA	/5Alex488N/TACGTTAGTGGACCA	CD11b
A29	/mal/ATAGGGCATTTGAAG	/5Alex647N/CTTCAAATGCCCTAT	CD56
A30	/mal/CACATGAGCGAATCA	/5ATTO550N/TGATTCGCTCATGTG	HBD-3
A32	/mal/TACCAAATCCTGATG	/5Alex647N/CATCAGGATTTGGTA	OGG1
A33	/mal/TTATCATGAGGAGCG	/5Alex647N/CGCTCCTCATGATAA	Collagen IV
A36	/mal/ACCTACACAATGCTA	/5ATTO550N/TAGCATTGTGTAGGT	pERK
A38	/mal/GCGTCTACTTATAAG	/5ATTO550N/CTTATAAGTAGACGC	CD34
A41	/mal/TGTATGAGTAGTAATCT	/5Alex488N/AGATTACTACTCATACA	LL37
A42	/mal/TCTAAGTCAGAGAGC	/5Alex647N/GCTCTCTGACTTAGA	pNFkB
A43	/mal/GACATTATCCGTGAT	/5Alex488N/ATCACGGATAATGTC	CD1a
A44	/mal/TCACTACTATTAGTACT	/5Alex488N/AGTACTAATAGTAGTGA	Mast cell tryptase
A45	/mal/GCCAGAATGCCA	/5Alex647N/TGGCATTCTGGC	CD163
A48	/mal/GCACGGCAAAGTG	/5ATTO550N/CACTTTGCCGTGC	CD20
A49	/mal/ATAACGCCTCGTATC	/5ATTO550N/GATACGAGGCGTTAT	CD11c
A51	/mal/CGTGCGGGAAAAT	/5Alex647N/ATTTTCCCGCACG	MPO
A55	/mal/AGGTCAACTCGCAC	/5ATTO550N/GTGCGAGTTGACCT	CD206
A56	/mal/GGTCACATGGTCGTT	/5ATTO550N/AACGACCATGTGACC	CD45
A57	/mal/GCGGATTTCGTATTT	/5ATTO550N/AAATACGAAATCCGC	Histone H3
A58	/mal/CGTCAGTACTTTCAG	/5Alex488N/CTGAAAGTACTGACG	S100A9
A60	/mal/ACAAAACTGCTGTCG	/5Alex647N/CGACAGCAGTTTTGT	HMGB1
A61	/mal/TCTTATTCCCGAATA	/5Alex647N/TATTCGGGAATAAGA	Foxp3
A62	/mal/TAGGGGAACAGGTTG	/5Alex488N/CAACCTGTTCCCCTA	CD62L
A63	/mal/AATTAGCTTAAGAGAGT	/5Alex488N/ACTCTCTTAAGCTAATT	Involucrin
A65	/mal/GATAAATATTTTACAGAGT	/5Alex488N/ACTCTGTAAAATATTTATC	HLA-DR
A66	/mal/TACGTGCTTTGGTT	/5Alex488N/AACCAAAGCACGTA	CD38
A67	/mal/GACGACGAAGGC	/5ATTO550N/GCCTTCGTCGTC	Cytokeratin

A68	/mal/CTTCTTGTGGAACC	/5ATTO550N/GGTTCCACAAGAAG	CD31
A69	/mal/CCCGGCAGTT	/5Alex488N/AACTGCCGGG	a-SMA
A70	/mal/AACCAAACTGACCG	/5Alex488N/CGGTCAGTTTGGTT	CD68
A71	/mal/TCACCCCCAGC	/5ATTO550N/GCTGGGGGTGA	Loricrin
A72	/mal/AACGCGACGGAT	/5Alex488N/ATCCGTCGCGTT	CD45RA
A74	/mal/ATTTGCTTCGACGA	/5ATTO550N/TCGTCGAAGCAAAT	citH3
A75	/mal/CGCTTGGGTGTTTA	/5ATTO550N/TAAACACCCAAGCG	Neutrophil Elastase
A76	/mal/CTGTCGGTCGTCA	/5Alex647N/TGACGACCGACAG	CD138
A77	/mal/ATTTCAACAAATATTGTT	/5Alex647N/AACAATATTTGTTGAAAT	CD3
A80	/mal/CGGGGCACCA	/5Alex647N/TGGTGCCCCG	Elafin
A81	/mal/CAAGGAACTACCGA	/5Alex647N/TCGGTAGTTCCTTG	Granzyme B

Table 3: List of oligo sequences and conjugated antibodies

2.2 Determination of suitable antibodies for characterization of AD and PS

To determine antibodies suitable for CODEX it is necessary to not only define the desired cellular targets but recommended to choose antibodies already established for IHC in FFPE tissues or even already tested for CODEX. Antibodies need to be purified, BSA free and specifically target human antigens. The skin as primary tissue of interest lays focus on epithelial and neutrophil markers, *S. aureus* and markers to portray possible DNA damage. Taking everything into account, a first panel approach was defined to then be validated after conjugation. The panel contained antibodies already established and tested in Schuerch Lab but also required many new markers specific for characterizing NET formation and the epidermis.

Antibodies that were used for initial conjugation and testing are listed in the table above. All antibodies marked with N or R were conjugated or reconjugated, unmarked antibodies were already conjugated and established by Prof. Dr. Christian Schürch, Yannick Palmowski and Christine Beschorner.

2.3 Tissue selection for patient samples and 3D models

All declarations concerning ethics approval can be found under the point Material and attached at the end. Two rounds of tissue selection were necessary, the first one being used for validation of the antibodies. In this step it is assured that the

antibodies perform specific binding and the dilution for CODEX multicycles is evaluated according to the intensity of the signal seen in fluorescent microscopy. For selection of the tissue the targets were analyzed using information provided on The Human Protein Atlas (https://www.proteinatlas.org/) (Uhlen *et al.*, 2010) to ensure expression of expected antigens. Most antibodies were tested on an AD patient sample, a T-cell induced 3D skin model as well as on a skin tissue microarray (TMA) to confirm positive staining. Some more specific targets were stained for validation on lung (RAGE, pNFkB, OGG1), tonsil (immune markers like TLR4) or radiated rectum carcinoma (pH2AX). The samples were provided by the Institute of dermatology or taken from archived cases at the Institute of Pathology. For the multicycle runs we designed tissue arrays (TA) including 5 3D skin equivalents samples for psoriasis, atopic dermatitis and control models or 5 patient samples for psoriasis, atopic dermatitis and healthy controls respectively.

2.4 3D human skin models

Preparation of the 3D models was performed at the Institute of Dermatology by Jasmin Scheurer and Birgit Sauer. Cell cultures of primary human fibroblasts and keratinocytes were isolated form human infantile foreskin as previously described (Bitschar *et al.*, 2019). Fibroblasts were cultured in tissue flasks in CnT-Prime Fibroblast Proliferation Medium (CELLnTEC) at 37 °C and 5 % CO_2. Keratinocytes were cultured in collagen-coated tissue flasks in CnT-BM.1 Basal Medium 1 with supplements (CELLnTEC) at 37 °C and 5 % CO_2. 2-3 days before using the keratinocytes for experiments, keratinocytes were cultured in CnT-Prime Epithelial Proliferation medium (CELLnTEC). For experiments cell passage 2 – 4 were used. Fibroblast and keratinocyte isolation from human foreskin were approved by the ethics committee of the medical faculty of the University Tübingen (093/2019B02). Keratinocyte cell lines N/TERT1 or N/TERT2G were cultured in tissue flasks in CnT-BM.1 Basal Medium 1 with supplements at 37 °C and 5 % CO_2. 2-3 days before using the keratinocytes for experiments, keratinocytes were cultured in CnTPrime Epithelial Proliferation medium. R2F/TERT fibroblast cell line was cultured in tissue flasks in Human Fibroblast Expansion Basal Medium (GibcoTM) and Medium 199 (GibcoTM) (1:1)

supplemented with iron-supplemented fetal calf serum (FCS) (Sigma Aldrich), 10 ng/ml epidermal growth factor and 0.4 µg/ml hydrocortisone. Culture conditions were at 37 °C and 5 % CO_2. N/TERT1, N/TERT2G and R2F/TERT cell lines were kindly provided by J. G. Rheinwald (Harvard Medical School, Boston, USA) (Dickson *et al.*, 2000).

2.4.1 Naïve CD4+ T cell isolation and TH1 cell generation

Untouched naive human CD4+ T cells were isolated from Peripheral Blood Mononuclear Cells (PMBCs) by magnetic-activated cell sorting using the Naïve CD4+ T Cell Isolation Kit II (Miltenyi) and an LS Column (Miltenyi) according to manufacturer's protocol. TH1 T cell polarization was induced by using 5 µl Dynabeads® Human T-Activator CD3/CD28 á $1x10^6$ cells, 10 ng/ml human IFN-γ (Peprotech), 10 ng/ml human IL-12 (Peprotech) and 1 µg/ml anti-IL-4 (Peprotech). T cells were cultured for 14 days in RPMI medium + L-Glutamine + 25 mM HEPES (Gibco) supplemented with 10 % FCS, 1 % penicillin-streptomycin (Thermo Fisher Scientific) and 0.02 mM sodium pyruvate (Thermo Fisher Scientific) at 37 °C and 5 % CO_2.

2.4.2 Bacterial strains and culture conditions

Staphylococcus aureus (USA 300 LAC) was used for infection experiments in this study. Bacteria were aerobically grown in tryptic soy broth medium at 37 °C and orbital shaking. Infection was performed with logarithmically growing bacteria (optical density = 0.5).

2.4.3 3D human skin equivalents on fibroblast matrix

The start was marked by directly seeding $5x10^5$ fibroblasts in 500 µl CnT-Prime Fibroblast Proliferation Medium supplemented with 200 µg/ml 2-phospho-L-ascorbic acid trisodium salt directly onto 12-Well inserts (0.4 µm, Greiner bio-one) at day 1, 3 and 5. CnT-Prime Fibroblast Proliferation medium supplemented with 200 µg/ml 2-phospho-L-ascorbic acid trisodium salt was added in the lower well, and the dermal compartment was cultured at 37 °C for at least 4 weeks.

Subsequently, medium in the upper well was removed and 2.5x10^5 keratinocytes in 500 µl CnT-Prime Epithelial Proliferation medium supplemented with 200 µg/ml 2-phospho-L-ascorbic acid trisodium salt were seeded on top of the dermis. Concurrently, the culture medium in the lower well was changed to CnT-Prime Epithelial Proliferation medium supplemented with 200 µg/ml 2-phospho-L-ascorbic acid trisodium salt and the 3D human skin equivalents were cultured at 37 °C for further 5-7 days. To induce stratum corneum formation, skin equivalents were then airlifted for 7-10 days only by adding CnT-Prime Airlift medium (CELLnTEC) supplemented with 200 µg/ml 2-phospho-L-ascorbic acid trisodium salt to the lower well. During the total generation procedure, media were changed twice a week.

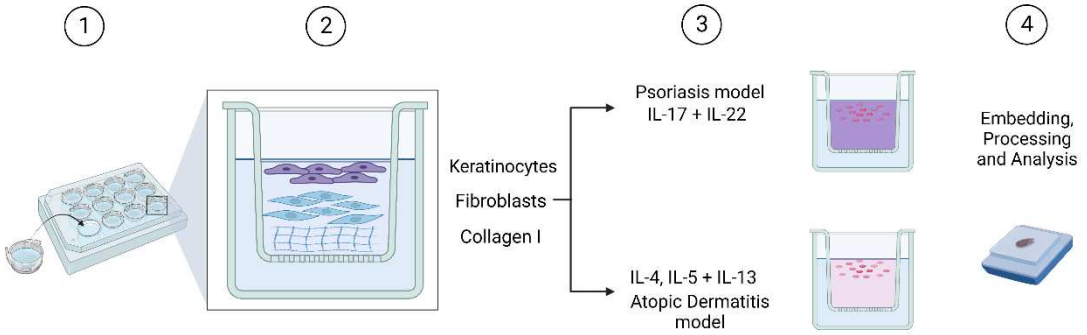

Figure 2: Schematic of production of 3D cytokine model. Figure created with Biorender.com.

2.4.4 3D human skin equivalents on collagen matrix

Firstly, an acellular collagen-layer was produced by adding 250 µl of 1.35 mg/ml neutralized (pH 7.2–7.4) collagen I (Corning) and CnT-Prime Fibroblast Proliferation medium to 12-well inserts (0.4 µm, translucent, Greiner bio-one). After 2 h of incubation at 37 °C, 2x10^5 fibroblasts were suspended in 500µl CnT-Prime Fibroblast Proliferation medium with 1.35 mg/ml neutralized (pH 7.2–7.4) collagen I (Corning) and were seeded on top of the collagen matrix. After a further 4-5h of incubation at 37 °C, CnT-Prime Fibroblast Proliferation medium was added in the upper and lower well, and the dermal compartment was cultured at 37 °C for 7 days. Subsequently, the medium in the upper well was completely removed and 2.5x10^5 keratinocytes in 10 µl CnT-Prime Epithelial Proliferation medium were pipetted directly onto the dermis. After 5h of incubation, the upper

well was filled up with CnT-Prime Epithelial Proliferation medium. Concurrently, the culture medium in the lower well was changed to CnT-Prime Epithelial Proliferation medium and the 3D human skin equivalents were cultured at 37 °C for further 5-7 days. From then on, skin equivalents were airlifted by only adding CnT-Prime Airlift medium in the lower well. After 7-10 days in the airlift phase, 3D human skin equivalents were used for experiments.

2.4.5 Equivalents of inflammatory skin

To mimic inflammatory phenotypes the skin equivalents were treated with cytokines or T cells to induce disease specific characteristics, such as thickening of the epidermis.

To induce a PS phenotype, 3D human skin equivalents were treated for 3-5 days with 30 ng/ml IL-17A and 30 ng/ml IL-22 after 5-7 days during the airlift phase.

Immunocompetent psoriasis-like 3D skin models were established by integrating type 1-polarized T cells into skin models. Therefore, $1x10^6$ TH1 cells in 500 µl CnT-Prime Epithelial Proliferation medium supplemented with 10 ng/ml IL-2 were seeded onto skin constructs one day before the start of the airlift phase. The lower well was filled up with CnT-Prime Epithelial Proliferation medium. Airlifting was than performed for by only adding CnT-Prime Airlift medium supplemented with 10 ng/ml IL-2 in the lower well. After 10 days in the airlift phase, 3D human skin equivalents were analyzed for experiments.

To induce an AD phenotype, 3D human skin equivalents were treated for 3-5 days with 20 ng/ml IL-4, 10 ng/ml IL-5, and 10 ng/ml IL-13 during the airlift phase.

2.4.6 Infection of 3D skin models with Staphylococcus aureus

3D human skin equivalents were infected with $1x10^8$ bacteria by topically applying bacteria for 3 h onto the epidermis by using 8 mm filter paper discs (Smart Practice). To determine *S. aureus* colonization, adhesion and invasion assays were performed. Therefore, the skin models were washed with PBS and then homogenized with a scalpel. Serial dilutions of the washing solution (determines loosely attached bacteria) and the homogenate (determines infiltrated bacteria)

were plated onto blood agar plates. After overnight incubation at 37 °C colony forming units were counted.

2.5 CODEX

2.5.1 Establishment of the CODEX technology

CODEX (CO-Detection by indexing, Figure 3) is a newly established highly multiplexed microscopy technology that uses DNA-conjugated antibodies with fluorescent nucleotides to reveal the spatial character of tissue. This helps in understanding complex interactions between cells, as it enables the visible detection of cell types as well as their activity using markers to detect proliferation and communication between cells and their surroundings. Currently up to 60 markers can be used in a single tissue sample (Black *et al.*, 2021). As our interest lies in visualizing the interplay of antimicrobial and inflammatory factors in *in vitro* skin models, a great number of simultaneous markers is needed. Some markers are needed to identify the cell types, but most markers will be targeted towards finding common and differing expression patterns between AD and PS samples. Thus, CODEX is the next step enabling the imaging of changes in the epidermal component, expression of antimicrobial peptides and pro-inflammatory cytokines.

2.5.2 Conjugation of selected antibodies to oligonucleotides

All procedures described in the following correspond to the protocol published by (Black *et al.*, 2021), only minor adaptations were made.

For successful conjugation of antibodies previous confirmation of all antibodies being purified and BSA free is needed. Measuring the specific concentration of the antibodies is essential to assure a 2:1 ratio of oligonucleotide to antibody. The workflow is mentioned in the following step by step protocol.

First the antibody was prepared for conjugation. The concentration of the purified antibody is measured using a UV-visible spectrophotometer (NanoDrop 2000) first blanking the spectrophotometer with 1x PBS and afterwards using 1 µl of antibody for calculation. Absorbance is measured at 280 nm.

This concentration is needed to calculate the volume of antibody needed for a conjugation with a ratio of 2:1. For example, if the oligonucleotide vial contains 208,2 µg of oligo, 104,1 µg of antibody are needed. Considering the concentration of the antibody of 1,63 µg/µl this means 63,87 µl of purified antibody are necessary to achieve the correct ratio.

$$\frac{Amount\ of\ antibody\ needed}{Antibody\ concentration} = \frac{104{,}1\ \mu g}{1{,}63\ \frac{\mu g}{\mu l}} = 63{,}87\ \mu l$$

Once the concentration is determined, the conjugation procedure was started by adding 500 µl of PBS-Tween solution onto a 50 kDA- molecular weight cutoff centrifugal filter column. The PBS-Tween solution was prepared beforehand by solving a 0.1 % (vol/vol) Tween solution in 1× DPBS. Blocking with PBS-Tween assured no unspecific antibody binding would happen to the column. Following centrifugation at 12,000 g for two minutes, the retained volume in the filter as well as the flow-through was discarded. Afterwards the entire measured volume of antibody was added to the filter and centrifugated at 12,000 g for eight minutes. The flow-through was discarded again, without emptying the contents of the filter column that now contains the concentrated antibody. During the centrifugation 2.5 mM TCEP solution was prepared for antibody reduction by adding 5 µl of 500 mM TCEP and 5 µl of 500 mM EDTA (pH 8.0) to 990 µl of 1× DPBS. 360 µl of the prepared 2.5 mM TCEP solution was added to the antibody in the filter column, the tube was briefly vortexed and centrifuged for 10 seconds before incubating for a maximum of 30 minutes at room temperature. This time needs be critically watched as a longer time in the TCEP may reduce disulfide bonds in the antibody thereby causing destabilization.

For some antibodies the protocol varied from this step on, after the results of testing them in FACS revealed negative conjugation. *S. aureus* antibody was therefore only reduced for 15 minutes instead of 30 minutes and instead of Buffer C High-salt PBS is used in the next step. This caused a successful conjugation of this antibody, that seems to be less stable in general.

In the meantime, a box for liquid nitrogen was put into the freezer at -80 °C which is needed for the oligonucleotide solution later. The oligonucleotides themselves

were transferred from the freezer to the fridge for thawing until needed in the described procedure.

To end incubation the column was spun down at 12,000g for eight minutes again. The flow-through was discarded before 400 µl of buffer C was added to stop the reduction. Buffer C was prepared by adding 1 ml of 1 M Tris (pH 7.0), 1 ml of 1 M Tris (pH 7.5), 30 ml of 5 M NaCl solution and 2 ml of 500 mM EDTA (pH 8.0) to 966 ml of ddH_2O. Add 200 mg of NaN_3 for a 0.02 % (wt/vol) concentration in this solution. Again, the column was centrifugated at 12,000 g for eight minutes, the flow-through discarded and another 400 µl of Buffer C added to ensure no left over TCEP is still in the column. During another centrifugation at 12,000 g for eight minutes, the oligonucleotide solution was prepared.

For preparation of the DNA oligonucleotide solution, 400 µl of PBS were added to an Eppendorf cup. Beforehand liquid nitrogen was collected and then poured into the box that was stored at -80 °C to cover the bottom. Using 150 µl of the PBS in the Eppendorf cups, the oligonucleotides were dissolved in the inert gas environment present on the rim of the box and then immediately transferred to the remaining PBS in the Eppendorf cup. After the flow-through was discarded, the entire 400 µl of oligonucleotide solution were added to the top of the filter and carefully mixed by pipetting up and down without puncturing the filter. The mixture was then incubated for two hours at room temperature.

After the two hours the column was centrifugated at 12,000 g for eight minutes, the flow-through discarded. Now 450 µl of high-salt PBS was added to the column, this marks the first washing step. Following centrifugation at 12,000 g for eight minutes and discard of the flow-through, this was repeated two more times. The high-salt solution was prepared as follows: 45 ml of 5 M NaCl solution and 25 ml of 10× DPBS to 180 ml of ddH_2O. 50 mg of NaN_3 for a 0.02 % (wt/vol) concentration in this solution. The three washing steps remove any unbound maleimide modified oligonucleotide.

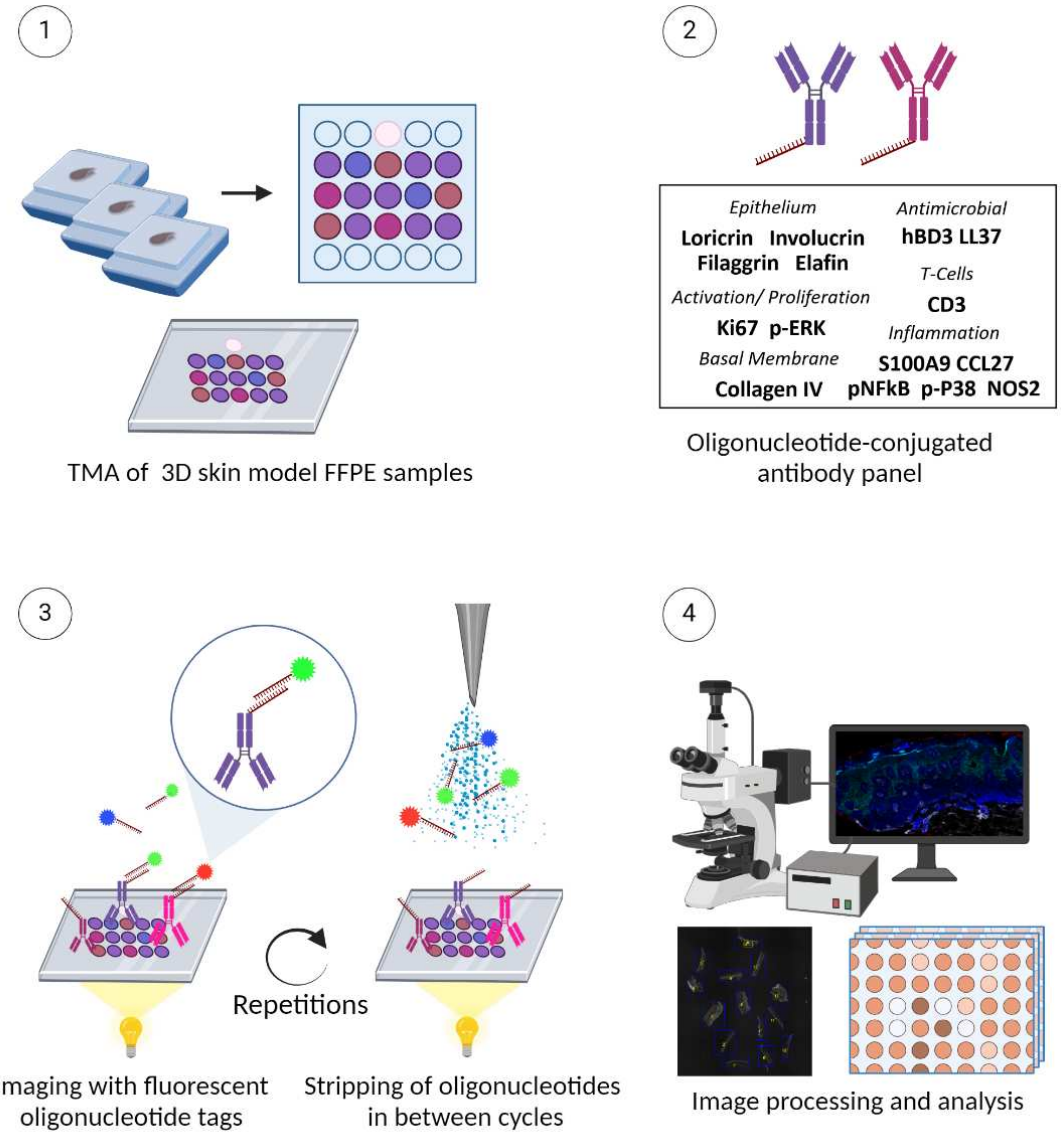

Figure 3: Schematic of CODEX procedure. Figure created with Biorender.com. Adaptation from publication in (Scheurer et al.*, 2024).*

The last step defines the resuspension of the conjugated antibody. This was done by adding antibody stabilizer solution to the column according to the initial volume of purified antibody. This means, for the previous example 208,2 µl of antibody being added. The antibody stabilizer consisted of 1 ml of 5 M NaCl solution and 100 µl of 500 mM EDTA (pH 8.0) in 9 ml of stock antibody stabilizer solution. This was briefly vortexed and then stored at 4 °C. For resuspension the stabilizer was pipetted up and down each side of the filter tip four times, to get all of the bound antibody. The mixture was then inverted into a fresh collection tube, which was

then centrifugated at 3,000g for just two minutes. The tube now contained the conjugated antibody and was labelled to be then stored at 4 °C until needed for testing.

2.5.3 Validation of conjugated antibodies using FACS analysis

For validation of the conjugation of DNA oligonucleotides to purified antibodies, analysis using flow cytometry is very helpful. The analysis, however, can only indicate positive conjugation of oligonucleotide to antibody rather than giving a quantitative measure. For all antibodies in the panel a FACS analysis was conducted, two out of all conjugations had to be repeated as they proved negative in the FACS. Another two were re-conjugated despite showing positive conjugation in the FACS due to bad staining results.

For the analysis using FACS a hybridization buffer and a hybridization solution were prepared before each experiment. The hybridization buffer consisted of 100 ml of DMSO and 400 ml of H2 buffer.

H2 buffer: 30 ml of 5 M NaCl solution, 10 ml of 1 M Tris (pH 7.5), 0.943 ml of Triton X-100, 2.03 g of $MgCl_2 \bullet 6H_2O$ and 0.02 % (wt/vol) NaN_3 to 960 ml of ddH_2O.

CODEX staining buffer 2 (S2): 250 ml of S1, 30.5 ml of 1 M Na_2HPO_4, 19.5 ml of 1 M NaH_2PO_4 and 25 ml of 5 M NaCl solution to 175 ml of ddH_2O. pH adjusted to 6.8–7.0 with sodium hydroxide. Stored at 4 °C for ≤ 1 year.

The FACS hybridization solution was prepared by adding 7 µl of B3 and 1 µl of the fluorescent oligonucleotide of interest to 92 µl of hybridization buffer for each antibody to be tested.

For the procedure itself, two tubes were labelled for each antibody, a positive sample and a negative control. 200 µl of S2 and 1 drop of UltraComp eBeads were added to each FACS tube. The beads would then bind to the oligonucleotide-conjugated antibodies, after they were added to the positive sample tubes (1 µl of conjugated antibody). The positive control tube was supplied with 1 µl of commercially available fluorescent FACS antibody. All was

properly vortexed to ensure a mixture of the added antibody and compensation beads, before incubation for 15 minutes.

Afterwards 4 ml of S2 buffer was added to all tubes to wash away any unbound antibody. The tubes were centrifugated at 500g for 5 minutes before inverting the FACS tubes to decant the supernatant. Then 4 ml of hybridization buffer was added to the tubes, again followed by centrifugation at 500g for 5 minutes. The supernatant was decanted again, leaving the pellet of beads at the bottom of the tubes. In the next step, 100 µl of the previously prepared hybridization solution was added to all tubes except the positive control and the tubes were incubated for 15 minutes in the dark at 4 °C.

CODEX staining buffer 4 (S4): 50 ml of 5 M NaCl solution to 450 ml of S1. Gently mix. Store at 4 °C for ≤1 year.

Afterwards the unbound fluorescent oligonucleotides were washed away by adding 4 ml of H2 buffer. This step was skipped for the positive control. The remaining tubes were centrifugated at 500g for 5 minutes, the supernatant was decanted afterwards. Then 4 ml of S4 were added to all tubes including the positive control, again centrifugating at 500g for 5 minutes. By inverting the tubes the supernatant was decanted and the remaining pellets holding beads with bound antibodies and tagged oligo were left at the bottom of the tubes. In the last step 250 µl of S4 was added and the tubes were vortexed for resuspension. For FACS analysis the tubes ran in the BD LSR II Cell Analyzer and events were ideally recorded until a total number of 30.000 events.

For gating of the fcs files the data was exported to cellengine.com. To determine the beads one of the negative controls was taken with forward scatter A (FSC A) on x axis, equaling the size measured in the flow cytometry, and sideward scatter A (SSC A) on y axis, equaling the granularity. The beads should now be visible as a close population, which was defined in the program. With the beads given as a known population, now the x axis is set to APC (Allophycocyanin), a fluorescent compound with an excitation peak at 651 nm and an emission peak at 660 nm. APC A is used to detect the fluorophores we want to see for the conjugated antibodies. All that is now seen for x values higher than where the

beads were defined can be interpreted as a positive conjugation. The steps for gating are also described in Table 4.

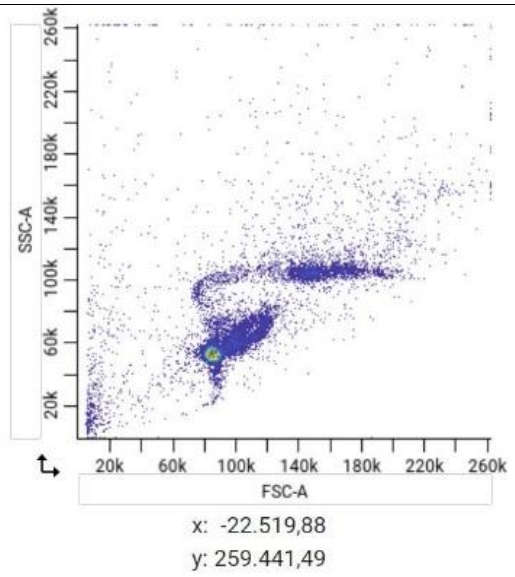	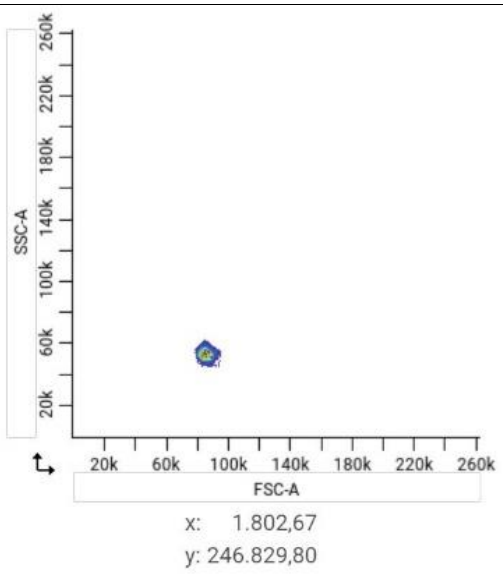
Raw data FSC A against SSC A	Gated beads, background subtracted
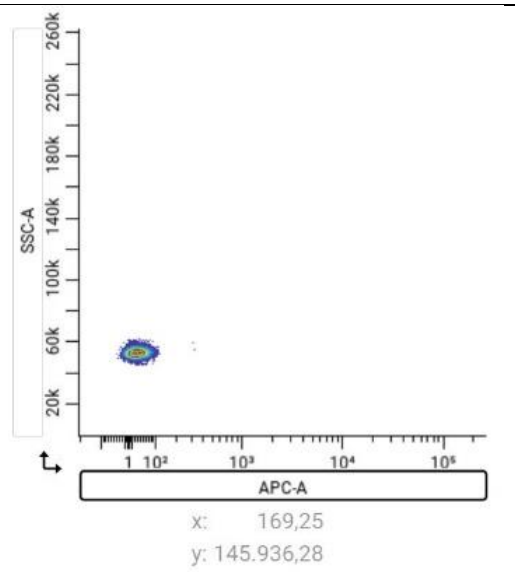	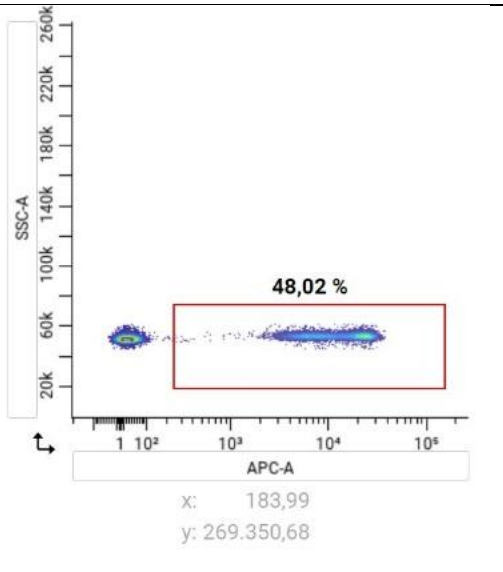
APC A against SSC A in negative control	APC A against SSC A in positively conjugated sample

Table 4: Gating of data generated in FACS. forward scatter A (FSC A), sideward scatter A (SSC A), Allophycocyanin A (APC A)

2.5.4 Validation of conjugated antibodies using hand-staining with fluorescent labeling

For further validation of the specific binding properties of the conjugated antibodies, they were tested on FFPE tissues and imaged using a fluorescent microscope. Two antibodies were tested on the same sample simultaneously and 2 tissue samples placed on one slide to minimize the amount of reagent needed. For the samples a 4 µm thick tissue section was taken from the FFPE blocks and sectioned to a TOMO glass slide. The slide was then baked at 70 °C for 1 hour, before being placed in xylene for 30 minutes in total, exchanging the xylene every 10 minutes. While the slides were baking a target retrieval solution was prepared for the antigen retrieval in the FFPE tissue. This was done by combining DAKO target retrieval solution with ddH_2O to a ratio of 1:10. The target retrieval solution was heated to 75 °C in a PT module. After the xylene step, the slide was put into 100 % ethanol, 100 % ethanol, 95 % ethanol, 95 % ethanol, 80 % ethanol, 70 % ethanol, ddH_2O and ddH_2O (vol/vol) for 3 minutes each.
This was followed by antigen retrieval. The slides were put into the preheated antigen retrieval solution, the PT module was set to 97 °C for 10 minutes, followed by 30 minutes at 60 °C. After those 30 minutes the slide was left to cool at room temperature in the retrieval solution for another 30 minutes.
The next step ensures a decrease of background signals when imaging in the last step. Bleaching is done in two cycles, each for 45 minutes between two LED-UV plates. The slides were placed in a petri dish containing a bleaching solution. The solution was prepared by combining 100 ml of 1x PBS with 18 ml of H_2O_2 and 3,2 ml of 1M NaOH and was exchanged after the first 45 minutes. The bleaching process was finished off by washing the slides in 1x PBS for 3 minutes four times.

After bleaching the slides were dried off by tapping with kimwipe tissue and the tissue was circled using a Bondic polyacrylamide gel pen to create a barrier for the solutions to be put onto it. First, the circled samples were put into 1x TBS IHC wash buffer with Tween 20 for 10 minutes on a shaker. In the meantime, the blocking solution was prepared by combining 156 µl of S2, 10 µl of B1, 10 µl of B2, 10 µl of B3 and 14 µl of BC4 for each tissue tested.

After the 10 minutes the slides were dried off again and placed in a humidity chamber, where 100 µl of blocking solution was added to each of the circled tissues making sure no area of the tissue remained dry. The slides were incubated at room temperature in the humidity chamber with the blocking solution for 1 hour.

During incubation the conjugated antibody solution was prepared by adding the antibody to be tested to blocking solution in the desired dilution to make a final volume of 100 µl. This means when testing two antibodies on one tissue, for a dilution of 1:100, 1 µl of antibody A, 1 µl of antibody B and 98 µl of blocking solution are combined. After the incubation, the excess blocking solution was tapped off the slides and 100 µl of the antibody mix was added to the slides. Incubation was performed overnight at 4 °C inside the humidity chamber and on a shaker at 50 rpm.

On the next day the specimen was washed in S2 twice for 2 minutes, after letting the S2 solution come to room temperature. Beforehand a PFA fixation solution was prepared by diluting 16 % (wt/vol) paraformaldehyde (PFA) at a 1:10 ratio with S4 (vol/vol). 100 µl of the PFA fixation solution were added to the samples after washing in S2 and the slides were incubated for 10 minutes in the humidity chamber at room temperature. This first fixation step is needed to fix the antibodies onto the tissue before washing in methanol in the next step: After 10 minutes the slides were washed in 1x PBS for 1 minute and then placed in ice cold methanol for 5 minutes. Methanol is used as a second fixation step to focus fluorescent markers in the cell membrane by removing lipids and therefore improves the imaging of antibodies located at the cell membrane. Afterwards the slides were washed in 1x PBS for 1 minute again.

For the following stripping steps, the hybridization and stripping puffers were prepared by combining 30 ml of DMSO with 120 ml of H2 buffer for the hybridization and adding 12,5 ml of H2 buffer to 37.5 ml of DMSO. Another solution that was prepared is the CODEX detection solution which consists of 7 µl B3, 1 µl of each matching bottom oligonucleotide for the respective antibodies on the tissue and 91 µl of H2 buffer.

The slides were placed in S4 and can be stored at 4 °C in the solution if needed for later use. Otherwise, the procedure continues with hybridization of the antibodies by incubation in the hybridization buffer for 1 minute. This was followed by placing the tissue in the stripping buffer for 10 minutes which removes the BC4 oligonucleotides binding to the antibodies and thereby aims for a more focused picture in the end. Afterwards the slides were placed in the hybridization solution for one minute again. The slides were then tapped off and 100 µl of the prepared hybridization solution were added onto the tissue. The slides were then placed back into the humidity chamber and incubated for ten minutes in the dark. Afterwards the slides were washed in hybridization buffer for 30 seconds, followed by washing in in S4 for 1 minute twice. The last step was careful removal of the Bondic polyacrylamide gel with a razor blade and drying the slides with a Kimwipe. Mounting was done by adding one drop of Cytoseal and gently covering the tissue with a cover slip, applying light pressure and avoiding air bubbles. The slides were left to dry in the dark for 30 minutes and then imaged.

The slides were imaged using the BZ-X710 inverted fluorescence microscope (Keyence) for both channels, always checking for background staining and auto-fluorescence to ensure correct interpretation of positive signals. The exposure time should be around ½ second, anything above 2 seconds can be defined as negative.

2.5.5 Multicycle imaging with CODEX

Tissue to be imaged for multicycle imaging in CODEX is prepared on coverslips of 1,5 mm thickness treated with Vecta-Bond. Other than that, the protocol does not vary from hand-staining for validation of antibodies described above. The protocol finishes with placing the slides into S4 after the third fixation step, treatment with hybridization solution only mimics the CODEX procedure is therefore unnecessary.

Results are taken from multiple runs with different samples, but statistical analysis was done on one multicycle ran on the TMA to ensure comparability of the values

as all tissues were located on a single coverslip and prepared under the exact same conditions and at the same time.

2.5.6 Panel design

For image processing the background signal is subtracted, therefore the first cycle should be a blank one to define the 'blank' signal. Fluorescent signal is generally strongest for the ALEXA647 channel and second strongest for ATTO550, the blue channel only gives good signal for antigens widely expressed along the tissue and was therefore left blank for the final panel run. Panel design is chosen accordingly, placing antibodies with an expectedly high expression in the blue channel, while rare antibodies should be put in either green or red. Antibody staining is relatively stable over the course of multicycles (Black *et al.*, 2021) so the final multicycle contained 50 markers spread over 28 cycles and 2 channels in total. The panels were tested in multiple runs, adjusting exposure times and concentrations if needed. The final panel designs for the tissue arrays with 3D skin models and patient samples can be found in Table 5 and in Table 6.

Cycle	Channel	Exposure Time	ATTO550	Oligo	Clone	Antibody Dilution	Exposure Time	Alexa647	Oligo	Clone	Antibody Dilution	Exposure Time
1	Hoechst	4	Blank				500	Blank				500
2	Hoechst	4	Collagen IV	33	polyclonal	1:100	500	Ki67	6	B56	1:100	500
3	Hoechst	4	Loricrin	71	Poly19051	1:100	500	LL37	41	poly	1:100	500
4	Hoechst	4	Filaggrin	26	AE21	1:400	20	HBD3	30	polyclonal	1:50	500
5	Hoechst	4	S. aureus	11	polyclonal	1:100	500	iNOS	74	polyclonal	1:50	500
6	Hoechst	4	Elafin	80	H-2	1:200	500	CD3	77	polyclonal	1:100	500
7	Hoechst	4	S100A9	58	MAC387	1:100	100	pNFkB	42	polyclonal	1:100	500
8	Hoechst	4	Involucrin	63	SY5	1:100	500	P-p38	14	polyclonal	1:100	500
9	Hoechst	4	CCL27	21	124308	1:50	500	Empty				1
10	Hoechst	4	pERK	36	polyclonal	1:25	500	DRAQ5				500
11	Hoechst	4	Blank				500	Blank				500

Table 5: Final Panel Design 3D skin equivalents

Cycle	Channel	Exposure Time	ATTO550	Oligo	Clone	Antibody Dilution	Exposure Time	Alexa647	Oligo	Clone	Antibody Dilution	Exposure Time
1	Hoechst	4	Blank				500	Blank				500
2	Hoechst	4	CD138	76	B-A38	1:100	150	Anti-*S. aureus*	11	polyclonal	1:50	500
3	Hoechst	4	CD3	77	MRQ-39	1:100	500	Neutrophil Elastase	75	ELA2	1:400	200
4	Hoechst	4	CD163	45	EDHu-1	1:50	500	OGG1	32	polyclonal	1:25	500
5	Hoechst	4	citH3	74	polyclonal	1:100	500	P-p38	14	polyclonal	1:100	700
6	Hoechst	4	Collagen IV	33	polyclonal	1:100	500	P53	25	DO7	1:25	500
7	Hoechst	4	Cytokeratin	67	AE1/AE3	1:100	500	pERK	36	polyclonal	1:25	500
8	Hoechst	4	Elafin	80	H-2	1:200	500	pH2AX	5	EP854(2)Y	1:50	500
9	Hoechst	4	Filaggrin	26	AE21	1:400	20	pNFkB	42	polyclonal	1:50	500
10	Hoechst	4	Foxp3	61	236A/E7	1:200	500	pSTAT3	20	BD-4	1:50	500
11	Hoechst	4	Granzyme B	81	EPR20129-217	1:100	250	S100A9	58	MAC387	1:100	100
12	Hoechst	4	HBD-3	30	polyclonal	1:100	500	TCR-b	3	G-11	1:50	500
13	Hoechst	4	Histone H3	57	E191	1:400	100	Vimentin	7	RV202	1:25	300
14	Hoechst	4	HLA-DR	65	EPR3692	1:100	500	NOS2	74	poly	1:25	500
15	Hoechst	4	HMGB1	60	polyclonal	1:100	500	CCL27	21	124308	1:25	500
16	Hoechst	4	Involucrin	63	SY5	1:100	500	LL37	41	polyclonal	1:100	500
17	Hoechst	4	Ki67	6	B56	1:200	500	CD62L	62	B-8	1:50	500
18	Hoechst	4	MPO	51	polyclonal	1:200	300	Beta Catenin	24	14	1:25	500
19	Hoechst	4	Loricrin	71	Poly19051	1:100	500	CD31	68	C31.3 + C31.7 + C31.10	1:200	166
20	Hoechst	4	Mast Cell Tryptase	44	AA1	1:400	50	CD34	38	QBEnd/10	1:50	500
21	Hoechst	4	CD68	70	KP-1	1:200	500	CD38	66	EPR4106	1:200	300
22	Hoechst	4	a-SMA	69	poly	1:200	250	CD45	56	2B11 + PD7/26	1:200	300
23	Hoechst	4	CD11b	28	EPR1344	1:100	250	CD45RA	72	HI100	1:400	500
24	Hoechst	4	CD11c	49	EP1347Y	1:50	300	CD45RO	2	UCH-L1	1:100	500
25	Hoechst	4	CD8	8	C8/144B	1:200	500	CD56	29	MRQ-42	1:200	300
26	Hoechst	4	CD15	15	HI98	1:400	500	CD20	48	rIGEL/773	1:400	300
27	Hoechst	4	CD1a	43	O10 + C1A/711	1:50	500	CD206	55	MM0820-48L31	1:100	300
28	Hoechst	4	Empty				1	DRAQ5			1:100	500
29	Hoechst	4	Blank				500	Blank				500

Table 6: Final panel design patient samples

2.6 Immunohistochemistry

Immunohistochemistry staining was done assisted by the Ventana Benchmark XT using the XT OptiView DAB IHC staining kit, therefore the steps are automated. The process begins by selecting EZ Prep to prepare the slides for the procedure. Once this step is completed, timed steps are initiated for the process of baking, deparaffinization up to staining. The slides are first heated to 60 °C and incubated for 4 minutes, a step referred to as "baking." Following this, the slides are further heated to 75 °C and incubated for another 4 minutes. The EZ Prep volume is then adjusted, and the slides are washed thoroughly. This process of adjusting the EZ Prep volume and washing the slides is repeated twice to ensure optimal preparation. Once cleaned, a coverslip is applied, and the slides are heated again, this time to 76 °C, and incubated for 4 minutes. After this incubation, the slides are washed once more, and the deparaffinization volume is adjusted. A coverslip is applied again before the slide heater is turned off. At this stage, the mixer is turned on, and the slides are washed. Cell Conditioner No. 1 is applied, followed by the dispensing of Cell Conditioner and a coverslip. The slides are then heated to 100 °C and incubated for 4 minutes. This incubation is followed by a series of incubation steps – first for 4 minutes, then 8 minutes. Afterward, Cell Conditioner No. 1 is applied again, followed by the application of

Cell Conditioner and a coverslip. The slides are incubated for 8 minutes, and this incubation is repeated several times to ensure thorough processing. After these cycles, the slide heater is turned off again. Next, the slides are rinsed with reaction buffer, and the volume is fine-tuned to ensure the reaction buffer is balanced. The process continues by applying a coverslip, after which the SSC Wash is selected. The procedures are synchronized, and the slides are warmed to 37 °C. The slides are then rinsed with reaction buffer, and the volume is adjusted as necessary. A drop of OV PEROX IHBTR is applied to each slide, followed by a coverslip, and the slides are incubated for 4 minutes. The slides are rinsed again with reaction buffer, and the buffer volume is fine-tuned. Another coverslip is applied before the slides are brought to the correct temperature for the incubation of the primary antibody. Following this, the slides are rinsed again with reaction buffer and fine-tuned before a coverslip is applied.

Meanwhile, the antibody solution is prepared manually by diluting the antibody according to its expected expression patterns in Zytomed Systems Antibody Diluent. The primary antibody then needs to be hand-applied, and the slides are incubated for 32 minutes. The slides are warmed to 37 °C and rinsed with reaction buffer. 460 µl of VA reaction buffer is applied, followed by a coverslip.

The slides are rinsed again, and 460 µl of VA reaction buffer is applied once more. This process of applying reaction buffer and coverslip, followed by rinsing, is repeated several times. Following this, 1 drop of OV HQ UNIV LINKR is applied, and the slides are incubated for 8 minutes. This step is repeated, with the slides being rinsed and the volume adjusted between applications of reaction buffer and coverslip. After this, OV HRP MULTIMER is applied, and the slides are incubated for 8 minutes. The slides are rinsed, and 900 µl of reaction buffer is added. After another round of rinsing, 460 µl of VA reaction buffer is applied, followed by the application of a coverslip. The final stages of the procedure begin with the application of OV H_2O_2 and OV DAB, along with the application of LCS. The slides are incubated for 8 minutes before being rinsed with reaction buffer. The volume is fine-tuned, and OV COPPER is applied, followed by a coverslip and 4 minutes of incubation. The slides are rinsed again, and the reaction buffer volume is fine-tuned. A final coverslip is applied before the slide heater is turned off. Finally, the

slides are manually washed in water and afterwards undergo staining before they can be examined under the microscope.

2.7 Cell culture

We tested two different lymphoma cell lines, HUT78 and HH cells. The cells were kept frozen in a liquid nitrogen tank until needed. Gentle thawing was assured using a water bath, but cells were not thawed fully to avoid cell damage by DMSO. Bottles for incubation of the cell culture were prepared with 25ml of the respective cell culture medium (FCS 10 % for HUT cells and FCS 20 % for HH cells). Thawed cells were washed with 10ml PBS and centrifugated at 1200 reps for 5 minutes at 20 °C. The supernatant was removed using vacuum suction and the remaining cells at the bottom were resuspended in 5 ml of FCS medium. The entire remaining volume containing cells and medium was added to the previously prepared bottles and positive transfer was validated using microscopy. The bottles were then put into the incubator for 3 – 5 days.

2.7.1 Cutaneous T-cell Lymphoma 3D skin model

In the first test we used both cell lines in varying cell concentrations to determine the optimal experimental setup for integration of the tumor cells. The experiments were either conducted as repetitive sowing of cells onto the growing skin equivalents or added to the fully developed models once.

Briefly, 3D equivalents from primary human fibroblasts on a 12-well collagen matrix were left to develop a dermal compartment for 7 days. Afterwards, primary human keratinocytes were added on top of the compartment. 24h later the first sowing of $5x10^4$ HH or HUT78 cells was carried out and 10 ng/ml of IL-2 cytokines were added into the medium at the bottom of the well. After another 3 and 6 days the sowing was repeated to achieve a total of $15x10^4$ HH or HUT78 cells. 24h after the final cell sowing the skin equivalents underwent airlift phase to support keratinization. During this phase the addition of IL-2 was continued into the medium. After 6 days the fully developed models were prepared for further

analyzation by paraffinization. Samples were then cut and stained for CD3 following protocol for immunohistochemistry as mentioned under 2.6.

We performed different variations of the experiment, testing cutaneous T-cell lymphoma models with repeated sowing of $5x10^4$ and 2 $x10^6$ HH/Hut 78 cells as well as single sowing of the HH/Hut 78 after the stratum corneum had formed. Furthermore, we followed another approach using a fibroblast matrix without collagen and adding Il-17 and Il-22 according to the respective protocols mentioned for preparation of inflammatory skin models.

2.8 Statistics and computation

Statistical analysis was done based on the data generated by the Akoya phenocycler after processing using the CODEX processor, creating hyperstacked images of all fluorescence channels following previous background subtraction. Processed images were analyzed using ImageJ/FIJI. Overlays and single-marker pictures shown in the figures were created using custom-made scripts for combinations of selected channels from focused CODEX hyperstacks. Quantification of marker intensities was performed by manual selection of epidermal regions using freehand selection and the measure tool for mean marker expression provided in ImageJ/FIJI. For further quantification of marker expression between the samples, segmentation analysis was performed using QuPath (Bankhead *et al.*, 2017). The brush tool was used for annotation of the epidermis, followed by detection of cells positive for nuclear staining with DRAQ5 (Cell Signaling Technology, 4084L). Single cell segmentation was managed after positive nuclei detection and validated visually. Subsequently measurements for mean nuclear expressions of respective markers were sorted in Excel (Version 2306). Significant differences between the means of the different treatments were evaluated using GraphPad Prism 9.0 (GraphPad Software, Inc.). Either unpaired, two-tailed Student’s t test or one-way analysis of variance followed by Dunnett’s multiple comparisons test was used for statistical analysis and indicated in the respective figure legends. Differences were considered statistically significant with a p value of < 0.05. Data were visualized using GraphPad 9.0 (GraphPad Software Inc.) or MS Excel (Microsoft Corporation).

3 Results

Partly, the results were previously published and are therefore cited in the following. The published results can be found under (Scheurer *et al.*, 2024) and (Focken *et al.*, 2023). See also 8.

To validate the panel design of antibodies for suitability and correct expression, antibodies were first tested on different FFPE tissues to ensure sufficient dilutions of antibodies. In example, Figure 5 shows expression of NOS2, OGG1 and pNFkB on lung and skin samples. It is evident that the expression of pNFkB is strictly cytoplasmic and shows high specificity. Therefore, dilution and exposure time were noted for further experiments to be kept. For expression of NOS2 antibodies were tested directly on skin tissue and showed strong expression rates, leading to a reduced dilution in further experiments as to not overshadow other markers. OGG1 expression seemed to be very unspecific on the tested lung tissue and led to a second try on skin tissue with a lower dilution of antibody. The second results showed more specific binding with very low to no background staining and can therefore be voted as positive staining results.

After conjugation all antibodies were checked for success of the experimental step by FACS analysis as described under 2.5.3. Gating showed positive conjugation of most antibodies, which can be seen by comparison to negative control and statistical analysis of gating by means. Some conjugations proved harder and had to be re-conjugated due to unspecific or insufficient staining or negative FACS analysis. Examples of FACS gating for conjugated antibodies can be seen below in Figure xx, depicting different qualities of conjugations. Results for S100A9 were positive with very low scattering, while the first conjugation of *S. aureus* antibody proved negative and showed some further difficulties in latter tries, which are mentioned under 2.5.2. The results for *S. aureus* for the final conjugation were labeled as positive but with lower quality because of a wider scatter.

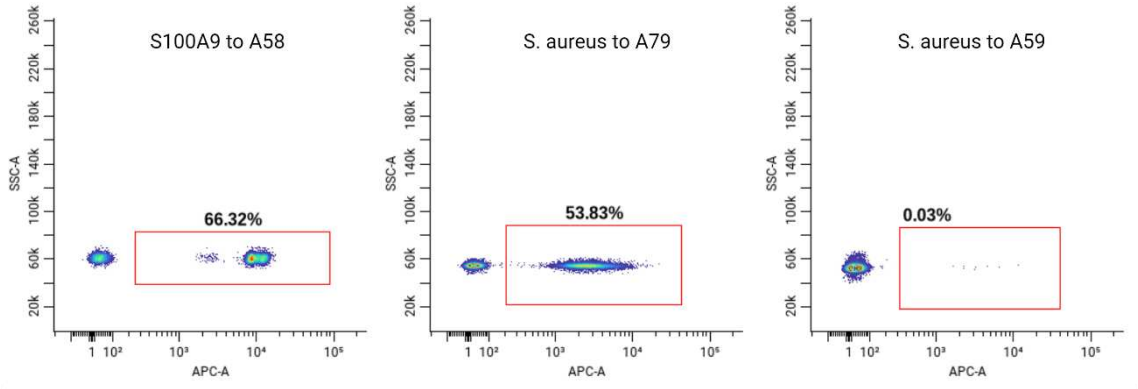

Figure 4: FACS analysis of conjugated antibodies.

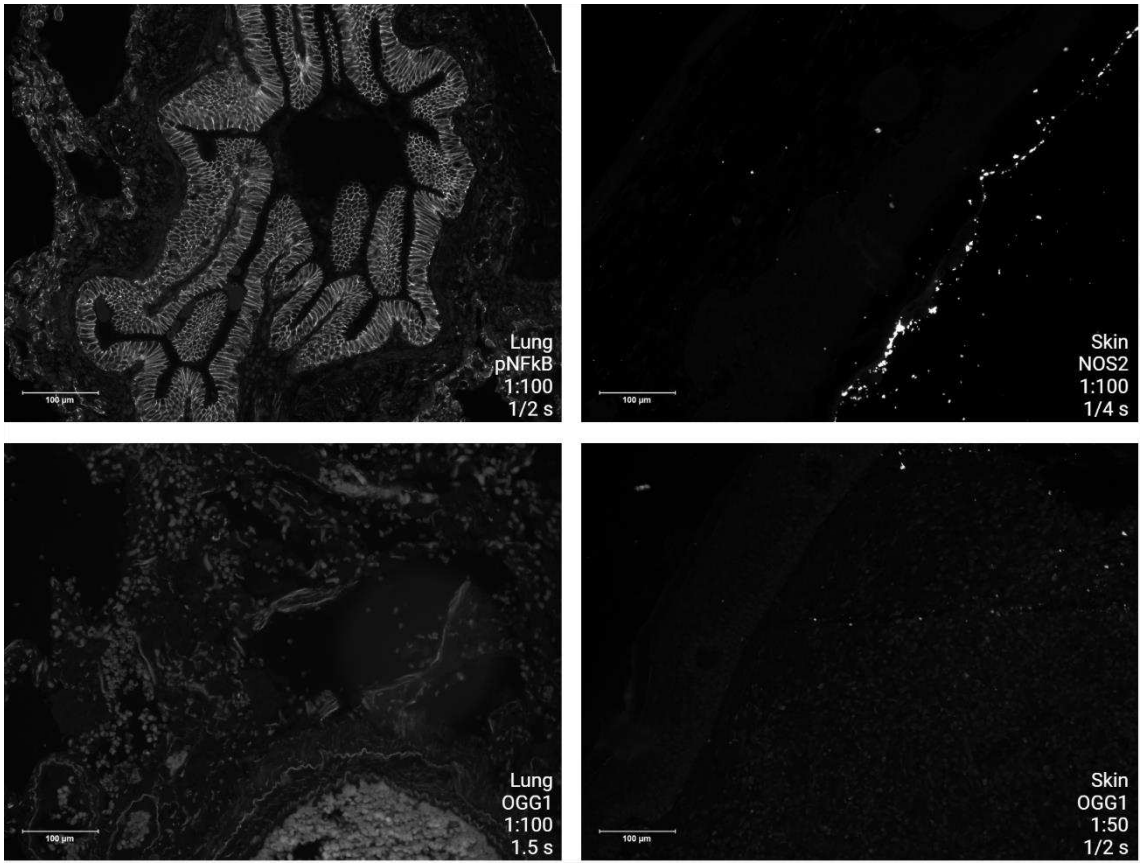

Figure 5: Hand staining of antibodies pNFkB, NOS2 and OGG1 on lung and skin. Dilutions and exposure times according to labels.

3.1 Skin equivalents

As skin equivalents have different properties in terms of tissue complexity and cell count, the panel design was smaller than for patient samples and focused on some key characteristics to be evaluated in the skin models.

3.1.1 Multiplexed imaging of phenotypic hallmark expression in 3D skin models

For CODEX analysis of phenotypic hallmarks, a tissue array with five samples of untreated skin models, five samples of cytokine models for the AD phenotype and five skin models for the psoriasis phenotype was used. The validated DNA-conjugated antibodies were used to detect epithelial, activation/proliferation and inflammation markers. Figure 6 represents an overlay of exemplary 3D human skin models, showing the epithelial markers Filaggrin, Loricrin and Elafin, Ki-67, NOS2 and the nuclear stain DRAQ5. On the left we see the untreated skin equivalent in a six-well collagen matrix, the middle shows the HSE treated with TH-17 cytokines for 3 days in a six-well collagen matrix and on the right is the HSE treated with TH-2 cytokines for 3 days in a six-well collagen matrix. The images are representative of at least three independent experiments. In Figure 7 – Figure 30 individual marker expression and quantitative analyses between the samples are depicted.

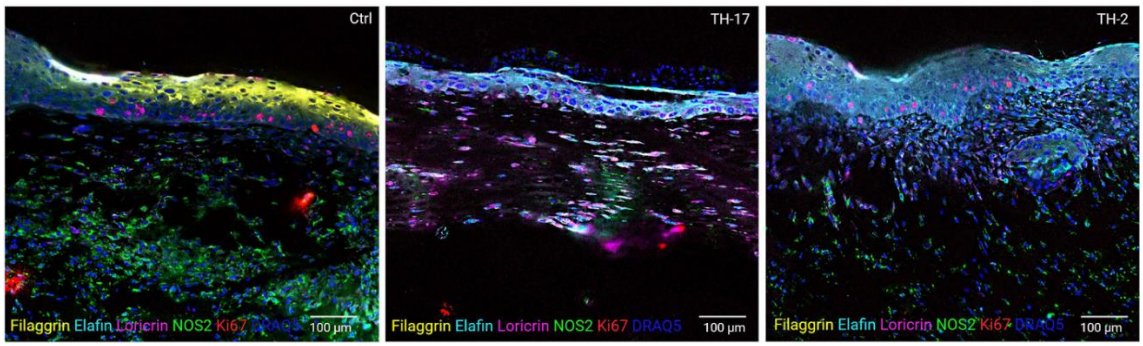

Figure 6: Overlay of representative 3D human skin models, showing the epithelial markers Filaggrin, Loricrin and Elafin, Ki-67, NOS2 and the nuclear stain DRAQ5. Published in (Scheurer et al.*, 2024).*

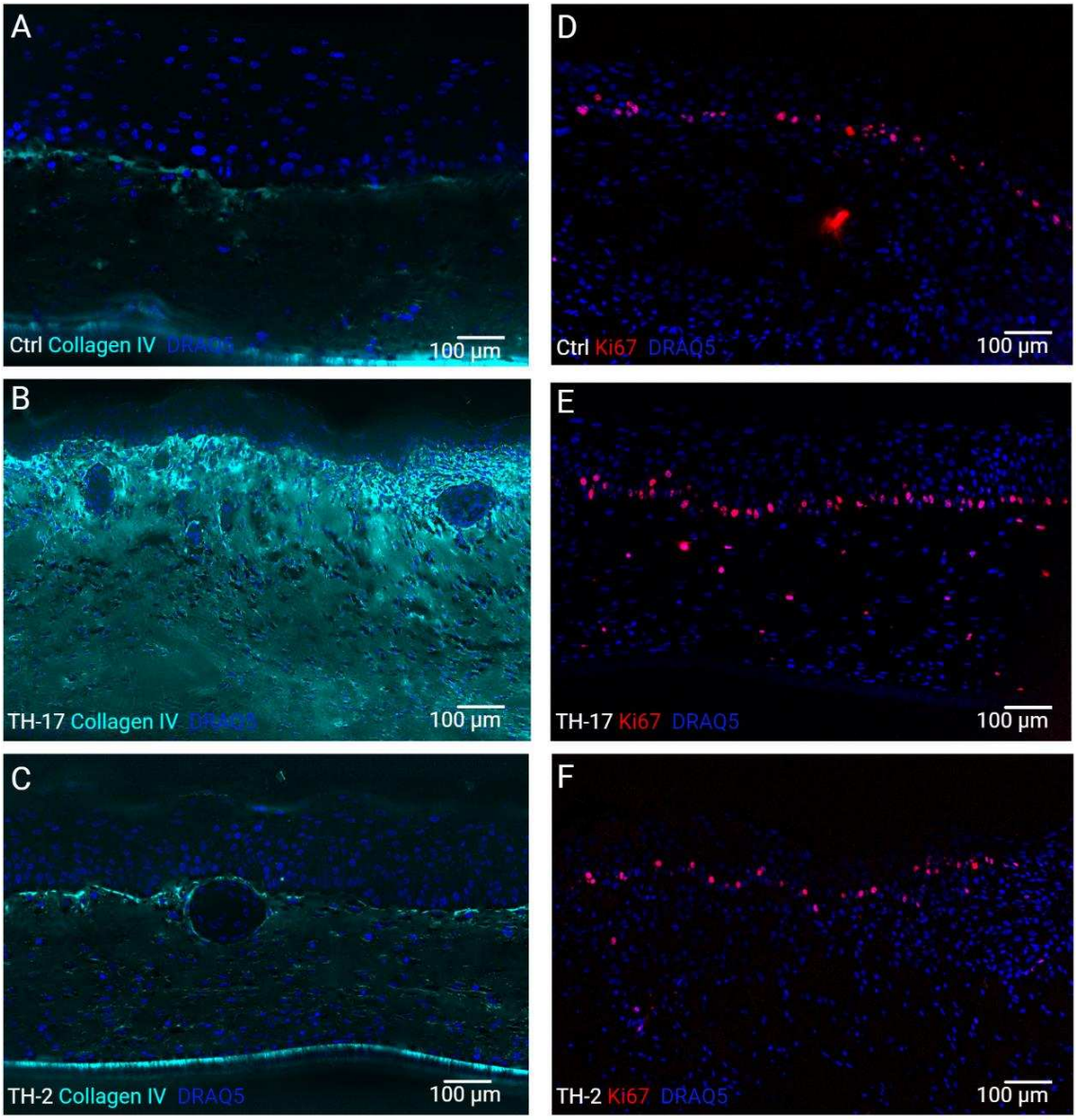

Figure 7: Collagen IV and Ki67 staining of human skin equivalents. Partly published in (Scheurer et al.*, 2024).*

For analysis of structural and histological validity of the skin models we performed CODEX analysis for basement membrane protein Collagen IV and proliferation marker Ki67 as shown in Figure 7. DRAQ5 was used as a nuclear marker. Expression of both markers is shown among an untreated control model, as well as on TH-2 and TH-17 cytokine models respectively. Pictures A-C represent CODEX fluorescent images of Collagen IV expression of an HSE built up on a collagen matrix. Pictures D-E show CODEX fluorescent images of Ki-67 expression of the same HSE. The same HSEs were used for expression analyses as for the analyses shown in Fig. 3. It becomes apparent that a clear distribution

pattern is formed along the suspected basement membrane showing an abundance of Collagen IV expression below the epidermal layer as well as a clearly visible line formed by the proliferating cells along the basement membrane.

3.1.2 Epithelial barrier in inflammatory skin equivalents

A big focus lay on characterization of the epithelial barrier. For instance, Filaggrin expression was visually and statistically analyzed as can be seen in Figure 8 and Figure 9. The CODEX analysis found a strong downregulation of Filaggrin expression in the AD and psoriasis models compared to the untreated control models. The abundance of Filaggrin in the control model cannot be found in either of the cytokine models (Figure 8). Quantitative analyses revealed the visually suspected differences in marker expression: A statistical comparison of the mean Filaggrin expression proved significant ($p < 0.05$) absence of Filaggrin expression among the epithelial cells of the cytokine models (Figure 9).

Furthermore, CODEX analysis of epithelial barrier proteins Loricrin and Elafin showed changes in the respective marker expression among the psoriasis and AD models (Figure 10). Figure 10 shows Elafin and Loricrin expression in HSEs. Pictured are CODEX fluorescent image comparisons of Elafin expression in untreated control, TH-17 and TH-2 3D human skin models for 3-day cytokine treatment in a 6-well collagen matrix. The outline shows the region of interest (ROI) for statistical analysis, specifically the respective parts of the histologically identified epidermis are marked in green. In A one can identify the visually notable elevation of Elafin expression in the cytokine models compared to the untreated control model. Statistical comparison of Elafin expression per epidermal cell by unpaired t-test proves a significantly ($p < 0.001$) higher Elafin expression per cell for the TH-2 treated AD phenotype.

On the bottom CODEX fluorescent image comparison of Loricrin expression in untreated control, TH-17 and TH-2 3D human skin models is visualized for 3-day cytokine treatment in a 6-well collagen matrix. The outline shows ROI for statistical analysis (epidermis green). The statistical comparison of Loricrin

expression per epithelial cell by unpaired t-test reveals significantly ($p < 0.001$) higher Loricrin expression per cell for the TH-2 treated AD phenotype and significantly ($p < 0.001$) lower expression of Loricrin for the PS phenotype compared to the untreated control.

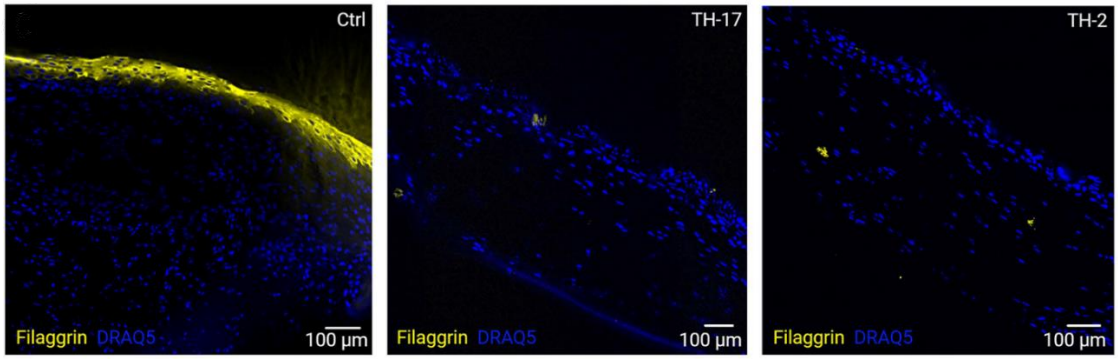

Figure 8: CODEX fluorescence image comparison of Filaggrin expression in untreated control, TH-17 and TH-2 3D human skin models. 3-day cytokine treatment, six-well collagen matrix. Published in (Scheurer et al.*, 2024).*

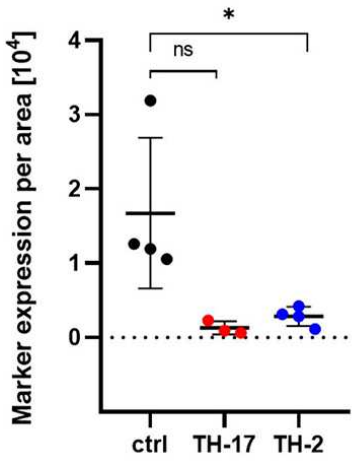

Figure 9: Comparison and unpaired two-tailed t-test of mean Filaggrin expression per unit area in the epidermis of all analyzed 3D human skin models (n=4). Bars represent the mean ± SD; ns, not significant; p < 0.05. Published in (Scheurer* et al.*, 2024).*

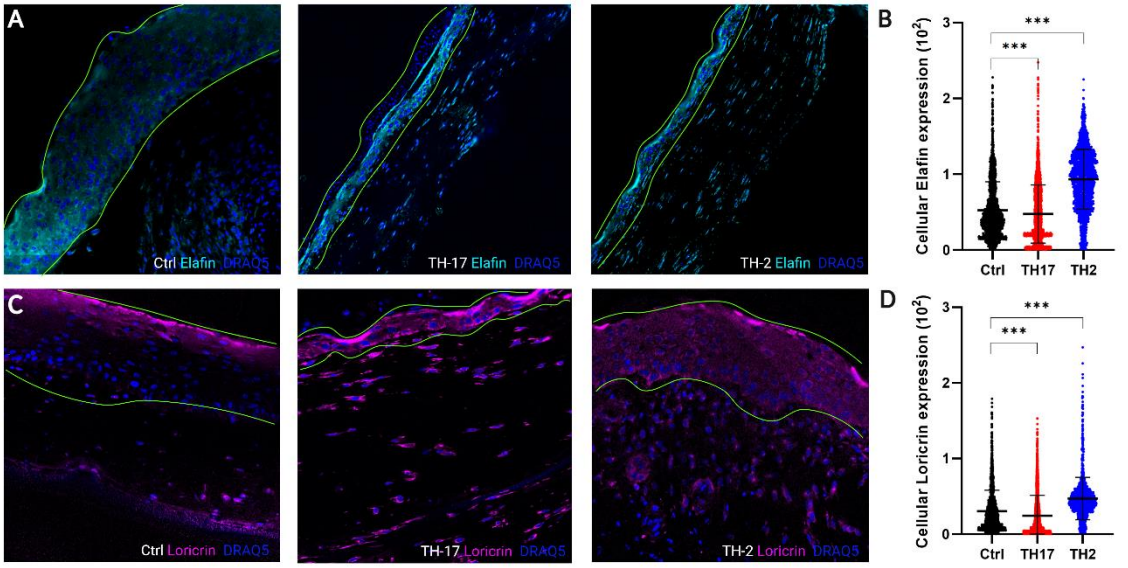

*Figure 10: Elafin and Loricrin expression in HSEs. Statistical comparison of Elafin and Loricrin expression per epidermal cell by unpaired t-test. Bars represent the mean ± SD; ns, not significant; p < 0.001***. Published in (Scheurer* et al.*, 2024).*

3.1.3 Inflammatory hallmarks and distinction markers

To further characterize the validity of the skin models we performed CODEX analysis for previously described markers of distinction between AD and PS. Figure 11 shows CODEX fluorescence image comparison of NOS2 expression in untreated control, TH-17 and TH-2 3D human skin models for 3 day cytokine treatment in a six-well collagen matrix. The outlines in the top row show regions of interest for statistical analysis (green, epidermis; magenta, dermis). The bottom row shows magnification of the ROIs for the TH-17- and TH-2-treated models visualizing epidermal NOS2 expression patterns in the psoriasis and AD model. Eminently, epidermal NOS2 expression cannot be seen within the untreated or TH-2 cytokine model while being prominently present in the TH-17 cytokine model. This becomes especially clear looking at the magnified pictures in the bottom row, where epidermal NOS2 expression is missing in the TH-2 model while analogous dermal NOS2 expression can be found for both cytokine models. To quantify the results, a statistical comparison of NOS2 expression per epithelial and per dermal cell by unpaired two-tailed t-test was performed. Results are found in Figure 12. NOS2 is expressed more prominently and is more widely

spread in the epidermis of the psoriasis model compared to the epidermis of the control HSE and the AD model (Figure 11, Figure 12).

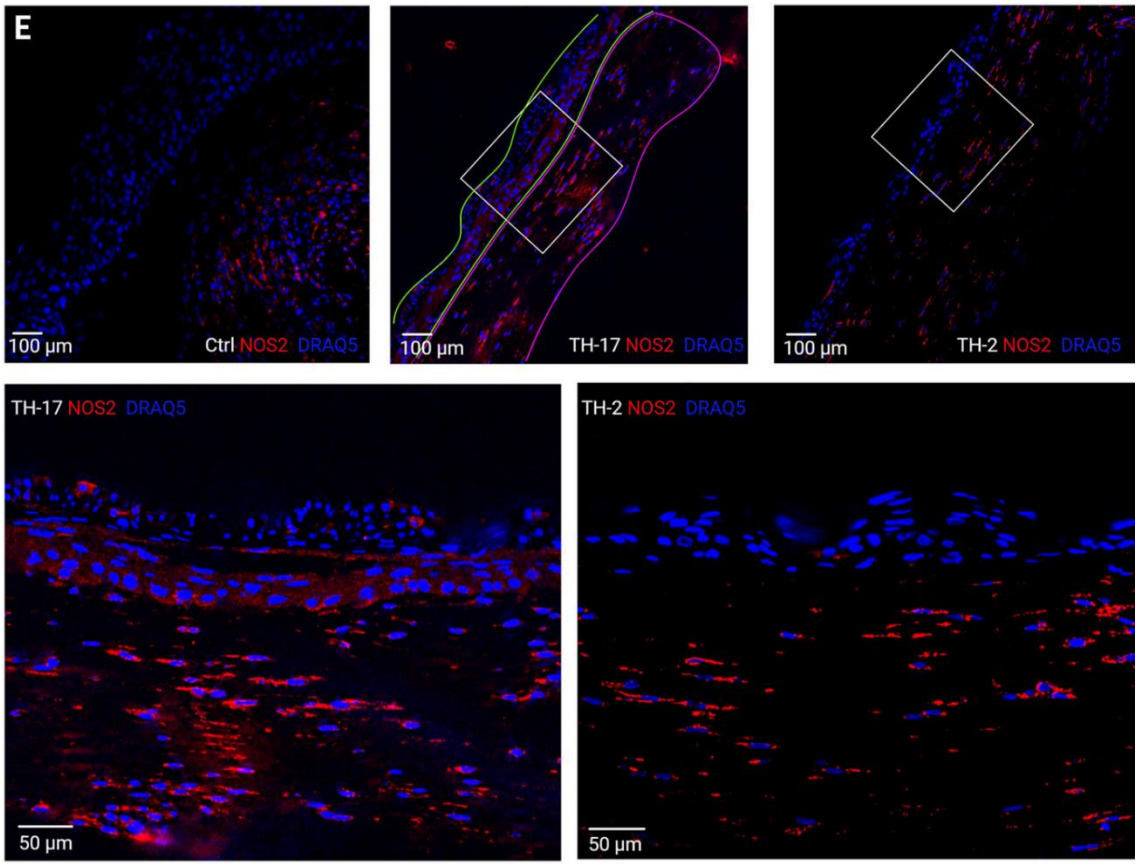

Figure 11: CODEX fluorescence image comparison of NOS2 expression in untreated control, TH-17 and TH-2 3D human skin models. 3-day cytokine treatment, six-well collagen matrix. Squares in top images indicate magnified regions in bottom images. Published in (Scheurer et al.*, 2024).*

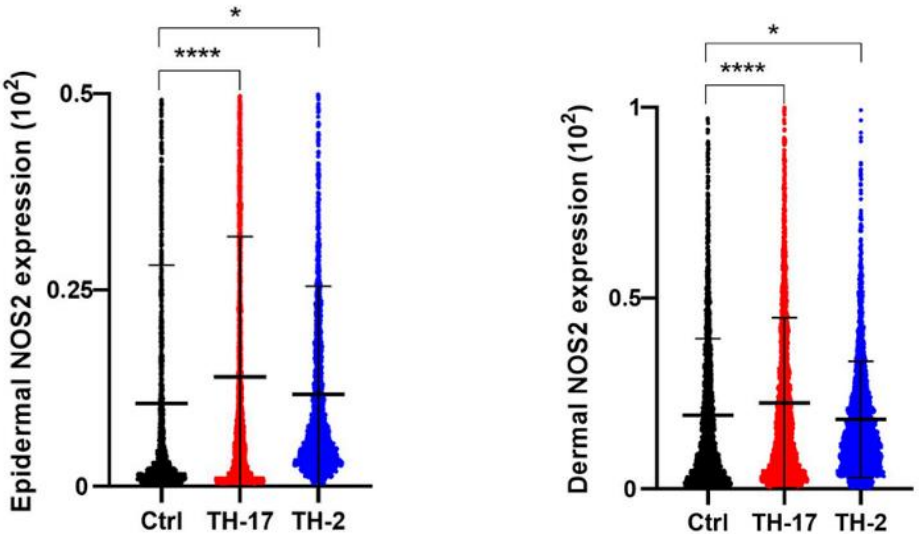

Figure 12: Statistical comparison of NOS2 expression per epithelial (left) or dermal (right) cell by unpaired two-tailed t-test. Bars represent the mean ± SD; p < 0.05; p < 0.0001****. Published in (Scheurer et al., 2024).*

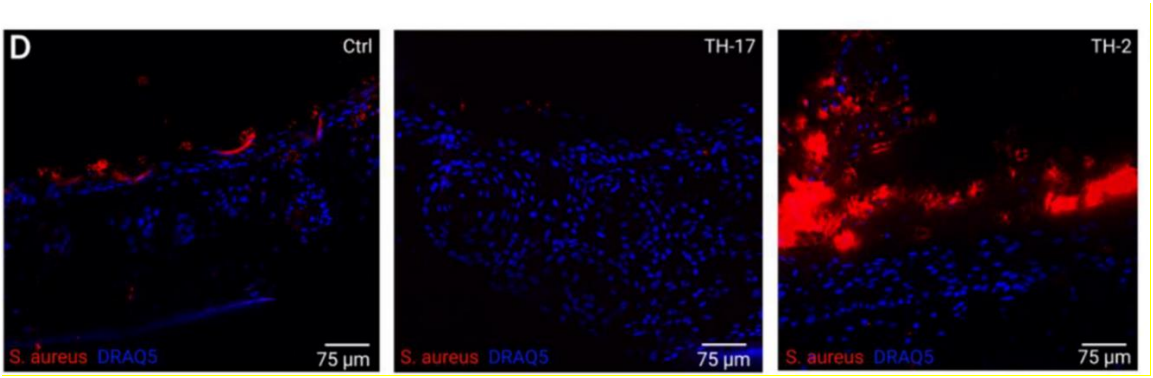

Figure 13: CODEX fluorescence image comparison of S. aureus expression in S. aureus-infected untreated control, S. aureus-infected TH-17 and S. aureus-infected TH-2 3D human skin models. 3-day cytokine treatment, six-well collagen matrix. Scale bars: 75 µm. Published in (Scheurer et al.*, 2024).*

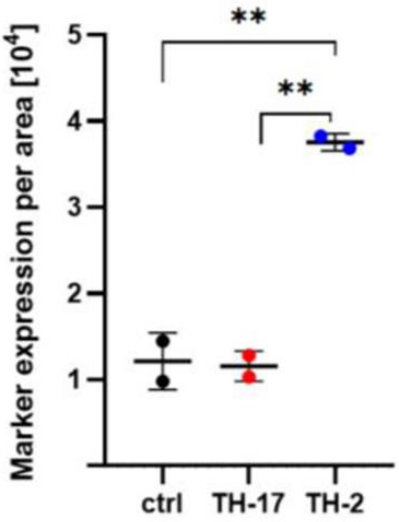

*Figure 14: Comparison and unpaired two-tailed t-test of mean marker expression of S. aureus per area in the epidermis of infected 3D human skin models (n=2). Unpaired two-tailed t-test was used. Bars represent the mean ± SD; p < 0.01**. Published in (Scheurer* et al.*, 2024).*

3.1.4 Staphylococcus aureus colonization

Figure 13 manages CODEX fluorescence image comparison of *S. aureus* expression in *S. aureus*-infected untreated control, *S. aureus*-infected TH-17 and *S. aureus*-infected TH-2 3D human skin models for 3-day cytokine treatment in a six-well collagen matrix. The scale bars indicate 75 µm. It becomes visible that the epidermal expression of *S. aureus* antigens is much more present in the TH-2 cytokine model even without taking the quantitative data of Figure 14 into account. Figure 14 shows a comparison and unpaired two-tailed *t*-test of the

mean marker expression of *S. aureus* per area in the epidermis of the 3D human skin models that were infected with Staphylococcus aureus before testing. It shows a significant difference in marker expression upon the cytokine models as well as in comparison to the model without any cytokine treatment used as control model. This model was also infected with the same concentration of Staphylococcus aureus cultures but shows a much weaker expression pattern than the TH-2 treated model.

3.2 Patient samples

3.2.1 Epithelial barrier proteins

In parallel with the approach for the skin models, the patient samples were analyzed after running the full panel as described previously. Figure 17 summarizes the expression patterns of two epithelial barrier proteins – Filaggrin and Elafin – for healthy controls and AD patient samples. The CODEX image is representative for a total of 5 samples per group. The samples were compared using the Mean Marker Expressions in the epidermis and dermis. It is apparent that neither visually nor statistically a difference in marker expression of Filaggrin nor Elafin can be found. The scatter of mean marker expression of Elafin between the samples of the healthy control is bigger than that of the AD patients. There is no statistical significance for differences in mean marker expression.

Figure 15 shows the line of action for another epithelial barrier protein. Loricrin can be found in the epidermis as part of the stratum granulosum of the healthy control group as well as in AD patient samples. Visually the expression of Loricrin seems more diffuse among the epidermal layer for the healthy controls, while Loricrin expression in the AD samples is visually more strictly focused on the stratum granulosum. Statistically no significance is found. There is much more of a scatter among the mean marker expressions in between the AD samples as there is for the samples of the healthy control.

To further regard this, an analysis was made using a different approach by taking single cell expression into account rather than solemnly considering the mean marker expression upon the entire sample. Therefore, after performing single cell

detection the respective marker expressions were calculated and compared. This data is depicted in Figure 16. Visually Loricrin expression now appears similar between AD and control samples, while the PS sample shows almost no Loricrin expression in the epidermis. Statistically we see a clear shift in results compared to the mean marker expression, as the epidermal Loricrin expression per cell normalized by nuclear expression of DRAQ5 is highest within the cytoplasm of the healthy control group followed by PS samples. Epidermal cytoplasmic Loricrin expression in AD patient samples is decreased with strong significance $p < 0.0001$.

The same procedure was used to analyze Filaggrin and Elafin expressions upon the epidermal regions. For Filaggrin CODEX images showed similar distributions of marker expression in the epidermis of all samples throughout all tested groups. The expression patterns are more apparent in the AD and PS samples visually due to the thickened epidermal layer in general. Moreover, the healthy control sample in Figure 19 portrays a preserved stratum corneum with high expression of Filaggrin. The statistical analysis now reveals elevated expression of Filaggrin upon the AD samples, while PS and healthy controls show comparably low levels of Filaggrin expression per epidermal cell.

Similarly, CODEX analysis of Elafin expression per epidermal cell is shown in Figure 20. Visually the expression patterns are similar upon all tested groups, while statistical analysis of marker expression per cell reveals elevation thereof for the AD samples. Furthermore, Elafin expression in PS samples is also slightly elevated compared to the healthy control group but much lower than the expression in AD patient samples.

A summary of the quantification of mean marker expression and Signal to noise ratio of the epidermal barrier proteins Elafin, Filaggrin and Loricrin can be seen Figure 18. There is significant elevation of Elafin expression found for the AD and PS samples compared to the healthy control. Elafin mean marker expression proves significantly higher than for the AD models, with a wider scatter of values between the individual analyzed samples. This scatter is not found for the AD or control samples. Contrariwise, Filaggrin expression is seen to be highest for the healthy control group and significantly lowered for the AD and PS samples. The

signal to noise ratio for the PS ratio is seen to be lower than seen for the control and AD samples with high significance p*** < 0.001 compared to the control group. For evaluation of Loricrin expression Signal to noise ratio as well as mean marker expression is depicted. The findings for quantitative Loricrin expression are not significant when looking at Signal to noise ratio between the 3 groups or comparison of mean marker expression for the AD and control group. There are statistical outliers found for the control and PS group.

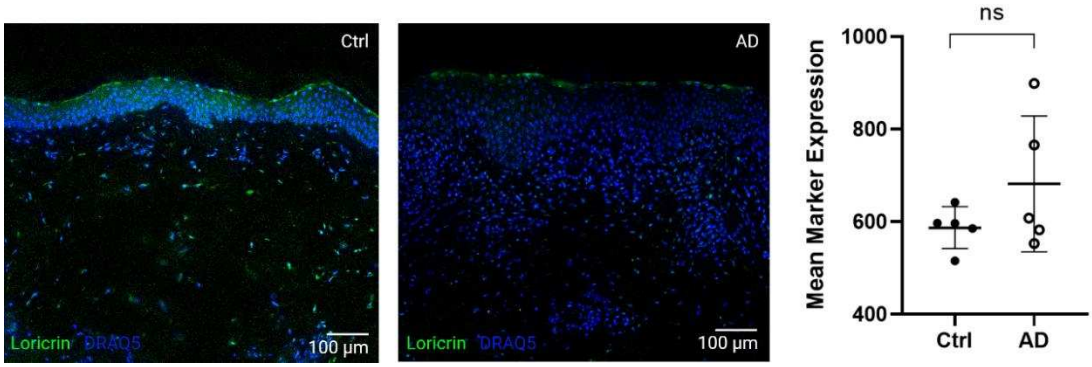

Figure 15: CODEX image of Loricrin expression and statistical comparison of mean epidermal marker expression. Bars represent the mean ± SD; ns, not significant.

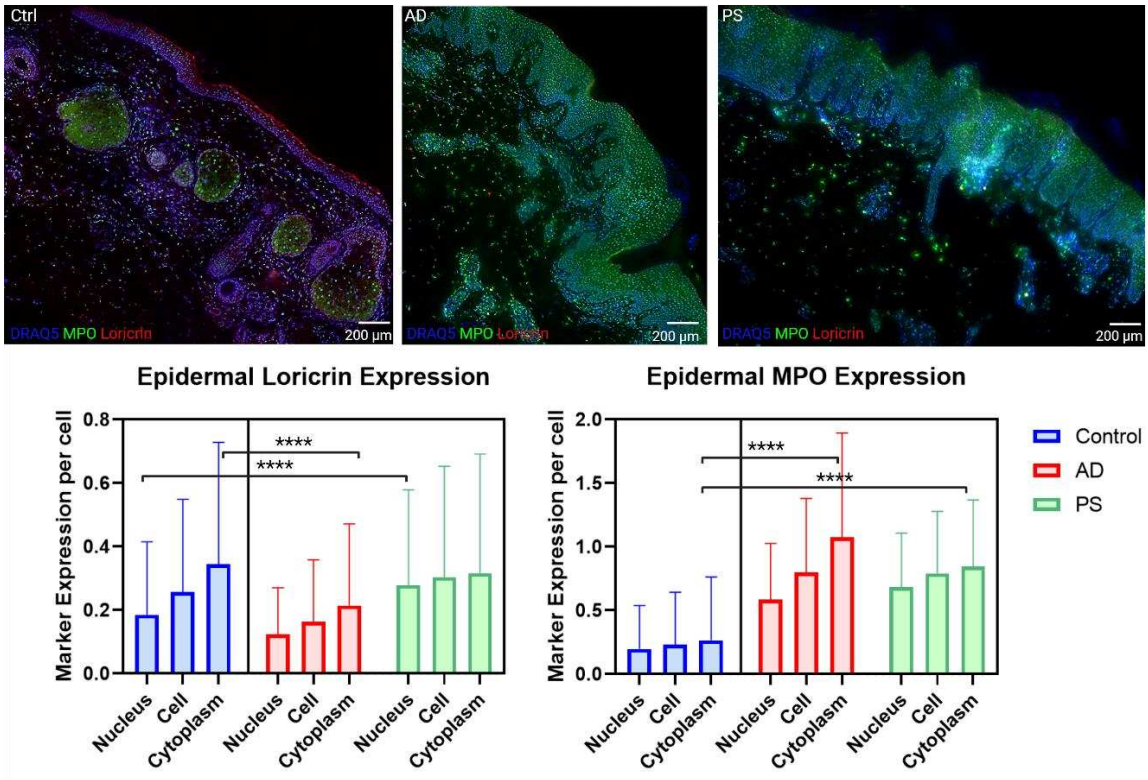

*Figure 16: CODEX images of Loricrin and MPO expression (top). Statistical analysis of epidermal Loricrin and MPO expression per cell (bottom). Total, nuclear and cytoplasmic marker expression quantified using QuPath; unpaired two-tailed t-tests, p < 0.0001****. Bars represent the mean ± SD.*

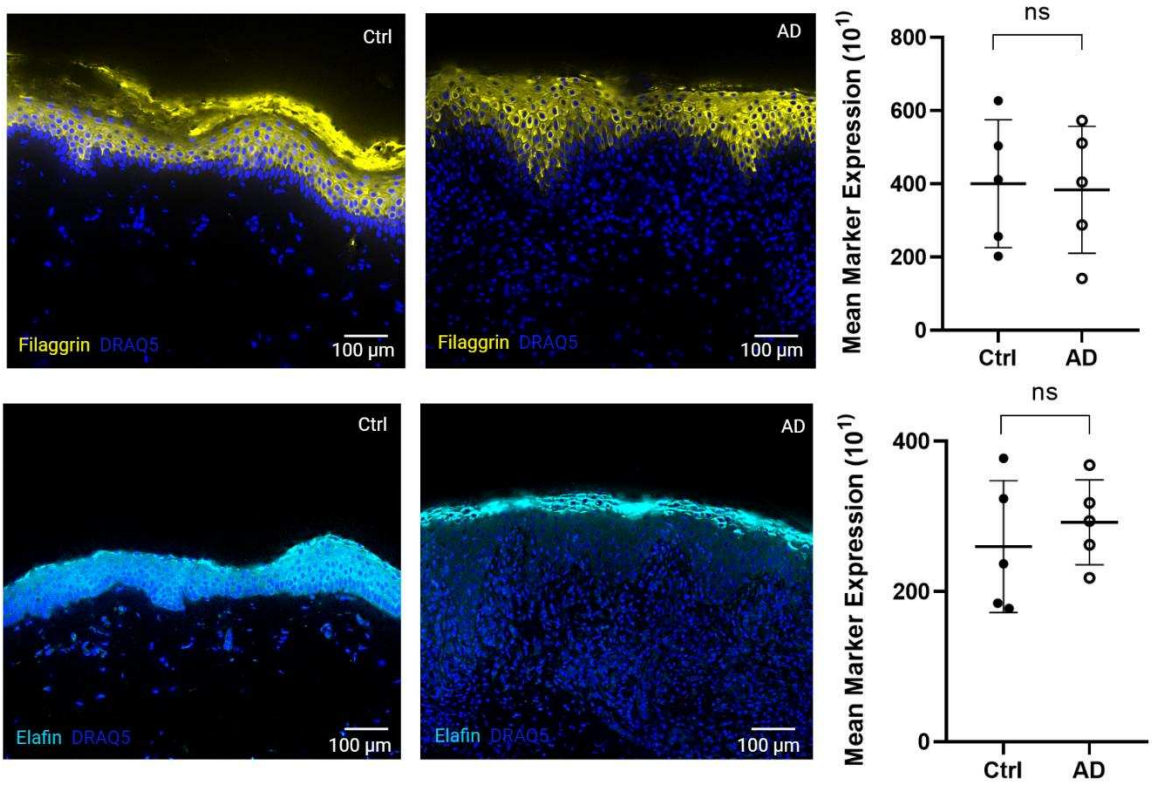

Figure 17: CODEX image comparisons of Filaggrin and Elafin expression and statistical analysis of mean marker expression. Bars represent the mean ± SD; ns, not significant.

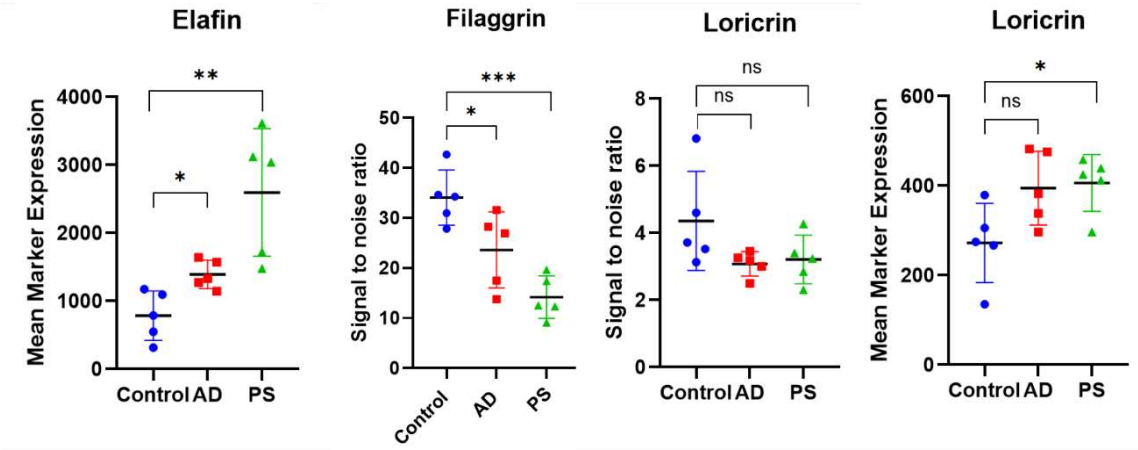

Figure 18: Comparison of Mean Marker Expression and Signal to noise ratio for epidermal barrier proteins Filaggrin, Elafin and Loricrin. Quantification and statistical analysis performed using QuPath, unpaired two-tailed t-tests. Bars represent the mean ± SD; ns, not significant, $p < 0.05$, $p < 0.01$**, $p < 0.001$***.*

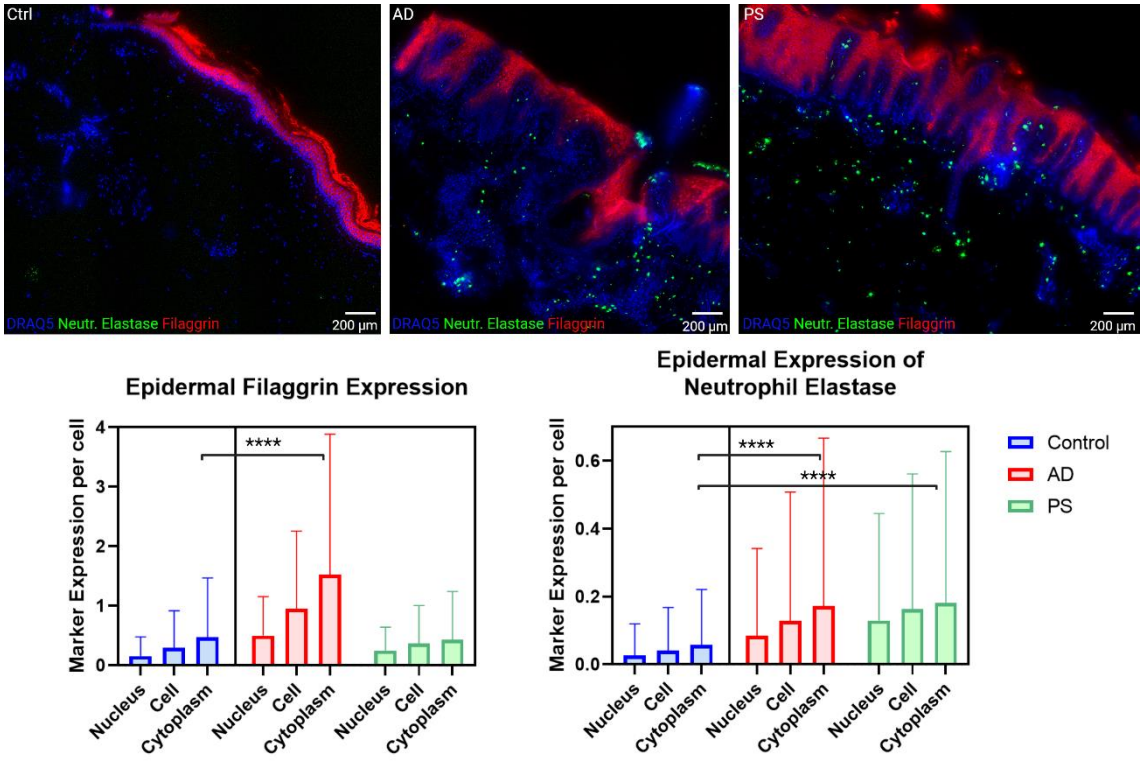

*Figure 19: CODEX images of Filaggrin and NE expression (top). Statistical analysis of epidermal Filaggrin and NE expression per cell (bottom). Total, nuclear and cytoplasmic marker expression quantified using QuPath; unpaired two-tailed t-tests, p < 0.0001****. Bars represent the mean ± SD.*

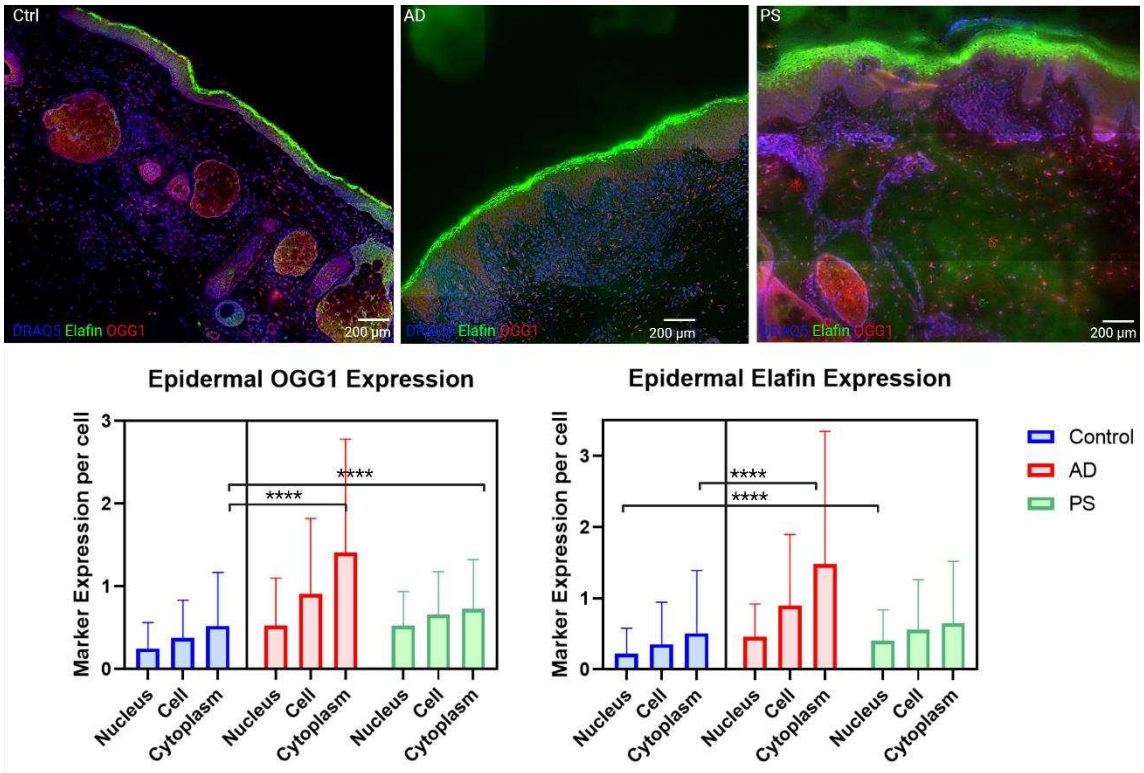

*Figure 20: CODEX images of OGG1 and Elafin expression (top). Statistical analysis of epidermal OGG1 and Elafin expression per cell (bottom). Total, nuclear and cytoplasmic marker expression quantified using QuPath; unpaired two-tailed t-tests, p < 0.0001****. Bars represent the mean ± SD.*

3.2.2 Inflammatory hallmarks

The data for MPO expression in AD and healthy control samples is shown in Figure 21 containing an analysis of the mean marker expression. CODEX imaging shows strong nuclear and epidermal cytoplasmic expression of MPO in both subgroups, though more strongly expressed in the AD samples. Analysis of the mean marker expression proves significant upregulation of MPO expression across all tested samples for the AD patients compared to the healthy control group. Further data on MPO is presented in Figure 16. The CODEX images on the top depict MPO expression in representative samples for the healthy control group, AD patients and PS patients. While there is little epidermal MPO expression visible in the healthy control sample, both AD and PS samples show strong cytoplasmic and nuclear MPO expression across the epidermis. Statistical analysis of epidermal MPO expression per cell proves highly significant increased expression of MPO with $p < 0.0001$ by unpaired two-tailed t-test in both inflammatory skin groups compared to the healthy control. Cytoplasmic MPO expression is highest in the AD group, while nuclear MPO expression is most prominent in the PS group.

Another important marker of inflammatory processes is Neutrophil Elastase, which is summarized in Figure 22. Shown are CODEX images of NE expression focused on the epidermal regions of representative samples for the healthy control and AD group. Very clearly, expression patterns can be seen epidermally and dermally for the AD sample, while there is much less visible NE expression in the healthy control sample. This is supported by mean marker expression of NE, which validates a significantly increased NE expression among the AD samples in contrast to the healthy control samples.

Additionally, Figure 19 shows similar results including the PS samples and manages statistical comparison of marker expression per epidermal cell. Even though NE expression is visibly found mainly in the dermal region below the basement membrane, there is still significantly higher expression of NE within the epidermis for the analyzed cells in AD and PS samples compared to the healthy

samples. There is no significant difference between the two inflammatory diseases regarding single cell expression of NE.

Figure 23 represents CODEX imaging and statistical analysis of OGG1 expression shown for representative images of healthy control and AD samples. OGG1 expression appears epidermally and dermally, the AD sample shows strong expression in the stratum granulosum, which does not become evident in the control group. Mean marker expression of OGG1 shows significantly increased expression of OGG1 by unpaired two-tailed t-tests with $p < 0.05$ in the AD group, but also much wider scattering of data between the different samples. Moreover, in Figure 20 CODEX images of OGG1 for all tested groups are shown. Visually there seems to be hardly any difference in OGG1 expression dermally between the subgroups, while epidermal expression is difficult to adequately evaluate with Elafin expression overlapping. Statistical analysis of epidermal OGG1 expression per cell reveals a significantly increased OGG1 expression among the AD group, especially for cytoplasmic marker expression by unpaired two-tailed t-tests with $p < 0.0001$.

The HMGB1 expression in the skin of AD patients compared to healthy controls is outlined in Figure 24 and Figure 25. CODEX images of representative samples show strong nuclear expression upon the two tested groups, while statistical analysis reveals significantly increased HMGB1 mean marker expression in the AD group by unpaired two-tailed t-test $p < 0.05$.
Figure 25 quantifies total, nuclear and cytoplasmic HMGB1 expression in the skin of AD patients compared to healthy control samples using QuPath. Significant differences were analyzed by unpaired two-tailed t-tests with significantly increased cellular and cytoplasmic HMGB1 expression upon AD samples with $p < 0.0001$ and nuclear expression with higher mean in the control group, but higher expressions in some single cells for the AD group.

Taking results for PS patient samples into account, another comparison of CODEX data for HMGB1 expression is presented in Figure 26. Representative

CODEX images for all subgroups are listed and HMGB1 expression can be seen mainly epidermally as nuclear staining. Visually HMGB1 expression appears to be prominent in AD and PS samples compared to the control group, which is validated looking at the statistical single cell analysis for HMGB1 expression. There is significantly higher nuclear HMGB1 expression in the epidermis for PS samples and even further elevated nuclear and cytoplasmic HMGB1 expression in AD samples.

CitH3 expression is shown in Figure 27 for AD and healthy control samples. While visually there is clearly a much more present expression of citH3 in the epidermis of the AD sample, this difference isn't statistically significant when comparing the mean marker expression of citH3 across the samples, even though showing a tendency towards elevated expression in the AD samples.

Further analysis is illustrated in Figure 26 for AD, PS and control samples and respective citH3 expression. Visually the pictures are congruent with the findings of Figure 27 and show strong epidermal expression of citH3 in the AD sample, while the control group and PS samples show a less vibrant expression of citH3 in the epidermal region. Statistically this proves to be significant on a single cell level, as marker expression per cell is highly significantly elevated across the AD group, especially looking at epidermal cytoplasmic citH3 expression.

Figure 28 shows statistical analysis of three proteins involved in inflammatory processes analyzed in the CODEX panel. Mean marker expression is portrayed for phospho-NF-κB, phospho-ERK and phospho-p38. The graphs represent significant elevation of phospho-NF-κB expression for AD and PS samples, significantly lower expression of phospho-ERK for the PS group when comparing PS and AD and a trend of elevation of pp38 among the inflammatory skin samples without statistical significance compared to the healthy control samples.

Figure 29 shows statistical analysis of three proteins involved in inflammatory processes analyzed in the CODEX panel. Mean marker expression is portrayed for HistoneH3, LL37 and HBD3. The graphs represent significant elevation of Histone H3 for the PS samples and a trend for elevation among the AD group

compared to the healthy control. For LL37 there is significantly higher expression for the PS group and a trend of elevation among the AD group that proves no statistical significance. When comparing HBD3 expression there is clear upregulation only upon the AD model, that cannot be found for the control or PS group.

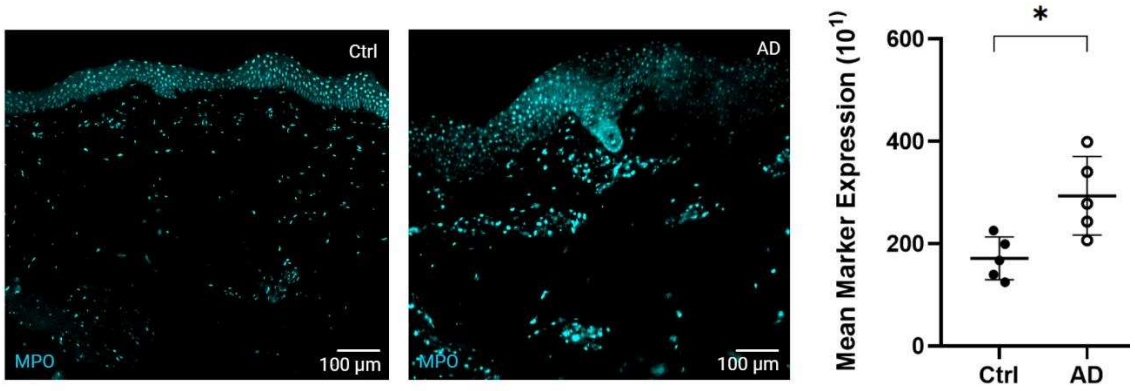

Figure 21: CODEX image comparisons of MPO expression and statistical analysis of mean marker expression by unpaired two-tailed t-tests. Bars represent the mean ± SD; p < 0.05.*

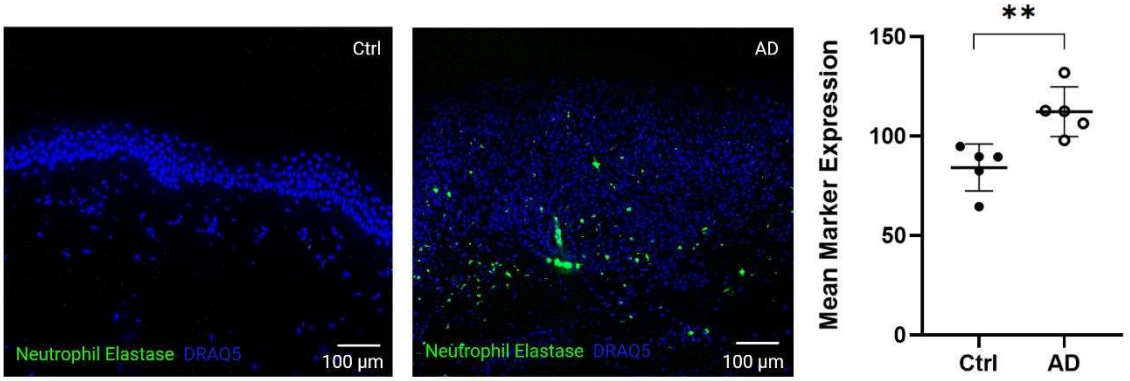

*Figure 22: CODEX image of Neutrophil Elastase expression and statistical comparison of mean epidermal marker expression by unpaired two-tailed t-tests. Bars represent the mean ± SD; p < 0.01**. Published in (Focken* et al.*, 2023).*

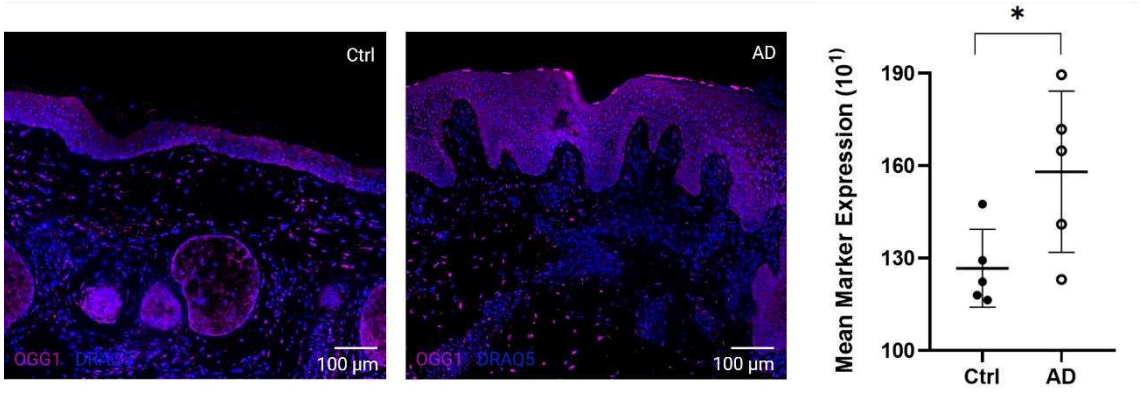

Figure 23: CODEX image of OGG1 expression and statistical comparison of mean epidermal marker expression by unpaired two-tailed t-tests. Bars represent the mean ± SD; p < 0.05.*

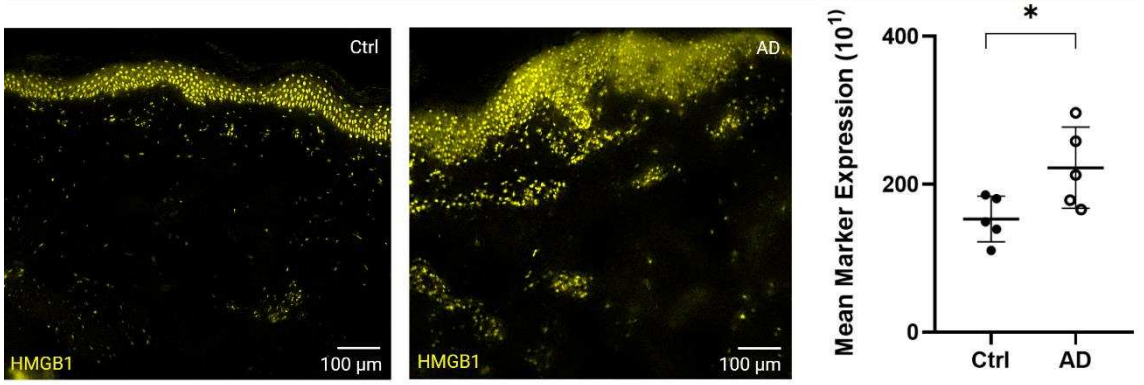

Figure 24: CODEX image of HMGB1 expression and statistical comparison of mean epidermal marker expression by unpaired two-tailed t-tests. Bars represent the mean ± SD; p < 0.05. Published in (Focken* et al.*, 2023).*

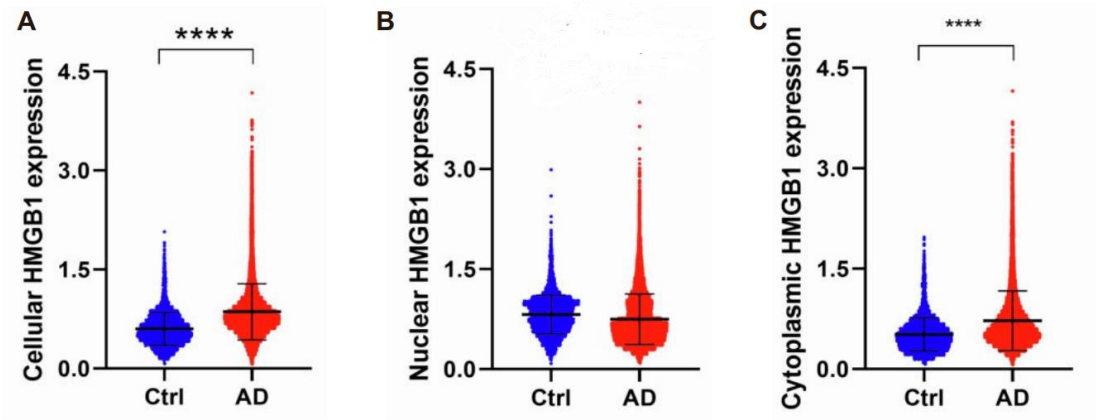

*Figure 25: HMGB1 expression in the skin of AD patients compared to healthy controls A-C: Total, nuclear and cytoplasmic HMGB1 expression quantified using QuPath; unpaired two-tailed t-tests. Bars represent the mean ± SD; p < 0.0001****. Published in (Focken* et al.*, 2023).*

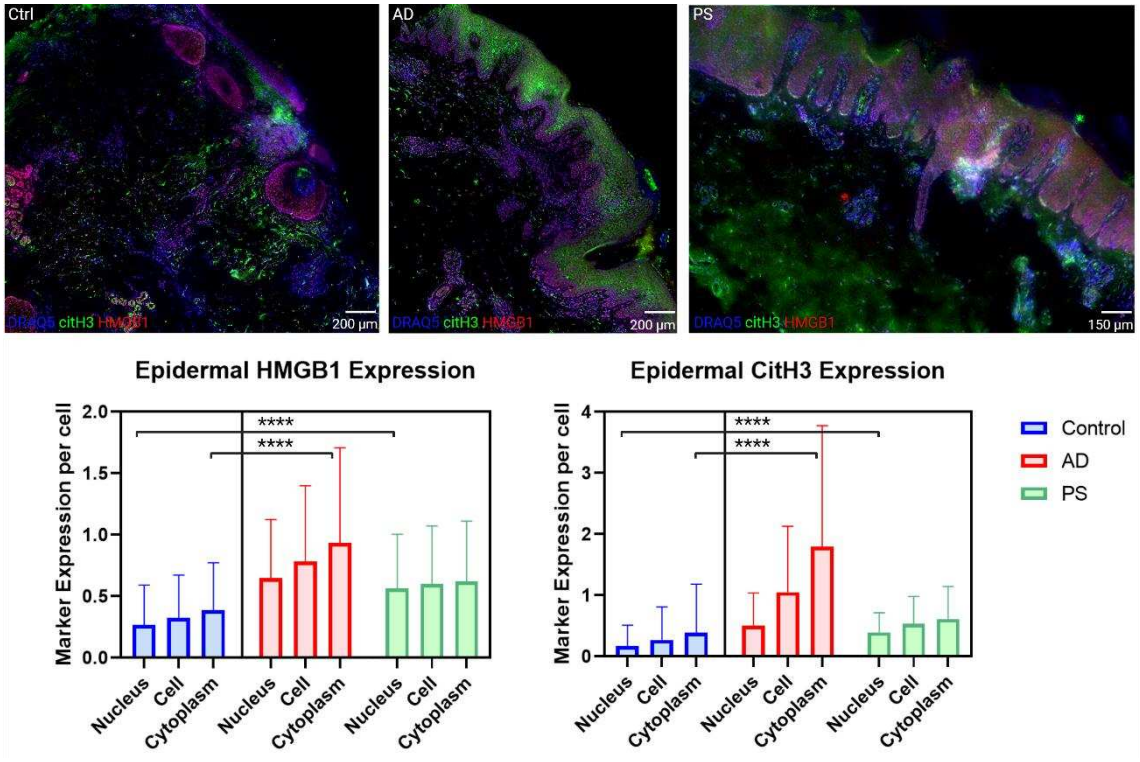

*Figure 26: CODEX images of HMGB1 and CitH3 expression (top). Statistical analysis of epidermal HMGB1 and CitH3 expression per cell (bottom). Total, nuclear and cytoplasmic marker expression quantified using QuPath; unpaired two-tailed t-tests, p < 0.0001****. Bars represent the mean ± SD.*

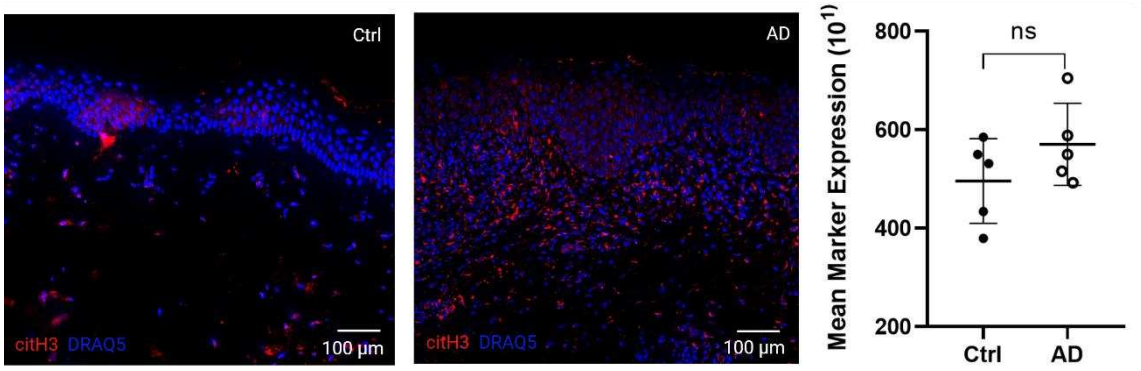

Figure 27: CODEX image of citH3 expression and statistical comparison of mean epidermal marker expression by unpaired two-tailed t-tests Bars represent the mean ± SD; ns, not significant.

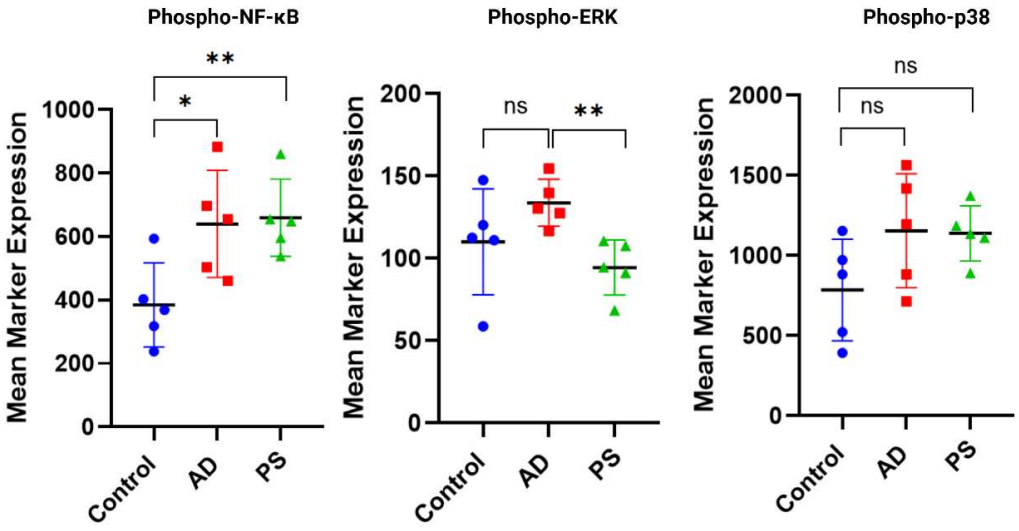

Figure 28: Comparison of mean marker expression of inflammatory hallmark proteins p-NF-kB, p-ERK and p-p38. Statistical analysis performed in QuPath, unpaired two-tailed t-tests. Bars represent the mean ± SD; p < 0.05, p < 0.01**.*

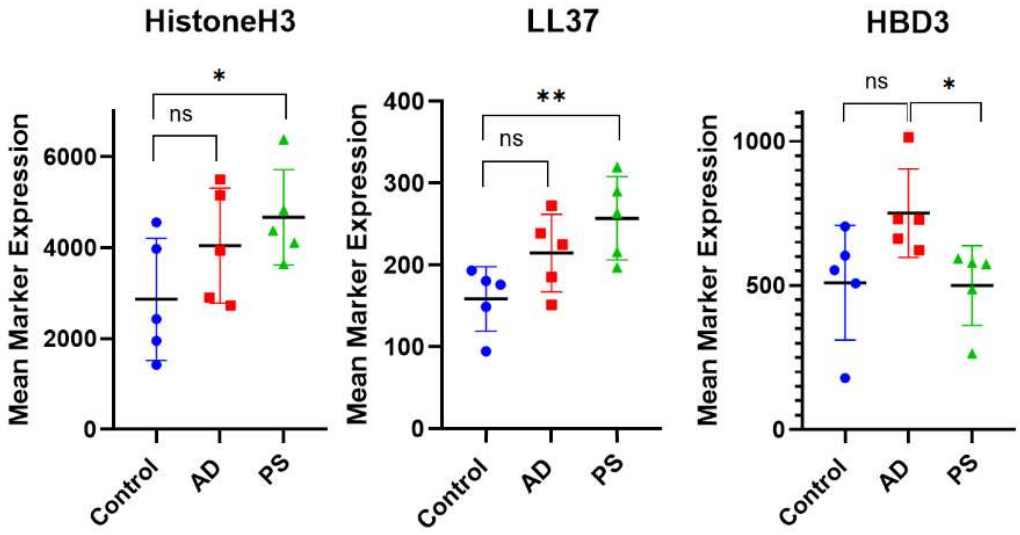

Figure 29: Comparison of mean marker expression of inflammatory hallmark proteins Histone H3, LL37 and HBD3. Statistical analysis performed in QuPath, unpaired two-tailed t-tests. Bars represent the mean ± SD; p < 0.05, p < 0.01**.*

3.2.3 S. aureus

Evaluation of colonization by Staphylococcus aureus among the tested skin samples can be found in Figure 31. The CODEX images show almost no expression of *S. aureus* in the control sample, the AD sample shows cytoplasmic *S. aureus* expression in the epidermis. Looking at the graph depicting a comparison of the mean marker expression it becomes eminent that there is

significantly higher expression of *S. aureus* within the AD samples. This can be seen as quantification by unpaired two-tailed t-test with $p < 0.05$.

The difference in expression patterns becomes even more prominently visible looking at Figure 30 which shows CODEX images for all tested subgroups. Epidermal and dermal expression of *S. aureus* is very substantial within the AD sample, while the samples for PS patients and the healthy control group show much less expression for *S. aureus*.

An analysis of the marker expression per cell within the epidermis reveals validity of the visual impression and proves significant for elevation of *S. aureus* expression within the AD samples for nuclear, cytoplasmic and global marker expression. The descriptive statistic gives an overview over the amount of data analyzed, as cell segmentation manages output of immense data amounts for each single cell to be put into comparison. The mean values for cytoplasmic S. aureus expression for healthy controls and PS samples are almost identical, while there is a strongly significant elevation for the AD samples.

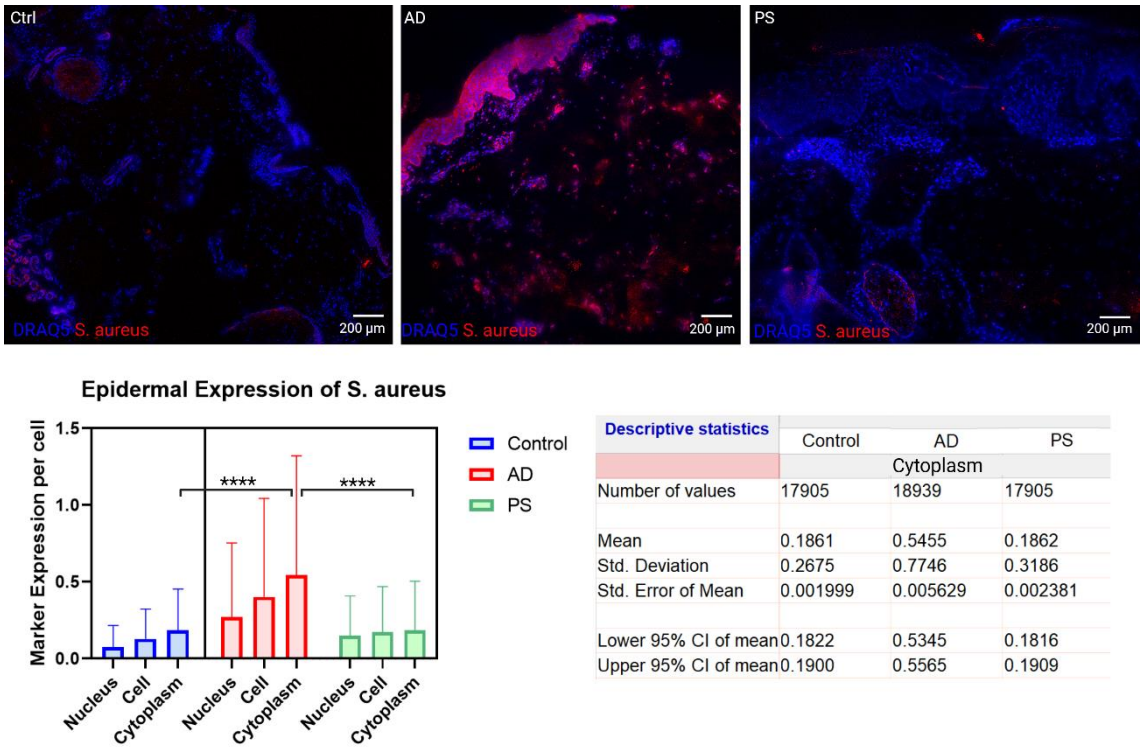

Descriptive statistics	Control	AD	PS
	Cytoplasm		
Number of values	17905	18939	17905
Mean	0.1861	0.5455	0.1862
Std. Deviation	0.2675	0.7746	0.3186
Std. Error of Mean	0.001999	0.005629	0.002381
Lower 95% CI of mean	0.1822	0.5345	0.1816
Upper 95% CI of mean	0.1900	0.5565	0.1909

*Figure 30: CODEX images of S. aureus expression (top). Statistical analysis of epidermal S. aureus expression per cell (bottom left). Descriptive statistics for epidermal cytoplasmic S. aureus expression per cell (bottom right). Total, nuclear and cytoplasmic marker expression quantified using QuPath; unpaired two-tailed t-tests, p < 0.0001****. Bars represent the mean ± SD.*

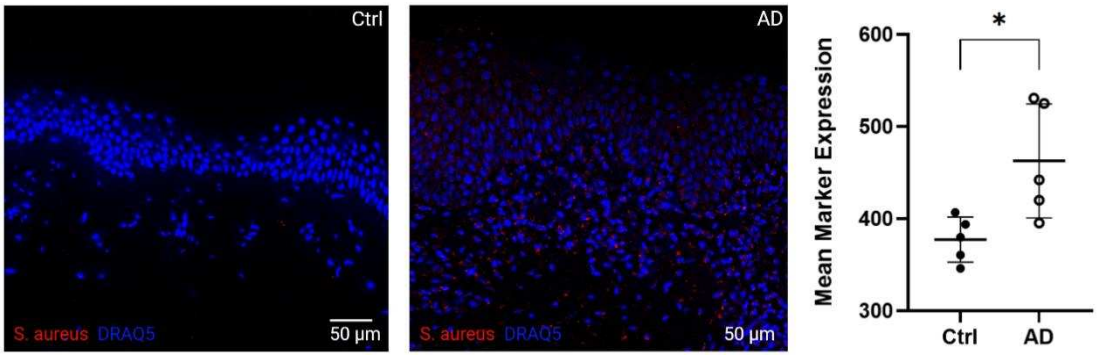

Figure 31: CODEX image of S. aureus expression and statistical comparison of mean epidermal marker expression by unpaired two-tailed t-tests, Bars represent the mean ± SD; p < 0.05. Published in (Focken* et al*., 2023).*

3.3 Cell culture and Lymphoma

3.3.1 CD3 staining for cell lines HH and HUT 78

CD3 staining for comparable models showed more successful integration of lymphoma cells for the HUT 78 cell line, all further experiments were therefore carried out using HUT 78 cell line. HH cells did show integrated cells in the epidermis, but to a much smaller extent and cell count.

3.3.2 CD3 staining for TH-17 HSEs with HUT 78

Following the first round of experiments testing for successful integration of lymphoma cells into the HSEs, Figure 32 and Figure 33 show results for the second round of experiments of CD3 staining on lymphoma skin models. The top shows sewing of $5x10^5$ HUT78 cells on a TH-17 cytokine treated model on the right side and non-cytokine treated model in the middle. The control is pictured on the left side and does not show any signs of integrated lymphoma cells. Both models treated with the HUT78 cells show strong epidermal CD3 staining on top of the stratum granulosum as well as integration into the epidermis below the basement membrane.

Figure 33 shows similar results for sewing with $6x10^6$ HUT78 cells on non-cytokine and TH-17 cytokine treated models. Both show CD3 staining on the rim of the stratum granulosum as well as integration into the epidermis below the stratum basale.

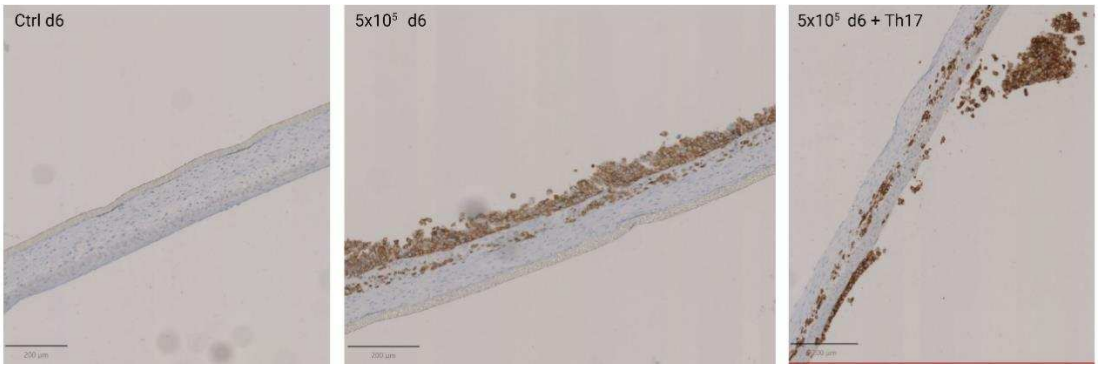

Figure 32: CD3 staining for sewed 5x10^5 HUT 78 cells on Control, non-cytokine and TH-17 cytokine model after 6 days. Scale bars indicate 200 µm.

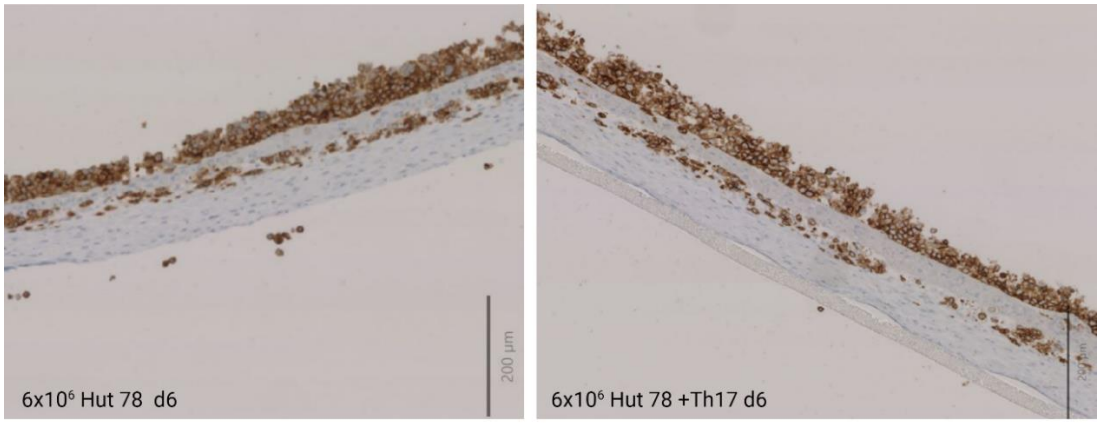

Figure 33: CD3 staining for sewed 6x10^6 HUT 78 cells on non-cytokine treated and TH-17 cytokine skin model after 6 days. Scale bars indicate 200 µm.

4 Discussion

4.1 Skin equivalents

4.1.1 Multiplexed imaging of phenotypic hallmark expression in 3D skin models

The panel design chosen for characterization of the skin models proved extensive enough, as tissue complexity and cell count cannot be equaled to patient samples especially in terms of epidermal thickness. In general, CODEX analysis was highly successful on all HSE models even though the samples are more fragile due to their stepwise construction.

Successfully, all samples were analyzed upon their characteristics for expression of epithelial barrier proteins, inflammatory markers and *S. aureus* colonization.

The validated DNA-conjugated antibodies were used to detect epithelial, activation, proliferation and inflammation markers identically as the procedure for the patient samples and showed no significant differences regarding antigen and antibody interactions. Comparing Figure 6 to the CODEX image overlays of patient samples visually there are superficially no compromises in terms of image quality and epidermal complexity, especially in the matter of TH-2 cytokine-induced models.

4.1.2 Multiplexed imaging validates phenotypic hallmark expression in 3D skin models

CODEX analysis of phenotypic hallmarks, like dermal and epidermal construction, revealed very satisfying results in terms of validating a correct assembly of epidermal layers with a strong and clear separation of Collagen IV expression within the dermal layer up to the basement membrane. The models were all built up in a collagen matrix and still manage to illustrate an eminent basement membrane with strong Collagen IV expression rather than a ubiquitous expression pattern of collagen. This can especially be seen for the control and TH-2 model in Figure 7. For the TH-17 induced cytokine model there is more of an unspecific staining and strong background expression to be suspected, which could be on account of incorrect development of the dermal compartment of the

HSE, incorrect experimental CODEX conduction or unspecific staining of the antibody. As all experiments were carried out under identical conditions using a tissue array to be able to eliminate this cause of error and the conjugated Collagen IV antibody is well established, portraying specific staining for the other models, an error in the development of the HSE model within the collagen medium is most likely.

For analysis of structural and histological validity of the skin models proliferation marker Ki67 showed promising results with no distinction between the HSE model types. Control group and cytokine models all showed strong, specific and strictly localized Ki67 expression in the stratum basale, ascribable to correct development of epidermal and dermal structures among all the HSE models.

4.1.3 Epithelial barrier function of HSEs mimics inflammatory skin

The epithelial barrier is not only a visually analyzable feature but also one of the main factors involved in the pathogenesis of inflammatory skin diseases. Therefore, CODEX characterization of epithelial markers and barrier proteins was one of the key assessments to be made. There are many different proteins that can and need to be considered when talking about epidermal barrier function, plenty of which were included in the CODEX panel. The results for individual marker expressions vary among the samples and different proteins and are to be discussed in the following.

For instance, CODEX analysis found a strong downregulation of Filaggrin expression in the AD and psoriasis models compared to the untreated control models. The abundance of Filaggrin in the control model cannot be found in either of the cytokine models, which was portrayed by quantitative comparison of mean Filaggrin expression per unit area in the epidermis of all analyzed 3D human skin models after unpaired two-tailed t-test proved significant absence of Filaggrin expression among the epithelial cells of the cytokine models. This lack of abundant Filaggrin expression as seen in the control model could be a sign of possible impairment of epidermal barrier function due to deficiency in the mentioned structural protein. As illustrated in (McGrath and Uitto, 2008) Filaggrin is known as a key protein for skin barrier maintenance and is downregulated in

diseases with epidermal barrier disruption, making the described findings congruent with the common scientific understanding of barrier impairment in inflammatory skin.

Furthermore, CODEX analysis of epithelial barrier proteins Loricrin and Elafin showed changes in the respective marker expression among the psoriasis and AD models (Figure 10). Visually notable elevation of Elafin expression in the TH-2 and TH-17 cytokine models can be found compared to the untreated control model and statistical comparison of Elafin expression proves higher expression per cell for the TH-2 treated AD phenotype. This is interesting in terms of epidermal structure as Elafin acts modificatory in immune processes of the epidermis and is previously described to be of abundance in psoriatic skin (Kamsteeg *et al.*, 2010). Elafin serves as an important antimicrobial peptide and serine protease inhibitor with anti-inflammatory properties as well as stimulatory effects on cellular proliferation (Elgharib *et al.*, 2018). The lack of significant Elafin elevation in the TH-17 treated cytokine model, especially in comparison to the TH-2 model, could be a demonstration of limitations of quantitative analysis of the skin models. It raises the question whether the HSE models can correctly portray inflammatory skin in vitro, as there is no elevation of Elafin expression described in current scientific literature for AD skin.

In the HSE skin models mimicking psoriasis epidermal Elafin expression is visually increased, while Filaggrin expression is decreased, thus recapitulating the disease *in vitro*. However, a thickening of the epidermis is expected but not detectable looking at the illustrated HSE models for AD and PS. On the contrary the epidermis is thicker within the untreated model. This may be due to restricted cell proliferation under the influence of the cytokine treatment for the TH-2 and TH-17 models. While the AD model does show significant increase in Elafin expression, the statistic does not suggest a trend of elevation for the PS model. However, visually the expression of Elafin appears to be much stronger in the epidermis of the TH-17 treated model than in the untreated control. This, together with the epidermal thickening seen in the untreated model, may suggest statistic limitations as consequently there are less cells included in the analysis for the TH-17 model. This may not be representative of actual Elafin

expression levels and should be reevaluated by further quantification of marker expression taking the analyzed area and cell count into consideration. This is a restriction to be noted for the HSE models as generally speaking cell count is of much lesser number than for the actual human patient samples.

Loricrin, similarly to Filaggrin, is involved in skin barrier integrity by affecting corneocyte function. It is also important to evaluate *S. aureus* colonization, as adherence to the squamous epithelial cells is achieved by binding to Loricrin and cytokeratin 10 (Mulcahy *et al.*, 2012). Release of IL-4 and IL-13 reduces Loricrin expression and induces oxidative stress (Furue, 2020). Looking at the results for the TH-2 type, that includes cytokines IL-4, IL-5 and IL-13, a downregulation of Loricrin expression in the TH-2 treated HSE models was expected. However, in contrary there is significant upregulation of Loricrin expression per epidermal cell for the AD model. The TH-17 treated model does show a downregulation but proved less reliable for statistical comparison due to much smaller overall epidermal cell count.

The results for the two epidermal barrier proteins Loricrin and Elafin clearly indicate limitations especially for statistical comparability of the HSE models, even though reliably representing the dermal and epidermal construct and integration of characteristic proteins. There seems to be too much variation in factors like thickness of the epidermis and respective cell count to ensure a consistent structure of the HSEs treated with cytokines to adequately assess or represent the highly complex epidermis of inflammatory skin. Some of the tested models did present expected results in terms of epithelial marker expression but in the sum of the samples considered for analysis the statistical marker expression per cell among the samples did vary greatly and therefore needs to be interpreted with respect to the mentioned limiting factors.

4.1.4 NOS2 as psoriatic disease classifier

For both skin diseases thickening of the epidermis and changes in epidermal barrier proteins have been described and are discussed above. For characterization of distinction markers between AD and PS CODEX analysis on NOS2 was performed. Nitric oxidase synthase 2 (NOS2) has been used as a

clinical diagnostic tool to differentiate between AD and PS, as it is known to be upregulated in lesional psoriatic skin, an effect that is IL-17 dependent, and correlates with clinical and histological characteristics of psoriasis (Garzorz-Stark *et al.*, 2016). Most importantly, this upregulation was not found in AD skin or healthy control samples.

As there is visual and statistic proof of upregulation of epidermal NOS2 expression, the TH-17 cytokine model accurately illustrates psoriatic features regarding inflammation hallmarks. The TH-2 model representing AD skin shows no presence of epidermal NOS2 expression and therefore also mimics AD skin satisfactorily. The statistical evidence and significance of the data despite the restrictions due to small epidermal cell count support the assumption of HSE models validity in accurate representation of inflammatory skin.

4.1.5 Nitric oxide donors present a new therapeutic perspective for psoriasis

Recent research shows clinical implications of NOS2 expression that can be employed in therapeutic approaches for treatment of psoriasis. Even though NOS2 expression levels are elevated in psoriasis, Köhler *et al.*, 2024 present a prevention of NOS2 translation by microRNA-31, which is involved in post-transcriptional regulation and translation of mRNAs (Yu *et al.*, 2018). This interferes with the completion of the translation process of NOS2 mRNA to protein. microRNA-31 is induced by IL-17 and therefore activated within psoriatic skin. Inhibition of NOS2 translation leads to lower levels of nitric oxide (NO), which increases keratinocyte proliferation. A therapeutic approach of increasing cellular nitric oxide levels to counteract the effect of microRNA-31 showed promising results in a mouse model, putting future treatment by NO donor therapy into prospect for psoriasis patients (Köhler *et al.*, 2024).
This is consistent with the data presented for the cytokine HSE models and could therefore be continued by further testing of the HSE models with NO treatment as done in the mouse model.

4.1.6 Staphylococcus aureus colonization is enhanced by an abundance of Polymorphonuclear Neutrophils

CODEX fluorescence image comparison of *S. aureus* expression in *S. aureus*-infected untreated control, *S. aureus*-infected TH-17 and *S. aureus*-infected TH-2 HSEs showed strong epidermal expression of *S. aureus* antigen in the TH-2 cytokine model. Quantitative data of Figure 14 portrayed comparison of *S. aureus* expression per area in the epidermis of the 3D human skin models infected with Staphylococcus aureus. The significant difference in marker expression upon the cytokine models as well as in comparison to the untreated control indicates a positive outcome of the experimental setup.

As all models were treated under the same conditions and with the same concentration of *S. aureus*, abundance of *S. aureus* expression in the TH-2 cytokine model shall be interpreted as valid representation of the AD phenotype. Due to defects in the epidermal barrier like previously discussed as well as inflammatory and microbial properties in the microenvironment of AD skin it is assumed that many factors play a role in *S. aureus* colonization. One epidermal protein occupies an important role as moisturizing factor of the skin and hereby stabilizing the natural barrier function. Filaggrin, more precisely its breakdown products, presents natural moisturization for the epidermis and enables correct function of corneocytes. As Filaggrin expression is downregulated in inflammatory skin the moisturizing effects are omitted which causes a change in corneocyte conformation. Corneocyte morphology is altered causing apical villus-like projections which is suspected as a location of accessibility for ligands in the skin's environment, such as *S. aureus* (Geoghegan, Irvine and Foster, 2018).

Another surface protein expressed on the *S. aureus* bacterium is clumping factor B (ClfB), a cell surface-associated protein implicated in virulence by promoting bacterial attachment and inducing the formation of bacterial clumps. ClfB mediates adherence to squamous epithelial cells by binding to epithelial proteins Loricrin and cytokeratin 10 (Mulcahy *et al.*, 2012). Interestingly, Loricrin expression is described to be downregulated by TH-2 cytokines which we could not observe for the TH-2 HSE model. Considering the notable abundance of *S.*

aureus in the TH-2 model and suspecting binding of the bacterium to the cell via Loricrin, this could explain the missing downregulation in Loricrin expression. *In vivo* TH-2 cytokines are present for the AD phenotype to occur in the first place, which then makes the skin susceptible to *S. aureus* colonization. *In vitro* cytokine treatment of the HSE models is contemporaneous with *S. aureus* infection. This leaves minimal time for TH-2 cytokines to take effect on Loricrin expression before binding of *S. aureus* occurs – therefore possibly interfering with the downregulation that would otherwise be caused by the cytokines. However, this hypothesis is in need of further experimental validation and so far shall not be taken as all-encompassing explanation of differences in *in vivo* and *in vitro* expression patterns.

4.2 Patient samples

In contrast to the analyzed HSE models, the patient samples were tested with a much broader panel design with consideration of the expected tissue complexity. As the panel included more than 50 different markers, not all markers can be discussed in the following. Proteins that were analyzed to validate established expression patterns within skin tissue are not mentioned below.

4.2.1 Changes to epithelial barrier proteins in inflammatory skin diseases

When looking at the results for Filaggrin expression between healthy skin samples and AD samples, Filaggrin expression visually appears to be stronger in the healthy tissue – especially considering expression in the stratum corneum that was preserved in the sample of the pictured CODEX image. Statistically there was no difference in mean marker expression between the two groups, which is most likely due to unsuitable analysis. Filaggrin is exclusively expressed in the epidermis, which makes analysis of mean marker expression in the whole tissue prone to inaccurately display expression patterns. Looking at the AD sample, thickening of the epidermis is visible, especially when compared to the healthy sample. Furthermore, it seems the typical layers of the epidermis are assembled less strictly in the AD sample as the stratum basale and dermis cannot be clearly

differentiated.

To enable data comparison of marker expression, another approach was chosen for statistical analysis taking expression per cell and location of marker expression into account. The results shown in Figure 19 display similar findings as seen in Figure 8 with eminent Filaggrin expression in all tissue samples. Again, there is preserved part of the stratum corneum of the healthy skin sample that depicts very strong Filaggrin expression. Visually Filaggrin expression seems to be spread only as far as the stratum spinosum, not reaching the stratum basale which can be observed across all groups. Statistical analysis per epidermal cell showed similar expression rates for the healthy tissue and PS sample, while the AD tissue displayed elevated Filaggrin expression per epidermal cell. This is a surprising result as visually expression per epidermal cell appears to be strongest in the healthy skin tissue. Therefore, limitations of the statistical cell analysis need to be considered:

The stratum corneum emitting strong Filaggrin signal may be one explanation, as for cell analysis vital nuclei are segmented and data is based only upon those cells. The Filaggrin expression in the stratum corneum thus is not included in the statistics as it does not contain vital cells. Moreover, higher cell density and cell count within the inflammatory skin samples may lead to less accurate segmentation and could thereby distort analysis of expression per cell. To assess the limitations, quantification of signal to noise ratio for Filaggrin was performed and showed satisfying results. As initially expected, Filaggrin signal can be seen to be downregulated for the AD and PS samples while being strongly emitted within the control group. Strong statistical significance of Filaggrin downregulation for the PS samples suggests consonant findings with the visual data of the CODEX images.

Visual Elafin expression patterns are similar upon all tested groups as strictly found in the stratum granulosum, while statistical analysis of marker expression per cell reveals elevation of Elafin expression for patient samples. When looking at the single cell analysis in Figure 20 it is apparent that in contrast to data for Filaggrin expression, Elafin is elevated not only in PS samples but also in AD samples when compared to the healthy control. Nuclear, cytoplasmic and overall

Elafin expression are found to be higher in PS samples than in samples of healthy skin. A summary of the quantification of mean marker expression of the epidermal barrier protein Elafin can be seen Figure 18. Elafin mean marker expression of the PS samples proves significantly higher than for the AD group, with a wider scatter of values between the individual analyzed samples. This scatter is not found for the AD or control samples, which may indicate generally less activity of the epidermal protein for those two groups. The variation in mean marker expression of Elafin for the PS samples could be a representation of different stages of the inflammatory processes Elafin is involved in. Elafin is considered to be a PS-specific biomarker and involved in keratinocyte proliferation leading to phenotypic epidermal hyperplasia seen in psoriasis patients. The disease is characterized by keratinocytes demonstrating abnormally high proliferation rates and differentiation errors, which is associated with infiltration of multiple inflammatory cells (Zhou *et al.*, 2022). In line with scattering data for Elafin expression among the PS samples, keratinocytes play a vital role in all phases of psoriasis pathogenesis and the varying levels but consistent elevation of Elafin expression could be indicative of the samples being taken from patients within different phases of psoriasis. This is supported by findings that found Elafin to be elevated even in non-lesional skin of psoriasis patients (Berekmeri *et al.*, 2024)

Loricrin expression is shown in Figure 15 and displays expression in the stratum granulosum of the healthy control group as well as in AD patient samples. Statistically there is no significant difference in mean marker expression, as there is a wide scatter of the mean marker expressions among the AD samples. This could be explained by the thickened epidermis of the AD samples and therefore less valid statistical representation of mean marker expression due to high epidermal cell count. As Loricrin expression focuses on the stratum granulosum, analysis of the epidermis and dermis for mean marker expression seems an inadequate form of data comparison.

To regard this, statistical analysis was made using single cell segmentation with respective marker expressions per cell. This data as visualized in Figure 16 suggests Loricrin expression to be similar between AD and control samples, while the PS sample shows almost no Loricrin expression in the epidermis. Statistically

we see a clear shift in results compared to the mean marker expression, as the epidermal Loricrin expression per cell normalized by nuclear expression of DRAQ5 is highest within the cytoplasm of the healthy control group followed by PS samples. Epidermal cytoplasmic Loricrin expression in AD patient samples is decreased with strong significance $p < 0.0001$.

Further analysis regarding mean marker expression and signal to noise ratio of Loricrin expression revealed mixed results and proved statistical outliers among the analyzed samples. The hypothesis upon overview of the different statistical approaches is an unsuitable quantitative approach for Loricrin analysis due to its strict localization in the stratum granulosum. Visually Loricrin signal is detected as a fine line in the upper epidermis and can therefore not statistically be accurately represented by analysis of the whole epidermis. This suggests necessity of statistical CODEX analysis to be made based on visual data and according to expression patterns of the induvial markers to be quantitatively accurate, representative of marker expression and ensure comparability between the groups.

4.2.2 Neutrophil abundance in inflammatory skin and NETosis

As atopic dermatitis and psoriasis both represent skin diseases with pathogenesis that excessively relies on inflammatory processes, analysis of markers visualizing the respective immune responses and protein activities is a priority in characterization of inflammatory skin. The processes involved in disease pathogenesis and inflammation progress are complex, diverse and interactions are not yet understood to the entire extent.

The first marker to be discussed is the granule enzyme myeloperoxidase (MPO) found as one of the main enzymes in neutrophils and known to be essential in formation of neutrophil extracellular traps (Metzler *et al.*, 2011). CODEX imaging shows strong epidermal nuclear and cytoplasmic expression of MPO in PS and AD samples, while MPO expression in the healthy control is not as presently found epidermally and focuses more on the dermal compartment. Analysis of the mean marker expression proves significant upregulation of MPO expression across all tested samples for AD patients and statistical analysis of epidermal

MPO expression per cell proves significant increase of MPO expression in both inflammatory skin groups compared to the healthy control. Cytoplasmic MPO expression is highest in the AD group, while nuclear MPO expression is most prominent in the PS group.
The abundance of neutrophils expressing MPO in samples of inflammatory skin is conclusive with the assumption of elevated immune response in lesional skin. Also, considering data on NET formation being enabled by MPO, the preposition of NET formation being induced in AD skin seems supported by the elevation of MPO expression seen in AD samples compared to PS samples. This needs to be correlated with other markers for NETosis like citH3 and Neutrophil Elastase and is discussed below.

Another important marker of inflammatory processes is Neutrophil Elastase (NE), which is found in neutrophils as a serine protease responsible for inflammation processes and progression of bacterial infections. Its activity is directly associated with disease state and severity (Zeng *et al.*, 2023). Figure 22 shows CODEX images of NE expression focused on the epidermal regions of representative samples for the healthy control and AD group with clear expression patterns of NE epidermally and dermally for the AD sample. This is supported by mean marker expression of NE, which validates a significantly increased NE expression among the AD samples in contrast to the healthy control samples.
Additionally, Figure 19 shows similar results including the PS samples and manages statistical comparison of marker expression per epidermal cell. Even though NE expression is visibly found mainly in the dermal region below the basement membrane, there is still significantly higher expression of NE within the epidermis for the analyzed cells in AD and PS samples compared to the healthy samples. There is no significant difference between the two inflammatory diseases regarding single cell expression of NE. Similarly to elevation of MPO expression, the significantly higher NE expression rates among the samples of inflammatory skin can be seen as indicators of an immune response taking place in lesional skin. Presence of neutrophils is expected and supported by previous

findings, especially in psoriatic skin the neutrophil abundance is correlated with initial and maintenance phases of the disease and seen as histopathological hallmark of psoriasis (Chiang *et al.*, 2019). For AD the exact function of neutrophils, though described as elevated, remains unclear but is suspected to play an important role in AD pathophysiology. It is supposed that formation of neutrophil extracellular traps mediated by Neutrophil Elastase and MPO may further worsen AD (Chiang *et al.*, 2024). This is congruent with the findings of the CODEX analysis performed and proves active neutrophil infiltration for samples of the AD and PS group.

Histone H3 forms the nucleosome as one of four core histones, presents a vital part of chromatin and is highly linked to DNA replication. Its citrullination results in activation and loosening of chromatin structure for gene transcription. For Histone H3 a close connection to NET formation is observed, citrullination being the critical step to initiating NETosis. Neutrophils then release DNA, histones, including Histone H3 being released in its citrullinated form, and proteins like MPO and NE (Osca-Verdegal *et al.*, 2022).
CODEX analysis reveals significant elevation of Histone H3 for the PS samples and a trend towards elevation among the AD group compared to the healthy control. The data for the citrullinated form revealed strong elevation of citH3 in the AD group, but none in the PS group. This could indicate active NETosis in the AD patient samples, while in the psoriasis samples NETosis may be less present. Elevated Histone H3 levels in its deactivated state as seen for the PS samples could reflect elevated DNA replication as part of the inflammatory processes without distinct apoptosis of neutrophils.
Citrullinated Histone H3 (citH3) is product of conversion of histone H3 and found to be a central marker for neutrophil extracellular traps (NETs). CitH3 is released upon strong stimulation of neutrophils and found in the bloodstream during NETosis. Also, current research suggests levels of citH3 correlating with levels of Neutrophil Elastase and myeloperoxidase, all known to induce NETosis (Thålin *et al.*, 2018). The expression of citH3 is shown in Figure 27 for AD and healthy control samples. While visually there is clearly a much more present expression

of citH3 in the epidermis of the AD sample, this difference isn't statistically significant when comparing the mean marker expression of citH3 across the samples, even though showing a tendency towards elevation among AD samples. Further analysis is illustrated in Figure 26 for AD, PS and control samples and respective citH3 expression. Visually the pictures are congruent with the findings of Figure 27 and show strong epidermal expression of citH3 in the AD sample, while the control group and PS samples show a less vibrant expression of citH3 in the epidermal region. Statistically this proves to be significant on a single cell level, as marker expression per cell is highly significantly elevated across the AD group, especially looking at epidermal cytoplasmic citH3 expression. There is a slight elevation of citH3 expression in the PS group compared to the healthy control group, but this does not prove significant. Visually citH3 expression in the PS sample appears more diffuse and is found dermally and epidermally, while AD shows more of an epidermal abundance. This supports the current understanding of neutrophil infiltration in inflammatory skin as well as high probability of NETosis in the AD sample.

As all markers known to be involved in NETosis are significantly overexpressed among the AD samples it is to be suspected that coexistence of MPO, NE and citH3 is a visual and quantitative representation of NET formation within inflammatory skin. The lack of citH3 elevation corelated with increased Histone H3 levels in psoriasis are likely an indication of distinguished DNA replication in response to inflammatory processes, in contrast to pronounced NETosis in the AD samples.

4.2.3 Interaction of inflammatory markers in response to reactive oxygen species

Oxidized DNA lesions by reactive oxygen species (ROS) are closely linked to inflammation (Karsten, 2021) and enzymes for regulation of oxidized and damaged DNA are therefore crucial for cell function and play a vital role in disease pathogenesis (Tumurkhuu *et al.*, 2020). Oxoguanisine glycolase 1 (OGG1) is a DNA repair enzyme known for its relevance regarding DNA lesions. Figure 23 represents CODEX analysis of mean marker expression of OGG1 and

shows significantly increased expression of OGG1 in the AD group, but also wider data scatter between the different samples.

Moreover, CODEX images of OGG1 for all tested groups presented in Figure 20 fail to demonstrate visual differences in OGG1 expression dermally between the subgroups, while epidermal expression is difficult to adequately evaluate due to the overlapping Elafin expression. Statistical analysis of epidermal OGG1 expression per cell reveals a significantly increased OGG1 expression among the AD group, especially for cytoplasmic marker expression.

OGG1 expression among the AD group marks probable exposure to reactive oxygen species that caused DNA damage and led to an upregulation of OGG1 within the inflammatory skin samples. The lack of OGG1 expression in the psoriasis samples indicates less exposure to ROS and therefore smaller extent of DNA damage. The high levels of ROS present in AD patients are associated with cytokines IL-4, IL-13 and IL-17 and attributed to environmental, physical or psychological stressors such as air pollution causing disruption of the skin barrier and thereby leaving the skin prone to further environmental harm (Md Jaffri, 2023). An overview of the stressors described and the pathway of inflammation as well as marker interaction can be seen in Figure 34.

For psoriasis patients ROS elevation is noted due to proinflammatory cytokines IL-6, IL-17 and IL-22. The cascade triggered by the induced ROS is depicted in a simplified form and shows interaction of many different inflammation markers. UV radiation and air pollution trigger ROS and thereby activate a pathway of MAPK, NF-kB and HMGB1. This is aggravated through LL37 and HBD3 by phosphorylation of p38 and ERK, leading to DNA damage and inflammation as well as triggering conformation change of Histone H3 to its citrullinated form. This again acts as a trigger for NETosis, releasing MPO, Neutrophil Elastase and citH3 into the extracellular space together with the chromatin strands that form the Neutrophil extracellular traps. The described signaling pathways are dysregulated affecting vital cell functions like proliferation and keratinization (Md Jaffri, 2023). Research found different stages of disease in psoriatic skin to closely be related with oxidative stress and subsequently to NET formation (Chiang *et al.*, 2019).

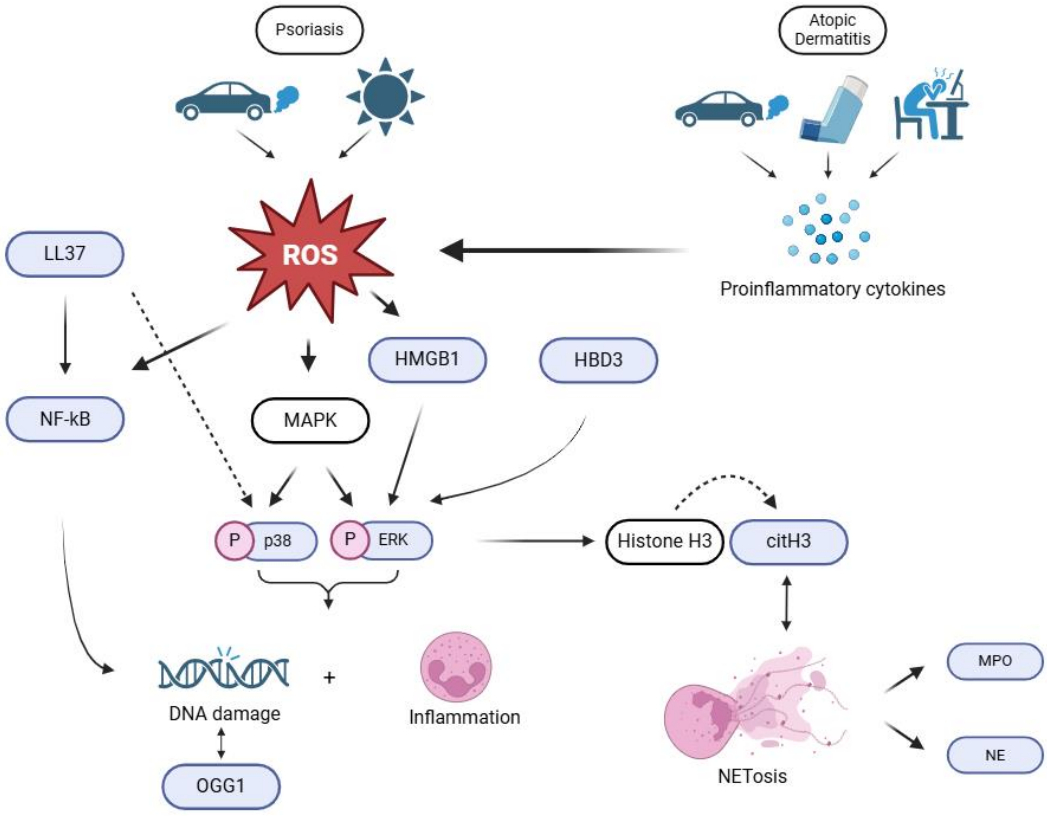

Figure 34: Overview of interactions between inflammation markers. Figure created using Biorender.com. Adapted from (Chen, Kang and Tang, 2022; Md Jaffri, 2023). Blue labels indicate markers included in the CODEX panel for characterization of inflammatory skin.

High mobility group box 1 (HMGB1) does not only promote inflammatory diseases but is closely associated with NETosis and disease severity correlates with HMGB1 levels (Satoh, 2022). As HMGB1 serves as a biomarker for inflammatory processes, CODEX analysis of its expression is interesting in terms of possible correlations with disease state and comparison between PS and AD. The HMGB1 expression in the skin of AD patients compared to healthy controls is outlined in Figure 24 and Figure 25 and reveals significantly increased HMGB1 mean marker expression in the AD group. Quantification of total, nuclear and cytoplasmic HMGB1 expression in AD skin compared to healthy control samples proves increase of cellular and cytoplasmic HMGB1 expression upon AD samples. Representative CODEX images for all subgroups show epidermal HMGB1 expression mainly as nuclear staining. Visually HMGB1 expression appears to be prominent in AD and PS samples compared to the control group with

significantly higher nuclear HMGB1 expression in the epidermis for PS samples and further elevation in AD samples.

The results support current knowledge upon the role of HMGB1 in inflammatory processes. The elevation among the two inflammatory skin diseases is representation of the pathway presented in Figure 34 which reveals involvement of HMGB1 in the immune response to external factors causing ROS as discussed above. Elevated levels of HMGB1 expression in AD patient samples compared to PS patients could be an implementation of NET formation and NETosis in Atopic Dermatitis as a result of co-upregulation of citH3, NE and MPO. The effect of this upregulation on *S. aureus* colonization is considered under 4.2.4.

As part of the downstream pathway of the mentioned factors causing phenotypic disease hallmarks in response to external stressors activated byproducts of the NF-κB and MAPK signal path play an important role in activation of neutrophils and regulation of the immune response.

Nuclear Factor-κB (NF-κB) is widely accepted as pivotal mediator of inflammatory processes as it is involved in regulation of cytokine release, activation and differentiation of immune cells and contributes to pathogenesis of several inflammatory diseases as transcription factor (Liu *et al.*, 2017). Activation of NF-κB is regulated by pro-inflammatory cytokines and critical for phosphorylation which modulates NF-κB activation and influence in acute and chronic inflammation (Viatour *et al.*, 2005). CODEX analysis of mean marker expression of phosphor-NF-κB proves significantly elevated for the AD and PS samples compared to the healthy control group and equivalent among the two inflammatory diseases.

Mitogen-activated protein kinase (MAPK) cascades mediate many cellular responses influencing proliferation, differentiation and inflammation processes. Two important members of the MAPK family are extracellular signal-regulated kinase (ERK) and p38 MAPK. Both kinases are activated by phosphorylation which leads to increased enzymatic activity and thereby changes to cell differentiation and proliferation. Interestingly, p38 can regulate the NF-κB pathway by interacting with respective transcription factors. The interactions are not only plentiful and highly complex but also still subject to further research as

they are involved in most cellular processes mediating proliferation, differentiation, inflammation and apoptosis and therefore present leading forces in the pathomechanism and treatment of inflammatory diseases and cancer (Zhang and Liu, 2002). CODEX analysis of phospho-ERK (pERK) and phospho-p38 (pp38) represent significantly lower expression of phospho-ERK for the PS group when comparing PS and AD and a trend of elevation of pp38 among the inflammatory skin samples without statistical significance compared to the healthy control samples.

Elevation of phospho-NF-κB, pERK and pp38 among the AD samples accounts for activity of inflammation processes within the lesional skin as described above. The significant upregulation of phospho-NF-κB in both inflammatory skin diseases is likely result of ROS damage among the samples and possibly associated with upregulation of LL37, leading to strong activation of the NF-κB pathway. As biomarker for inflammation an upregulation of phospho-NF-κB is expected for both samples of inflammatory skin diseases and shows expression of a very similar extent for both subgroups. Looking at the MAPK pathway, trends of upregulation of the phosphorylated kinases can be seen in the AD group while there is no indication for an upregulation of pERK in the PS group. This correlates with findings for HMGB1 expression levels being significantly higher among the AD samples and therefore priming upregulation of pERK in the downstream cascade. Similarly to the AD group, there is a visible trend towards an upregulation of pp38 in the PS group that is not statistically significant but could correspond with elevated LL37 levels, that could thereby lead to an elevated expression of pp38, while not influencing the MAPK pathway of pERK. In summary it seems activation of the MAPK pathway is more present among the AD group, while the NF-κB pathway is elevated equally.

Antimicrobial peptides (AMPs) are pivotal as the first line of defense and therefore key factors of innate immunity. They are involved in cytokine production and many immunomodulatory processes are mediated by AMPs as part of signaling cascades. Main AMP production is found in keratinocytes presenting an important mechanism for immune responses in the epidermis. Two of the most

important AMPs are human cathelicidin LL37 and human β-defensin (HBD3), both carrying antiviral and immunomodulatory properties (Chessa *et al.*, 2022). Figure 29 shows significantly higher expression of LL37 for the PS group and a trend of elevation among the AD group that proves no statistical significance. When comparing HBD3 expression there is clear upregulation only upon the AD model, that cannot be found for the control or PS group. Research showed attenuation of barrier disruption mediated by HBD3 in a mouse model of atopic dermatitis and suggests positive immunomodulatory effects of HBD3 that could also be used for therapeutic purpose (G *et al.*, 2022). The lack of HBD3 expression among the PS samples is not described in literature so far but does correspond with missing pERK upregulation, that is inter alia mediated by HBD3. Hollox *et al.*, 2008 described elevated genomic copy numbers of beta-defensin but discussed that due to the location of the genes encoding HBD2, HBD3 and HBD4 distinction between one gene or a combination of all three genes cannot be made. Therefore, upregulation of HBD2 and HBD4 is possible with missing upregulation of HBD3.

LL37 shows significant elevation in the PS samples correlating with the increase of pp38 and NF-κB discussed above. The differences in expression levels of antimicrobial peptides between the two inflammatory skin diseases could be a sign of suspected bacterial colonization and subsequent effects on epidermal barrier and immunomodulatory mechanisms. The abundance of LL37 seen for psoriasis but not for AD suggests a counteractive mechanism of HBD3 and LL37 that trigger the downstream pathways leading to DNA damage, barrier dysfunction and disease specific inflammation in determined ways.

To conclude influence of ROS on inflammatory skin it is to say that the high abundance of OGG1 found among the AD samples stands in support of the assumption that external stressors activate a cascade of cytokine release leading to elevation of ROS and thereby damaging DNA strands. This presents a trigger mechanism for OGG1 elevation to reduce the DNA damage. Elevated levels of HMGB1 in combination with upregulation of neutrophil markers MPO, NE and citH3 implement indicators of NET formation and NETosis in AD patients. Changes to the activation states of MAPK and NF-κB pathways vary in both

inflammatory skin diseases, are results of ROS damage and seem to be associated with upregulation of LL37 and HBD3.

4.2.4 S. aureus colonization is enhanced by presence of PMNs and NET formation

In lesioned skin the compromised diversity of the microflora allows growth of pathogens like *S. aureus* (Nakatsuji *et al.*, 2017). For patients suffering from atopic dermatitis a strong *S. aureus* colonization has been observed and known for many years, but explanation for this exclusive bacterial abundance that cannot be found in other inflammatory diseases with flaws to epidermal barrier function is unaccounted for. With CODEX analysis of *S. aureus* expression it becomes eminent that epidermal and dermal expression of S. aureus is very substantial within the AD sample, while the samples for PS patients and the healthy control group show much less expression of *S. aureus*. Quantification of the images proves significant elevation of *S. aureus* expression within the AD samples. The results exhibit colonization of *S. aureus* for the AD group and a lack thereof for the PS group. Looking at the CODEX findings for the presence of neutrophils, elevated levels of neutrophil markers MPO, NE and citH3 were found in AD patients, that could not be seen to the same extent for PS samples. Furthermore, upregulation of OGG1, HBD3 and HMGB1 that all play a vital part in neutrophil activation and pathways triggered by ROS, was seen for AD samples and may stand as starting point for AD pathogenesis. These data indicate that PMNs in the skin of atopic dermatitis patients might increase *S. aureus* skin colonization by the induction of ROS and increased levels of HMGB1. The unique mechanism of PMNs to form NETs likely takes part in the pathomechanism that enables *S. aureus* colonization: Research supports the idea that initially NET formation can have positive effects as part of the innate immune system but needs to be strictly balanced. Strong induction of NETs, for example by increased levels of HMGB1 and HBD3 or generally higher counts of ROS, reveal negative impacts of NETosis as it leads to an imbalance to macrophage clearance. Thereby the process of NETosis can turn out to be a driver of chronic inflammation, hinder wound healing and damage skin tissue (Sabbatini, Magnelli and Renò, 2021). The negative

effects of a dysregulation in NETosis stand in line with elevated *S. aureus* colonization seen for lesional AD skin and are plausibly induced by an upregulation of AMPs and other proteins involved in inflammatory pathways.

4.3 Cell culture

CD3 staining for comparable models showed more successful integration of lymphoma cells for the HUT 78 cell line than the HH line but with successful visible integration for both cell lines. To minimize any errors both cell cultures were handled identically and sewed onto the skin models simultaneously under the same conditions. The integration of HH cells into the skin models to a much smaller extent than seen for the HUT 78 cell line may be due to the derivation of HUT 78 cells from a patient with Sezary syndrome known to be an especially aggressive form of cutaneous T-cell lymphoma, which may have led to more rapid or more sufficient infiltration of the tumor cell line (Vakiti, Padala and Singh, 2025).

4.3.1 CD3 staining for TH-17 HSEs with HUT 78

The positive CD3 staining on top of the stratum granulosum cannot be seen as positive cell integration (Figure 33). It is to be assumed that the cells on top just attached to the outer layer of the epidermis but did not successfully penetrate the epidermal barrier. Those cells are likely to be wiped or washed off, which can also be suspected is what happened for the skin model portrayed in Figure 32 on the right-hand side. Fortunately, CD3 staining is also found positive beneath what can be interpreted as the stratum basale due to less dense cell configuration. This indicates successful integration into the epidermis down to the dermal layer of the skin models, as those tumor line cells must have passed the epidermal barrier after sewing of the HUT 78 Cutaneous T-cell lymphoma (CTCL) cells.

As for a difference regarding cytokine treatment on the skin models there is no eminent change in cell integration, neither positive nor negative. This may be due to the thin epidermal barrier of the skin models, that may already be easily penetrable for the aggressive tumor cell line. Looking at the results found in

patient samples for PS and AD skin samples, it is possible that cytokine treatment with TH-2 cytokines for AD phenotype may lead to even higher cell count of integrated CTCL cells due to the impaired epidermal barrier. This is subject for further experiments and shall be evaluated also by CODEX imaging of the existing models. Furthermore, tests are to be carried out on the models using common chemotherapeutics for CTCL to verify the accuracy and conformity to reality of the CTCL skin models.

4.4 Outlook

There are several therapeutic approaches for the treatment of inflammatory skin diseases, most relying on topical steroid or systemic immune treatment. Recent advances give prospect to new treatment possibilities by inhibition of NOS2 translation through increasing cellular nitric oxide levels (Köhler *et al.*, 2024) or by the targeted oral peptide Icotrokinra that selectively blocks the IL-23 receptor and demonstrated promising results in a Phase 3 trial for severe plaque psoriasis (*Icotrokinra delivered an industry-leading combination of significant skin clearance with demonstrated tolerability in a once daily pill in Phase 3 topline results*, 2024).

Furthermore, successful clinical trials expanded therapeutic options for AD patients and include therapies targeting cytokines IL-4, IL-13, and IL-31 (Meledathu, Naidu and Brunner, 2025).

However, many underlying mechanisms of the diseases remain unclear and are subject to further research that may continue to bring forth novel therapeutic prospects and broaden the knowledge and understanding on inflammatory pathways and pathomechanisms of Psoriasis and Atopic Dermatitis. CODEX presents a method enabling close study of marker interaction and neighborhood analysis that can take part in opening new possibilities for research on molecular mechanisms and complex pathways. Analysis of inflammatory diseases on HSE models, that aim to better represent human skin than mouse models, demonstrates a novel chance for faster testing of auspicious therapeutics and possibly more accurately represent favorable as well as adverse effects on human skin.

5 Conclusion

Accounting for omnipresent diseases, inflammatory skin defects like Psoriasis and Atopic Dermatitis deserve close and thorough research to investigate pathological mechanisms and drivers of inflammation. Using CODEX to characterize the complex constructs of inflammation cascades and antimicrobial pathways describes a novel approach to better understand molecular interactions of inflammatory skin diseases. This work demonstrates a method aiming to visualize and quantitatively analyze the effects of inflammation on immune as well as DNA damage and epithelial markers.

Suitability of 3D human inflammatory skin models for use in functional assays *in vitro* was successfully visually validated and proved histological accordance to inflammatory skin. However, quantification of marker expression evinced limitations due to small cell count and missing uniformity.

CODEX analysis of patient samples revealed enhanced presence of Polymorphonuclear neutrophils, showing high expression of the neutrophil marker Neutrophil Elastase in skin of AD patients and an elevation of NET markers MPO and citH3, as well as a significant increase of HMGB1 expression in AD skin. This correlated with more severe *S. aureus* colonization, DNA damage by reactive oxygen species and activation of inflammatory cascades. The presented data hereby confirms preliminary findings *in vitro* that illustrated an enhancement of bacterial colonization in Atopic Dermatitis through NET formation and adds a possible explanation for phenotypical differences between PS and AD by revealing dissimilarities between the samples in reaction to ROS exposure.

Furthermore, this work lays the foundation for more detailed exploration of CTCL progression in skin models and the prospects of viable reflection of CTCL in HSE models for testing potential therapeutics in vitro. Tailored analysis methods that account for marker-specific localization and expression patterns are essential for advancing our understanding of inflammatory skin diseases and identifying precise therapeutic strategies.

Zusammenfassung

Entzündliche Hauterkrankungen wie Psoriasis und atopische Dermatitis sind allgegenwärtig, was die Notwendigkeit der Forschung an pathologischen Mechanismen und Triebkräfte der zugrundeliegenden Entzündung nahelegt. Die Verwendung von CODEX zur Charakterisierung von Entzündungskaskaden und antimikrobiellen Stoffwechselwegen stellt einen neuen Ansatz dar, um die molekularen Interaktionen bei entzündlichen Hauterkrankungen besser zu verstehen. Diese Arbeit demonstriert daher eine Methode, die darauf abzielt, die Auswirkungen von Entzündungen auf das Immunsystem sowie auf DNA-Schäden und epitheliale Proteine zu visualisieren und quantitativ zu analysieren. Die Eignung der menschlichen 3D-Hautmodelle für funktionelle Tests in vitro wurde erfolgreich visuell validiert und die histologische Übereinstimmung mit entzündeter Haut nachgewiesen. Die Quantifizierung der Markerexpression war jedoch aufgrund der geringen Zellzahl und der fehlenden Einheitlichkeit eingeschränkt.

Die CODEX-Analyse der Patientenproben zeigte ein verstärktes Vorkommen polymorphkerniger neutrophiler Granulozyten, der neutrophilen Marker Neutrophile Elastase, MPO und citH3, sowie eine signifikante Zunahme der HMGB1-Expression bei Patienten mit atopischer Dermatitis.
Dies korrelierte mit einer stärkeren S. aureus-Besiedlung, DNA-Schäden durch reaktive Sauerstoffspezies und der Aktivierung von Entzündungskaskaden. Die vorgestellten Daten bestätigen vorherige in vitro Ergebnisse, die eine Verstärkung der bakteriellen Besiedlung bei atopischer Dermatitis durch NET-Bildung zeigten, und liefern darüber hinaus eine mögliche Erklärung für die phänotypischen Unterschiede zwischen PS und AD durch gezeigte Abweichungen in der Reaktion auf die ROS-Exposition. Darüber hinaus legt diese Arbeit den Grundstein für eine detailliertere Untersuchung der Progression des kutanen T-Zell-Lymphoms in Hautmodellen und deren Testung therapeutischer Interventionen für CTCL.

6 Bibliography

Abreu-Velez, A.M. and Howard, M.S. (2012) ‘Collagen IV in Normal Skin and in Pathological Processes’, *North American Journal of Medical Sciences*, 4(1), pp. 1–8. Available at: https://doi.org/10.4103/1947-2714.92892.

Baertsch, M.-A., Nolan, G.P. and Hickey, J.W. (2022) ‘Multicellular modules as clinical diagnostic and therapeutic targets’, *Trends in Cancer*, 8(3), pp. 164–173. Available at: https://doi.org/10.1016/j.trecan.2021.11.004.

Balato, A. *et al.* (2019) ‘Human Microbiome: Composition and Role in Inflammatory Skin Diseases’, *Archivum Immunologiae Et Therapiae Experimentalis*, 67(1), pp. 1–18. Available at: https://doi.org/10.1007/s00005-018-0528-4.

Bankhead, P. *et al.* (2017) ‘QuPath: Open source software for digital pathology image analysis’, *Scientific Reports*, 7(1), p. 16878. Available at: https://doi.org/10.1038/s41598-017-17204-5.

Berekmeri, A. *et al.* (no date) ‘Epidermal proteomics demonstrates Elafin as a psoriasis-specific biomarker and highlights increased anti-inflammatory activity around psoriatic plaques’, *Journal of the European Academy of Dermatology and Venereology*, n/a(n/a). Available at: https://doi.org/10.1111/jdv.20289.

Bitschar, K. *et al.* (2019) ‘Lugdunin amplifies innate immune responses in the skin in synergy with host- and microbiota-derived factors’, *Nature Communications*, 10(1), p. 2730. Available at: https://doi.org/10.1038/s41467-019-10646-7.

Bitschar, K. *et al.* (2020) ‘Staphylococcus aureus Skin Colonization Is Enhanced by the Interaction of Neutrophil Extracellular Traps with Keratinocytes’, *Journal of Investigative Dermatology*, 140(5), pp. 1054-1065.e4. Available at: https://doi.org/10.1016/j.jid.2019.10.017.

Black, S. *et al.* (2021) ‘CODEX multiplexed tissue imaging with DNA-conjugated antibodies’, *Nature Protocols*, 16(8), pp. 3802–3835. Available at: https://doi.org/10.1038/s41596-021-00556-8.

Bowcock, A.M. (2004) ‘The genetics of psoriasis, psoriatic arthritis and atopic dermatitis’, *Human Molecular Genetics*, 13(90001), pp. 43R – 55. Available at: https://doi.org/10.1093/hmg/ddh094.

Chessa, C. *et al.* (2022) ‘Antiviral Effect of hBD-3 and LL-37 during Human Primary Keratinocyte Infection with West Nile Virus’, *Viruses*, 14(7), p. 1552. Available at: https://doi.org/10.3390/v14071552.

Chiang, C.-C. *et al.* (2019) ‘Neutrophils in Psoriasis’, *Frontiers in Immunology*, 10, p. 2376. Available at: https://doi.org/10.3389/fimmu.2019.02376.

Chiang, C.-C. *et al.* (2024) ‘Neutrophils in Atopic Dermatitis’, *Clinical Reviews in Allergy & Immunology*, 67(1–3), pp. 21–39. Available at: https://doi.org/10.1007/s12016-024-09004-3.

Chieosilapatham, P., Ogawa, H. and Niyonsaba, F. (2017) ‘Current insights into the role of human β-defensins in atopic dermatitis’, *Clinical and Experimental Immunology*, 190(2), pp. 155–166. Available at: https://doi.org/10.1111/cei.13013.

Cho, S.H. *et al.* (2001) ‘Fibronectin and fibrinogen contribute to the enhanced binding of Staphylococcus aureus to atopic skin’, *The Journal of Allergy and Clinical Immunology*, 108(2), pp. 269–274. Available at: https://doi.org/10.1067/mai.2001.117455.

Cornelissen, C. *et al.* (2012) ‘IL-31 regulates differentiation and filaggrin expression in human organotypic skin models’, *Journal of Allergy and Clinical Immunology*, 129(2), pp. 426-433.e8. Available at: https://doi.org/10.1016/j.jaci.2011.10.042.

Dhingra, N. *et al.* (2013) ‘Attenuated neutrophil axis in atopic dermatitis compared to psoriasis reflects TH17 pathway differences between these diseases’, *The Journal of allergy and clinical immunology*, 132(2), p. 10.1016/j.jaci.2013.04.043. Available at: https://doi.org/10.1016/j.jaci.2013.04.043.

Dickson, M.A. *et al.* (2000) ‘Human keratinocytes that express hTERT and also bypass a p16(INK4a)-enforced mechanism that limits life span become immortal yet retain normal growth and differentiation characteristics’, *Molecular and Cellular Biology*, 20(4), pp. 1436–1447. Available at: https://doi.org/10.1128/MCB.20.4.1436-1447.2000.

Elgharib, I. *et al.* (2018) ‘Serum elafin as a potential inflammatory marker in psoriasis’, *International Journal of Dermatology*, 58. Available at: https://doi.org/10.1111/ijd.14217.

Focken, J. *et al.* (2023) ‘Neutrophil extracellular traps enhance S. aureus skin colonization by oxidative stress induction and downregulation of epidermal barrier genes’, *Cell Reports*, 42(10). Available at: https://doi.org/10.1016/j.celrep.2023.113148.

Foster, T.J. *et al.* (2014) ‘Adhesion, invasion and evasion: the many functions of the surface proteins of Staphylococcus aureus’, *Nature Reviews. Microbiology*, 12(1), pp. 49–62. Available at: https://doi.org/10.1038/nrmicro3161.

Furue, M. (2020) ‘Regulation of Filaggrin, Loricrin, and Involucrin by IL-4, IL-13, IL-17A, IL-22, AHR, and NRF2: Pathogenic Implications in Atopic Dermatitis’, *International Journal of Molecular Sciences*, 21(15), p. 5382. Available at: https://doi.org/10.3390/ijms21155382.

G, P. *et al.* (2022) ‘Human β-defensin-3 attenuates atopic dermatitis-like inflammation through autophagy activation and the aryl hydrocarbon receptor signaling pathway’, *The Journal of clinical investigation*, 132(17). Available at: https://doi.org/10.1172/JCI156501.

Garzorz-Stark, N. *et al.* (2016) ‘A novel molecular disease classifier for psoriasis and eczema’, *Experimental Dermatology*, 25(10), pp. 767–774. Available at: https://doi.org/10.1111/exd.13077.

Geoghegan, J.A., Irvine, A.D. and Foster, T.J. (2018) ‘Staphylococcus aureus and Atopic Dermatitis: A Complex and Evolving Relationship’, *Trends in Microbiology*, 26(6), pp. 484–497. Available at: https://doi.org/10.1016/j.tim.2017.11.008.

Gochnauer, H. *et al.* (2017) ‘The Psychosocial Impact of Atopic Dermatitis’, in E.A. Fortson, S.R. Feldman, and L.C. Strowd (eds) *Management of Atopic Dermatitis: Methods and Challenges*. Cham: Springer International Publishing (Advances in Experimental Medicine and Biology), pp. 57–69. Available at: https://doi.org/10.1007/978-3-319-64804-0_6.

Goldblum, J.R. *et al.* (2018) *Rosai and Ackerman’s Surgical Pathology*. 11th ed. Elsevier.

Ho, A.W. and Kupper, T.S. (2019) ‘T cells and the skin: from protective immunity to inflammatory skin disorders’, *Nature Reviews. Immunology*, 19(8), pp. 490–502. Available at: https://doi.org/10.1038/s41577-019-0162-3.

Hoffmann, J.H.O. and Enk, A.H. (2016) ‘Neutrophil extracellular traps in dermatology: Caught in the NET’, *Journal of Dermatological Science*, 84(1), pp. 3–10. Available at: https://doi.org/10.1016/j.jdermsci.2016.07.001.

Hollox, E.J. *et al.* (2008) ‘Psoriasis is associated with increased beta-defensin genomic copy number’, *Nature genetics*, 40(1), pp. 23–25. Available at: https://doi.org/10.1038/ng.2007.48.

Hu, S.C.-S. *et al.* (2016) ‘Neutrophil extracellular trap formation is increased in psoriasis and induces human β-defensin-2 production in epidermal keratinocytes’, *Scientific Reports*, 6(1), p. 31119. Available at: https://doi.org/10.1038/srep31119.

Icotrokinra delivered an industry-leading combination of significant skin clearance with demonstrated tolerability in a once daily pill in Phase 3 topline results (2024) *JNJ.com*. Available at: https://www.jnj.com/media-center/press-releases/icotrokinra-delivered-an-industry-leading-combination-of-significant-skin-clearance-with-demonstrated-tolerability-in-a-once-daily-pill-in-phase-3-topline-results (Accessed: 4 February 2025).

Irvine, A.D., McLean, W.H.I. and Leung, D.Y.M. (2011) ‘Filaggrin Mutations Associated with Skin and Allergic Diseases’, *New England Journal of Medicine*, 365(14), pp. 1315–1327. Available at: https://doi.org/10.1056/NEJMra1011040.

Kamsteeg, M. *et al.* (2010) ‘Molecular diagnostics of psoriasis, atopic dermatitis, allergic contact dermatitis and irritant contact dermatitis’, *British Journal of Dermatology*, 162(3), pp. 568–578. Available at: https://doi.org/10.1111/j.1365-2133.2009.09547.x.

Karsten, S. (2021) *The DNA repair enzymes MTH1 and OGG1 as targets to treat inflammation*. thesis. Karolinska Institutet. Available at: https://openarchive.ki.se/articles/thesis/The_DNA_repair_enzymes_MTH1_and_OGG1_as_targets_to_treat_inflammation/26896003/1 (Accessed: 25 January 2025).

Kezic, S. *et al.* (2011) ‘Levels of filaggrin degradation products are influenced by both filaggrin genotype and atopic dermatitis severity’, *Allergy*, 66(7), pp. 934–940. Available at: https://doi.org/10.1111/j.1398-9995.2010.02540.x.

Köhler, I. *et al.* (2024) ‘NOS2-derived low levels of NO drive psoriasis pathogenesis’, *Cell Death & Disease*, 15(6), p. 449. Available at: https://doi.org/10.1038/s41419-024-06842-z.

Kuswanto, W., Nolan, G. and Lu, G. (2023) ‘Highly multiplexed spatial profiling with CODEX: bioinformatic analysis and application in human disease’, *Seminars in Immunopathology*, 45(1), pp. 145–157. Available at: https://doi.org/10.1007/s00281-022-00974-0.

Landgren, E. *et al.* (2006) ‘Psoriasis in Swedish conscripts: Time trend and association with T-helper 2-mediated disorders’, *The British journal of dermatology*, 154, pp. 332–6. Available at: https://doi.org/10.1111/j.1365-2133.2005.07004.x.

Leyden, J.J., Marples, R.R. and Kligman, A.M. (1974) ‘Staphylococcus aureus in the lesions of atopic dermatitis’, *British Journal of Dermatology*, 90(5), pp. 525–525. Available at: https://doi.org/10.1111/j.1365-2133.1974.tb06447.x.

Liu, T. *et al.* (2017) ‘NF-κB signaling in inflammation’, *Signal Transduction and Targeted Therapy*, 2(1), pp. 1–9. Available at: https://doi.org/10.1038/sigtrans.2017.23.

McGrath, J.A. and Uitto, J. (2008) ‘The filaggrin story: novel insights into skin-barrier function and disease’, *Trends in Molecular Medicine*, 14(1), pp. 20–27. Available at: https://doi.org/10.1016/j.molmed.2007.10.006.

Md Jaffri, J. (2023) ‘Reactive Oxygen Species and Antioxidant System in Selected Skin Disorders’, *The Malaysian Journal of Medical Sciences : MJMS*, 30(1), pp. 7–20. Available at: https://doi.org/10.21315/mjms2023.30.1.2.

Megna, M. *et al.* (2016) ‘Systemic Treatment of Adult Atopic Dermatitis: A Review’, *Dermatology and Therapy*, 7(1), pp. 1–23. Available at: https://doi.org/10.1007/s13555-016-0170-1.

Meledathu, S., Naidu, M.P. and Brunner, P.M. (2025) ‘Update on Atopic Dermatitis’, *Journal of Allergy and Clinical Immunology* [Preprint]. Available at: https://doi.org/10.1016/j.jaci.2025.01.013.

Metzler, K.D. *et al.* (2011) ‘Myeloperoxidase is required for neutrophil extracellular trap formation: implications for innate immunity’, *Blood*, 117(3), pp. 953–959. Available at: https://doi.org/10.1182/blood-2010-06-290171.

Mulcahy, M.E. *et al.* (2012) ‘Nasal Colonisation by Staphylococcus aureus Depends upon Clumping Factor B Binding to the Squamous Epithelial Cell Envelope Protein Loricrin’, *PLOS Pathogens*, 8(12), p. e1003092. Available at: https://doi.org/10.1371/journal.ppat.1003092.

Nakatani, T. *et al.* (2001) *CCR4 memory CD4+ T lymphocytes are increased in peripheral blood and lesional skin from patients with atopic dermatitis - PubMed*. Available at: https://pubmed.ncbi.nlm.nih.gov/11174204/ (Accessed: 23 September 2022).

Nakatsuji, T. *et al.* (2016) ‘Staphylococcus aureus Exploits Epidermal Barrier Defects in Atopic Dermatitis to Trigger Cytokine Expression’, *The Journal of Investigative Dermatology*, 136(11), pp. 2192–2200. Available at: https://doi.org/10.1016/j.jid.2016.05.127.

Nakatsuji, T. *et al.* (2017) ‘Antimicrobials from human skin commensal bacteria protect against Staphylococcus aureus and are deficient in atopic dermatitis’, *Science Translational Medicine*, 9(378), p. eaah4680. Available at: https://doi.org/10.1126/scitranslmed.aah4680.

Nguyen, M.T. *et al.* (2016) ‘Skin-Specific Unsaturated Fatty Acids Boost the Staphylococcus aureus Innate Immune Response’, *Infection and Immunity*, 84(1), pp. 205–215. Available at: https://doi.org/10.1128/IAI.00822-15.

Noormohammadpour, P. *et al.* (2015) ‘Evaluation of Some Psychological Factors in Psoriatic Patients’, *Iranian Journal of Psychiatry*, 10(1), pp. 37–42.

Nørreslet, L.B., Agner, T. and Clausen, M.-L. (2020) ‘The Skin Microbiome in Inflammatory Skin Diseases’, *Current Dermatology Reports*, 9(2), pp. 141–151. Available at: https://doi.org/10.1007/s13671-020-00297-z.

Osca-Verdegal, R. *et al.* (2022) ‘Histone Citrullination Mediates a Protective Role in Endothelium and Modulates Inflammation’, *Cells*, 11(24), p. 4070. Available at: https://doi.org/10.3390/cells11244070.

Pompili, M. *et al.* (2016) ‘Suicide risk and psychiatric comorbidity in patients with psoriasis’, *Journal of International Medical Research*, 44(1_suppl), pp. 61–66. Available at: https://doi.org/10.1177/0300060515593253.

Quaranta, M. *et al.* (2014) ‘Allergic Contact Dermatitis in Psoriasis Patients: Typical, Delayed, and Non-Interacting’, *PLoS ONE*. Edited by J. Schauber, 9(7), p. e101814. Available at: https://doi.org/10.1371/journal.pone.0101814.

Rada, B. (2019) ‘Neutrophil Extracellular Traps’, *Methods in Molecular Biology (Clifton, N.J.)*, 1982, pp. 517–528. Available at: https://doi.org/10.1007/978-1-4939-9424-3_31.

Robert, C. and Kupper, T.S. (1999) ‘Inflammatory skin diseases, T cells, and immune surveillance’, *The New England Journal of Medicine*, 341(24), pp. 1817–1828. Available at: https://doi.org/10.1056/NEJM199912093412407.

Sabbatini, M., Magnelli, V. and Renò, F. (2021) ‘NETosis in Wound Healing: When Enough Is Enough’, *Cells*, 10(3), p. 494. Available at: https://doi.org/10.3390/cells10030494.

Satoh, T.K. (2022) ‘The role of HMGB1 in inflammatory skin diseases’, *Journal of Dermatological Science*, 107(2), pp. 58–64. Available at: https://doi.org/10.1016/j.jdermsci.2022.07.005.

Scheurer, J. *et al.* (2024) ‘Histological and functional characterization of 3D human skin models mimicking the inflammatory skin diseases psoriasis and atopic dermatitis’, *Disease Models & Mechanisms*, 17(1), p. dmm050541. Available at: https://doi.org/10.1242/dmm.050541.

Schürch, C.M. *et al.* (2020) ‘Coordinated Cellular Neighborhoods Orchestrate Antitumoral Immunity at the Colorectal Cancer Invasive Front’, *Cell*, 182(5), pp. 1341-1359.e19. Available at: https://doi.org/10.1016/j.cell.2020.07.005.

Sieprawska-Lupa, M. *et al.* (2004) ‘Degradation of human antimicrobial peptide LL-37 by Staphylococcus aureus-derived proteinases’, *Antimicrobial Agents and Chemotherapy*, 48(12), pp. 4673–4679. Available at: https://doi.org/10.1128/AAC.48.12.4673-4679.2004.

Sun, Y. *et al.* (2012) ‘Fatty acids regulate stress resistance and virulence factor production for Listeria monocytogenes’, *Journal of Bacteriology*, 194(19), pp. 5274–5284. Available at: https://doi.org/10.1128/JB.00045-12.

Thålin, C. *et al.* (2018) ‘Citrullinated histone H3 as a novel prognostic blood marker in patients with advanced cancer’, *PLoS ONE*, 13(1), p. e0191231. Available at: https://doi.org/10.1371/journal.pone.0191231.

Tumurkhuu, G. *et al.* (2020) ‘Oxidative DNA Damage Accelerates Skin Inflammation in Pristane-Induced Lupus Model’, *Frontiers in Immunology*, 11, p. 554725. Available at: https://doi.org/10.3389/fimmu.2020.554725.

Uhlen, M. *et al.* (2010) ‘Towards a knowledge-based Human Protein Atlas’, *Nature Biotechnology*, 28(12), pp. 1248–1250. Available at: https://doi.org/10.1038/nbt1210-1248.

Vakiti, A., Padala, S.A. and Singh, D. (2025) ‘Sezary Syndrome’, in *StatPearls*. Treasure Island (FL): StatPearls Publishing. Available at: http://www.ncbi.nlm.nih.gov/books/NBK499874/ (Accessed: 18 January 2025).

Valdimarsson, H. *et al.* (1995) ‘Psoriasis: a T-cell-mediated autoimmune disease induced by streptococcal superantigens?’, *Immunology Today*, 16(3), pp. 145–149. Available at: https://doi.org/10.1016/0167-5699(95)80132-4.

Viatour, P. *et al.* (2005) ‘Phosphorylation of NF-κB and IκB proteins: implications in cancer and inflammation’, *Trends in Biochemical Sciences*, 30(1), pp. 43–52. Available at: https://doi.org/10.1016/j.tibs.2004.11.009.

Weidinger, S. *et al.* (2018) ‘Atopic dermatitis’, *Nature Reviews Disease Primers*, 4(1), pp. 1–20. Available at: https://doi.org/10.1038/s41572-018-0001-z.

Williams, M.R. *et al.* (2017) ‘Staphylococcus aureus Induces Increased Serine Protease Activity in Keratinocytes’, *The Journal of Investigative Dermatology*, 137(2), pp. 377–384. Available at: https://doi.org/10.1016/j.jid.2016.10.008.

Williams, M.R. and Gallo, R.L. (2015) ‘The Role of the Skin Microbiome in Atopic Dermatitis’, *Current Allergy and Asthma Reports*, 15(11), p. 65. Available at: https://doi.org/10.1007/s11882-015-0567-4.

Yu, T. *et al.* (2018) ‘Functions and mechanisms of microRNA-31 in human cancers’, *Biomedicine & Pharmacotherapy*, 108, pp. 1162–1169. Available at: https://doi.org/10.1016/j.biopha.2018.09.132.

Zeng, W. *et al.* (2023) ‘Neutrophil elastase: From mechanisms to therapeutic potential’, *Journal of Pharmaceutical Analysis*, 13(4), pp. 355–366. Available at: https://doi.org/10.1016/j.jpha.2022.12.003.

Zhang, W. and Liu, H.T. (2002) ‘MAPK signal pathways in the regulation of cell proliferation in mammalian cells’, *Cell Research*, 12(1), pp. 9–18. Available at: https://doi.org/10.1038/sj.cr.7290105.

Zhou, X. *et al.* (2022) ‘Advances in the pathogenesis of psoriasis: from keratinocyte perspective’, *Cell Death & Disease*, 13(1), pp. 1–13. Available at: https://doi.org/10.1038/s41419-022-04523-3.

7 Declaration of Originality

This work was conducted in the Institute of Pathology, University Hospital Tübingen, and supervised by Univ.-Prof. Dr. med. Christian Schürch, MD, PhD.

Conception of the study was done in cooperation with Prof. Dr. rer. nat. Birgit Schittek, Institute of Dermatology, University Hospital Tübingen.

All experiments were conducted by myself following the introduction by Christine Beschorner and Karen Greif, except for cutting of the tissue samples. 3D skin equivalents were prepared and provided by Jasmin Scheurer and Birgit Sauer. Computational work for the analyzed CODEX data was supported by Ahmad Makky. Antibodies that were used from existing conjugations were listed as such.

Statistical analysis was done independently by me.

I hereby declare that this thesis represents my original work and that I have used no other sources except as noted by citations.

Innsbruck, den 12.02.2025

_____

8 Publications

Focken, J. *et al.* (2023) 'Neutrophil extracellular traps enhance S. aureus skin colonization by oxidative stress induction and downregulation of epidermal barrier genes', *Cell Reports*, 42(10). Available at: https://doi.org/10.1016/j.celrep.2023.113148.

Cell Reports

Article

Neutrophil extracellular traps enhance *S. aureus* skin colonization by oxidative stress induction and downregulation of epidermal barrier genes

Graphical abstract

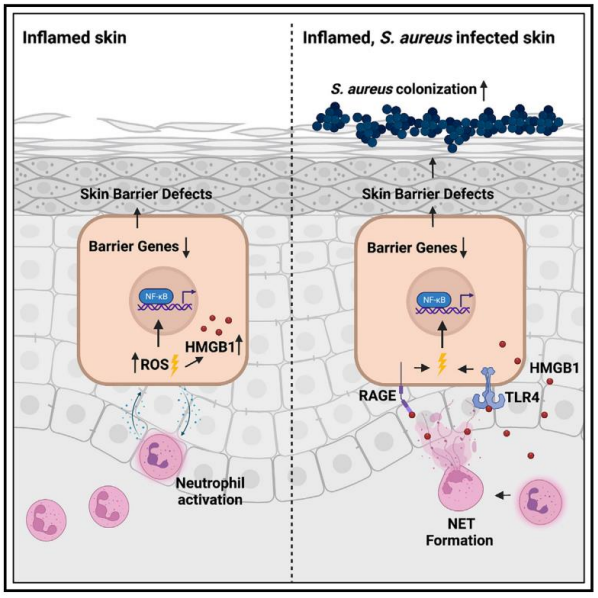

Authors

Jule Focken, Jasmin Scheurer, Annika Jäger, ..., Martin Schaller, Bettina Weigelin, Birgit Schittek

Correspondence

birgit.schittek@uni-tuebingen.de

In brief

Focken et al. show that in inflamed skin, the enhanced presence of neutrophils and NETs induces ROS-mediated secretion of HMGB1, which in turn mediates the downregulation of epidermal barrier genes, thus driving *S. aureus* skin colonization.

Scheurer, J. *et al.* (2024) 'Histological and functional characterization of 3D human skin models mimicking the inflammatory skin diseases psoriasis and atopic dermatitis', *Disease Models & Mechanisms*, 17(1), p. dmm050541. Available at: https://doi.org/10.1242/dmm.050541.

© 2024. Published by The Company of Biologists Ltd | Disease Models & Mechanisms (2024) 17, dmm050541. doi:10.1242/dmm.050541

The Company of Biologists

RESOURCES & METHODS

Histological and functional characterization of 3D human skin models mimicking the inflammatory skin diseases psoriasis and atopic dermatitis

Jasmin Scheurer[1], Birgit Sauer[1], Jule Focken[1], Martina Giampetraglia[3,4], Annika Jäger[2], Christian M. Schürch[2,4], Bettina Weigelin[3,4] and Birgit Schittek[1,4,*]

9 Acknowledgment

First and foremost, I want to thank my supervisor Prof. Dr. med. Christian Schürch for providing continuous guidance and knowledge, sharing his passion for science and especially for keeping me motivated during the times I failed to see the positive progress made.

Thanks also to the whole team of AG Schürch, without whom I would not have been able to complete this research. Everyone was always willing to help with every small or big problem and most importantly helped to laugh about failed experiments to keep up the spirit.

Furthermore, I would like to thank my co-supervisor Prof. Dr. rer. nat. Birgit Schittek and her team Jasmin Scheurer and Jule Focken who never failed to show great excitement over presented results and provided all samples, helped with the cell cultures and enabled publication of the data achieved.

I want to thank Sina and Tilman for spending their lunch breaks with me and listening to my rants and complaints.

I want to thank my family for always believing in whatever I did was certainly going to be a success. And for holding me accountable by asking about the completion of my dissertation every chance they could get.

Lastly, I want to thank Florian, who refused to proof-read but prevented my laptop from damage out of frustration over Excel sheets. But mostly for always supporting me with kind words, home-cooked meals and much needed distraction.

Thank you.